Available online at www.sciencedirect.com
SCIENCE DIRECT®
ELSEVIER
Progress in Energy and Combustion Science 31 (2005) 75–121
PROGRESS IN ENERGY AND COMBUSTION SCIENCE
www.elsevier.com/locate/pecs

Tracer-LIF diagnostics: quantitative measurement of fuel concentration, temperature and fuel/air ratio in practical combustion systems

Christof Schulz[a,1], Volker Sick[b,*]

[a]*Institut für Verbrennung und Gasdynamik, Universität Duisburg-Essen, Lotharstr. 1, 47057 Duisburg, Germany*
[b]*Department of Mechanical Engineering, The University of Michigan, 2023 W.E. Lay Automotive Laboratory, 1231 Beal Avenue, Ann Arbor, MI 48109-2133, USA*

Received 17 April 2004; accepted 27 August 2004

Abstract

The safe, clean, and reliable operation of combustion devices depends to a large degree on the exact control of the fuel/air mixing process prior to ignition. Therefore, quantitative measurement techniques that characterize the state of the fresh gas mixture are crucial in modern combustion science and engineering. This paper presents the fundamental concepts for how to devise and apply quantitative measurement techniques for studies of fuel concentration, temperature, and fuel/air ratio in practical combustion systems, with some emphasis on internal combustion engines. The paper does not attempt to provide a full literature review of quantitative imaging diagnostics for practical combustion devices; rather it focuses on explaining the concepts and illustrating these with selected examples. These examples focus on application to primarily gaseous situations.

The photophysics of organic molecules is presented in an overview followed by discussions on specific details of the temperature-, pressure-, and mixture-dependence of the laser-induced fluorescence strength of aliphatic ketones, like acetone and 3-pentanone, and toluene. Models that describe the fluorescence are discussed and evaluated with respect to their functionality. Examples for quantitative applications are categorized in order of increased complexity. These examples include simple mixing experiments under isothermal and isobaric conditions, fuel/air mixing in engines, temperature measurements, and mixing studies where fuel and oxygen concentrations vary.

A brief summary is given on measurements of fuel concentrations in multiphase systems, such as laser-induced exciplex spectroscopy. Potentially adverse effects that added tracers might have on mixture formation, combustion, and the faithful representation of the base fuel distribution are discussed. Finally, a brief section describes alternative techniques to tracer-based measurements that allow studies of fuel/air mixing processes in practical devices.

The paper concludes with a section that addresses key issues that remain as challenges for continued research towards the improvement of quantitative, tracer-based LIF measurements.

Keywords: Laser imaging; Fluorescence tracers; Fuel imaging; Temperature imaging; Photophysics; Diagnostics; Practical combustion

* Corresponding author. Tel.: +1 734 647 9607; fax: +1 734 764 4256.
E-mail addresses: christof.schulz@uni-duisburg.de (C. Schulz), vsick@umich.edu (V. Sick).
[1] Tel.: +49 203 3792995; fax: +49 203 3793087.

0360-1285/$ - see front matter © 2004 Elsevier Ltd. All rights reserved.
doi:10.1016/j.pecs.2004.08.002

Contents

1. Introduction

1.1. Motivation: use of fluorescent tracers

The safe, clean, and reliable operation of combustion devices depends to a large degree on the exact control of the fuel/air mixing process prior to ignition. Therefore, quantitative measurement techniques that characterize the state of the fresh gas mixture are crucial in modern combustion science and engineering. The mixture determines not only the homogeneity of the combustion process but also the ignition process in unsteady combustion systems, such as internal combustion engines. It therefore affects pollutant formation and release of unburned hydrocarbons in many ways, and its control is crucial for the development of energy-efficient, low-emission devices. The mixture is characterized by a number of key quantities. While the fuel concentration determines the total energy available for the process, the actual chemical process depends mostly on the *ratio* of fuel, oxygen and inert gases. The temperature of the mixture in turn has a strong influence on ignition, flame speed and flame orientation. Turbulence, finally, significantly increases the volumetric reaction rates.

In practical combustion devices the presence of large quantities of premixed (and therefore highly explosive) fuel/air mixtures is typically avoided for safety reasons. The aim is then to mix the components rapidly either shortly before the combustion process or while combustion is already in progress. In technical burners this is accomplished by turbulent mixing, i.e. in swirling flows. In internal combustion engines, injection of fuel into the compressed air provides fast mixing. Typically, no perfectly homogeneous mixture is achieved within the available time.

In contrast, a well-defined stratification of fuel/air mixtures is often attempted in modern internal combustion engines. This allows the operation of overall lean mixtures while still providing high enough fuel concentrations close to the spark plug to ensure reliable ignition. Direct-injection

Nomenclature

E	energy
f	focal length
FRET	fluorescence resonance energy transfer
h	Planck constant
IC	internal conversion
ISC	intersystem crossing
k_{abs}	rate of absorption
k_{coll}	rate of vibrational relaxation
k_{fl}	rate of spontaneous fluorescence
k_{ic}	rate of internal conversion
k_{isc}	rate of intersystem crossing
k_{nr}	rate of non-radiative depopulation processes
$\tilde{k}_q$	rate coefficient of collisional quenching
k_{SV}	Stern–Volmer coefficient
k_{tot}	total rate of all depopulation processes of electronically excited state
LIF	laser-induced fluorescence
n_{fl}	number density of fluorescence tracer
n_q	number density of quenching species
Oh	Ohnesorge number
P_n	probability of energy transfer in FRET
$\langle p \rangle$	probability of effective collision
r_0	critical radius in FRET
S_{fl}	fluorescence signal intensity (proportional to number density)
S_{fl}^{+}	fluorescence signal intensity (proportional to mole fraction)
S_{fl}^{0}	fluorescence signal intensity in the absence of collisional quenching
SI	spark ignition
V	volume
VR	vibrational relaxation
We	Weber number
x_{fl}	mole fraction of fluorescing species
Z_{coll}	collision rate
ΔE_{coll}	energy difference in collisional relaxation
$\Delta E_{thermal}$	average thermal ground state energy
$\Omega/4\pi$	solid angle of detection
ϕ	equivalence ratio
ϕ_{fl}	fluorescence quantum yield
η	detector efficiency
λ	wavelength
ν	frequency
σ_{abs}	absorption cross-section
σ	surface tension
τ_{eff}	effective lifetime
τ_{rad}	radiative lifetime

engines allow the control of the amount of fuel independent of the air load, which minimizes pumping losses and therefore increases the energy efficiency. In terms of characterizing the starting conditions of the combustion processes, an additional level of complication is added. The mixing of fuel vapor and air happens at the same time as fuel vaporization. The evaporation changes liquid and gas phase temperatures, and deposition of liquid films on the surfaces of the combustion chamber can occur.

Laser diagnostics are widely used in fundamental combustion science, research, and development to investigate transient phenomena without influencing the system under study by inserting probes and surfaces. Laser-induced fluorescence (LIF) is frequently used for remote detection of concentration and temperature. Within the duration of a single laser pulse (typically a few nanoseconds) volume elements in the sub-millimeter range can be observed. Two-dimensional cross-sections can be illuminated with light sheets and the resulting signal light can be imaged on CCD (charge-coupled device) cameras. Often, these cameras employ image intensifying devices to enhance signal levels and to provide temporal gating to suppress luminosity from flames.

Laser-induced fluorescence is emitted from electronically excited levels that are populated by absorption of photons, typically in the ultraviolet and visible spectral region. Usually the absorption wavelength increases with increasing size of the chromophore of the excited molecule (i.e. the active part of the molecule that absorbs light). Aliphatic (saturated, i.e. no double bonds) hydrocarbons that form the major part of combustion fuels are transparent within the spectral range of interest and therefore do not give any LIF signal at all. On the other hand, many commercial fuels contain unsaturated and aromatic components that strongly absorb light, leading to strong fluorescence. This fluorescence, however, typically does not come from a single component but is composed from signal light from numerous species. While this signal can be used for qualitative imaging of the fuel cloud, quantitative interpretation of the signals is typically not feasible. Each component exhibits a fluorescence signal that depends not only on the concentration of the fluorescing species but—in its own characteristic way—also on temperature, pressure and local gas composition. The simultaneous detection of signal from various species leads therefore to a complicated dependence of the integrated signal intensity on these variables. The various fluorescing compounds of commercial fuels furthermore might differ in their physical properties (boiling points, diffusion, and transport coefficients). LIF images of commercial fuels therefore do not perfectly represent the fuel distribution during fuel evaporation and mixing.

For quantitative analysis, systems are preferred where the fluorescence signal can be attributed to single species. Therefore, it is popular to add well-characterized fluorescing tracers to otherwise non- (or weakly) fluorescing fuels.

There is, however, not a single best tracer-LIF approach that covers all possible applications. The tracer signal intensities depend on the environment, which has to be corrected for when quantitative tracer concentration measurements are desired. In turn, these interdependencies can be used to gain further information on the system under study, yielding information about temperature and fuel/air ratios.

1.2. Desired quantities

There are a number of quantities that would be desirable to measure with non-intrusive in situ techniques in order to completely characterize the mixing process in the fresh gas. These quantities include:

- Fuel concentration
- Fuel/air ratio
- Temperature
- Fuel composition (i.e. concentration of individual components)
- Residual gas concentration.

In order to visualize the mixing process and to facilitate the interpretation of the results, these quantities should be imaged in at least two dimensions with temporal resolution faster than the time scale of mixing and chemical reaction.

When using tracers as representatives for the local fuel concentration in spatially well resolved experiments or in high-temperature applications, an important question must be addressed. The fuel and the tracer experience chemical reactions well before the flame front (the region of maximum heat release) in both time and space. Therefore, the disappearing of the fuel parent molecule and the tracer is not necessarily indicative for the onset of the high-temperature combustion process. The distinction of burned and unburned areas is based on the assumption of a single-step reaction, which is not a good model for many combustion situations.

1.3. Range of experimental situations

Mixing processes can be categorized according to the level of difficulty in terms of quantitative imaging measurements. They are listed here in order of increasing complexity:

- Constant pressure vs. temporally fluctuating pressure
- Constant temperature vs. temporally fluctuating temperature (spatially homogeneous)
- Spatially homogeneous temperature vs. spatially varying temperature
- Temperature approaches the stability limit of the tracer
- Homogeneous vs. inhomogeneous bath gas composition (mainly oxygen concentration is relevant)
- Single-component fuel vs. multi-component fuel
- Non-fluorescing vs. fluorescing fuel
- Homogeneous (gas-phase) vs. heterogeneous (two-phase flows).

1.4. The ideal tracer

The ideal tracer should behave exactly like the fluid to which it is added (i.e. the fuel or the desired component of a multi-component fuel) in terms of droplet formation, evaporation, convection, diffusion, reactivity, and reaction rate. It is obvious that these requirements cannot be met in full. However, practical tracers are often very similar to the fuel or are components which are present in commercial fuels. Therefore, in some situations, tracers must not be understood as 'added' to the fuel. Rather, the other fluorescing substances are replaced. The modification of the system must be kept to a minimum, and the influence of the tracers on a given experimental situation must be critically reviewed.

Ideally, the tracer should yield LIF signal intensities that are directly proportional to the desired quantity and should not be influenced by the ambient conditions. Unfortunately, signals from all fluorescent tracers show at least some dependence on local temperature, pressure, and bath gas variation. Therefore, in experiments where ambient conditions change in time or space, the underlying interdependencies with the tracer signal must be understood in order to obtain quantitative results.

1.5. Roadmap through the paper

This paper is organized as follows. We emphasize tracers for gas phase diagnostics. The tracers typically applied in these environments are discussed in Section 2. Section 3 introduces the photophysics of organic molecules necessary to explain the spectroscopic behavior of the most frequently used tracer classes and the dependence of signal intensities on ambient conditions. The two most frequently and best studied tracer classes—aliphatic ketones (e.g. acetone and 3-pentanone) and single-ring aromatics (e.g. toluene)—are discussed in Section 4. In Section 5 applications of the aforementioned tracers in gas phase systems are shown, using data evaluation based on the photophysical understanding. Section 6 gives a brief overview of the techniques that are currently used to characterize two-phase flows. Section 7 critically reviews the adverse effects of tracers added to fuel in practical combustion devices, and Section 8 describes alternative approaches to measuring fuel concentrations in single- and two-phase situations.

2. Tracers for gas-phase systems

Tracer-based LIF techniques have been used for experimental studies in fluid mechanics and combustion for several years. Tracers are single components

(molecules or atoms) with well understood spectral behavior that represent the local concentration of the fluid of interest or that allow remote measurements of a quantity of interest (e.g. temperature or pressure). Typically, compounds are chosen that yield strong enough LIF signal intensities to allow two- (or even three-) dimensional visualization of the desired quantity with sufficient temporal resolution to freeze the motion.

There are two opposite cases that require the application of tracers for the measurement in fluids. First, the components of the fluid *do not (or only weakly) fluoresce*. This is the case for air and typical exhaust gases (H_2O [1], CO_2 [2]). At room temperature these species are excited in the vacuum-UV only, and only at high temperatures do their spectra extend into the spectral range that is of practical use for combustion diagnostics. The resulting signal in O_2 [3] and CO_2 [2] is then strongly temperature-dependent and the practical use for concentration measurements is limited. In the second case the fuel contains *too many fluorescing compounds*. This is true for commercial fuels. Their fluorescence has been used to obtain qualitative and semi-quantitative measurements of fuel vapor concentrations [4]. However, because all these compounds have different physical properties in terms of volatility, transport, and spectral response on variations in ambient conditions, the overall signal cannot be quantified. In both situations it is desirable to add a single tracer that can be selectively observed within the fluid. In the case of fuels (gasoline or Diesel-type fuels) this often means replacing the fluorescing compounds of the fuel by non-fluorescing compounds, leaving only one, or adding an additional compound that was not part of the original mixture.

Different 'classes' of molecules have been used as tracers. The choice of potential tracers is driven by the desire to add a minimum concentration of tracer that yields a maximum LIF signal intensity, while not perturbing the system under study. To provide high enough seeding concentrations especially at low temperatures (room temperature), the tracer must have a high enough vapor pressure. While the main part of this paper focuses on the fuel-like hydrocarbon-based tracers, we include other concepts in the following overview.

2.1. Added tracers

2.1.1. Atoms

Atoms have large absorption cross-sections, and they are candidates that emit strong fluorescence upon excitation in the UV and the visible. The atomization of the material, however, requires high temperatures that are present in flames. Some metal salts (like thallium chloride or indium chloride) can be dissolved in the fuel. In the flame front metal atoms are then generated that can be used to measure temperature in the burned gases [5,6]. The strong transition moments in atoms allow the use of extremely low (and therefore non-perturbing) seeding levels; this is also required to avoid attenuation of the incident laser beam and fluorescence trapping. The strong transitions, in turn, are easily saturated. This needs to be avoided for quantitative temperature measurements. Excitation laser intensities are therefore limited and signals are weak, despite of the favorable spectroscopic properties. This class of fluorescing species is not suited for the observation of fuel distributions prior to combustion.

2.1.2. Small inorganic molecules

Di- and tri-atomic inorganic molecules are frequently used in combustion diagnostics. While unstable radicals like OH, CH, and C_2 that appear during the combustion process can be used for flame front localization and combustion diagnostics [7], they are not suited for observations in the mixing process prior to ignition. Strongly fluorescing stable species, however, are potentially interesting as tracers for the airflow. NO has been used, despite its toxicity, for studies in gaseous mixing processes [8,9], and its spectroscopy is well understood for a wide range of possible applications [10]. It could, therefore, be used as a tracer for gaseous fuels or mixed with air to 'inversely' trace the fuel in practical combustion situations prior to the onset of combustion. The latter application would circumvent several problems that are connected with tracing the fuel flow, e.g. non-ideal co-evaporation of fuel and tracer. This approach has not yet been demonstrated to our knowledge other than qualitatively with toluene to address mixture homogeneity and location of reaction sites in an engine [11]. OH and NO can also be photolytically generated in flow systems. While not suited for studying mixing on a large scale, these flow-tagging techniques give detailed insight in the fluid motion within the lifetime of the generated species. OH was generated following photodissociation of vibrationally hot water [12], while NO was produced from NO_2 photolysis [13] and from O_2-photolysis in air [14].

Molecular oxygen was used to 'trace' the air flow [15] and to measure temperatures during mixture formation in a Diesel engine [3]. It was also used for flow tagging following the excitation of higher vibrational states by stimulated Raman scattering (RELIEF, [16]).

Iodine was applied as a fluorescing tracer that can be excited and detected in the visible spectral range [17]. Its toxicity, corrosiveness, and the difficulty of seeding iodine at constant rates limit its practical applicability.

SO_2 can be excited at various wavelengths below 390 nm and subsequently emits fluorescence from the UV to the violet [18–20]. This corrosive and toxic gas (bp: $-10\,^{\circ}C$) can be either doped to the flow or can be generated in a flame from sulfur containing precursors [21]. The latter application was suggested to mark residual burned gases in internal engine combustion and to visualize their mixing with fresh air and fuel. SO_2 fluorescence is strongly quenched by many molecules including N_2 [19,22–25]. Its applicability in high-pressure environments could therefore be restricted.

NO_2 has been used as a tracer as well. It can be excited conveniently with a frequency-doubled Nd-YAG laser [26] and has been used to address cyclic variability of mixture concentration in an SI engine [27].

The LIF properties of high-temperature CO_2 upon excitation in the UV have been recently presented [2]. This observation offers a potential for new diagnostics for the observation of mixing of hot burned gases with air and fuel.

2.1.3. Organic molecules

In contrast to the excitation of atoms and di- and tri-atomic molecules, poly-atomic organic molecules have a high density of states and therefore show broad-band absorption spectra. Excitation is possible at various wavelengths that are often accessible with standard laser sources. The organic tracers are chemically close relatives of hydrocarbon fuels. Some of the molecules that are attractive tracers are present in commercial fuels at the percent level. Therefore, relatively high tracer concentrations can be applied without significantly disturbing the combustion process (cf. Section 7.3).

The chemical similarity between tracer and fuel has the additional advantage that the tracer disappears (burns) with the fuel close to the flame front. In measurements with limited spatial resolution ($\sim$1 mm) this is a good match to identify and visualize the position of reactive zones. However, since the reaction kinetics of the tracer are not identical to that of the fuel, tracers are not in general suited for highly resolved measurements close to the flame front because their concentration might no longer represent the fuel concentration accurately. It should be noted that during combustion of hydrocarbon fuels, the parent fuel molecules are consumed in a step-wise process [28]. While not much heat is released during the first steps of this oxidation mechanism, the original fuel molecules are already consumed. The same can happen to tracer molecules. For measurements in many combustion systems this has no real negative implications on the interpretation of the data since high-resolution measurements are either not needed or cannot be achieved. However, there are situations when the interpretation of tracer-LIF signals becomes difficult because of the early disintegration of the fuel and the fuel tracers (cf. Section 2.2.3).

Fluorescing organic tracers come in different sizes and structures with different volatilities. Using their boiling points as a first criterion they can be used to represent different volatility classes of multi-component fuels [29]. At the same time, care must be taken to avoid distillation processes that separate fuel and tracer due to non-ideal boiling behavior during fuel evaporation [30–32].

2.1.3.1. Aromatic hydrocarbons. Aromatic hydrocarbons are typical components of commercial fuels. These species are responsible for the strong absorption in the UV and the subsequently emitted fluorescence [33]. Single-ring aromatics like benzene, toluene, and xylene are part of gasoline fuels at the percent level, while two-ring aromatics like naphthalene and its derivatives are present in Diesel fuels. They typically have high fluorescence quantum yields (toluene: $\phi_{fl}=0.17$, benzene: $\phi_{fl}=0.22$, fluorene: $\phi_{fl}=0.66$, dimethyl anthracene: $\phi_{fl}=0.82$), and their absorption and emission spectra shift towards the red with increasing size of the aromatic system. The wide variety of molecular sizes (and therefore boiling points) makes this class of molecules attractive as tracers that can be adjusted to the boiling behavior of the fuel or that are representative for boiling classes in multi-component fuels. Compounds larger than benzene and toluene have vapor pressures too low for seeding room temperature gas flows.

A major drawback of aromatic tracers is the strong quenching by oxygen. The signal intensities do not only depend on the tracer but also (inversely) on the oxygen concentration. This effect was taken advantage of by interpreting the signal as proportional to fuel/air ratio which is of major practical interest (for this approach and its limitations, cf. Section 4.3.2).

The aromatic compounds in commercial fuels have been used for qualitative and semi-quantitative measurements, both in the vapor [34] and the liquid phases [35,36]. Benzene as a fuel tracer is typically avoided because of its carcinogenic effects. Toluene is less toxic and not considered carcinogenic. Therefore, it has been most frequently chosen as a fuel tracer [37], and recent publications shed more light on its fluorescence dependence on pressure, p, temperature, T, and oxygen number density, n_{O_2} [38,39]. We describe the properties of toluene in more detail in Section 4.3. α-Methyl-naphthalene was investigated by LIF, e.g. [40], because it is part of a model two-component fuel that is used in experimental and numerical studies as a substitute for Diesel or JP8 fuel. Like naphthalene, it is used in combination with *N*,*N*,*N*′,*N*′-tetra-methyl-*p*-phenylendiamine (TMPD) in exciplex studies to simultaneously visualize liquid and vapor phases [41] (ref. Section 6).

2.1.3.2. Aliphatic compounds. Typical saturated aliphatic hydrocarbons like alkanes and saturated alcohols do not fluoresce. They have their first absorption bands in the vacuum UV and excitation typically leads to photodissociation. Non-saturated hydrocarbons with extended conjugated systems that would have useful spectroscopic properties are unstable and tend to polymerize.

Fluorescing aliphatic candidates contain chromophores that allow excitation into stable states that subsequently fluoresce (see Table 1 for some examples). This class of molecules contains ketones (R_2CO), aldehydes (R-CHO), and amines (R_3N, where R is a saturated aliphatic hydrocarbon chain). The (conjugated) combination of chromophores (like in diketones R-CO-CO-R) typically shifts the absorption and fluorescence spectra to the red.

Ketones are the most frequently used class of fluorescent tracers. Their properties have been extensively studied

Table 1
Physical and thermodynamic properties of the most frequently used organic tracer molecules in comparison to typical fuels

	iso-Octane	Propane	Methane	Acetone	3-Pentanone	Acetaldehyde	Biacetyl	Toluene
Molecular weight (g/mol)	114.2	44.1	16.0	58.1	86.1	44.1	86.1	92.1
Density at 25 °C (g/cm^3)	0.69	0.49	–	0.79	0.81	0.77	0.98	0.87
Boiling point (°C)	99.2	−42.1	−161.5	56.1	102.0	20.1	88.0	110.6
Heat of vaporization at 25 °C (kJ/mol) [200]	35.1	14.8	–	31.0	38.5	25.5		38.0
Heat of combustion (MJ/mol) [200]	5.50	2.22	0.89	1.82	3.14	1.31		3.95
Max. burning velocity at 25 °C and $\phi =$ (cm/s) [201]	41.0 at 0.98	46.4 at 1.06	44.8 at 1.08	44.4 at 0.93		42.4 at 1.05		
Flash point (°C) [202]	−12 to 22	−104	−188	−18	7 [203]	−27 [203]	3 [203]	4.5–7
Autoignition temperature in air (°C) [201]	415–561	450–504	537–632	465–727	425–608	175–275	365 [203]	480–810
Flammability limits in 1 bar air (% vol) [201]	0.95–6.5	2.1–9.5	5.0–15	2.6–13	1.6–8	4.0–60	2.4–13 [203]	1.2–7.1
Gas-phase viscosity at 100 °C (μPa s) [204]	7.7	10.2	13.4	9.5	8.2	10.7		8.8
Gas-phase diffusion coeff. (1 bar air, 100 °C) ($cm^2\ s^{-1}$) [204]	0.102	0.181	0.344	0.166	0.129	0.218	0.135 [205]	0.132
Gas-phase diffusion coeff. (8 bar air, 130 °C) ($cm^2\ s^{-1}$) [204]	0.0148	0.0261	0.0493	0.0239	0.0187	0.0311	0.0283 [205]	0.0190

Compilation taken from [205].

[42–48], and they have been applied to various practical situations [49–52]. The high vapor pressure makes acetone (bp: 56 °C) an ideal tracer for gaseous flows [53,54]. 3-Pentanone (bp: 100 °C) [43,55,56] or mixtures of 3-pentanone and 3-hexanone [30] were suggested as tracers that mimic the boiling and transport properties of gasoline. In most of those cases, *iso*-octane was substituted as a representative for the mean boiling point characteristics of gasoline. This has the advantage that *iso*-octane is non-fluorescent and, as a single component, is more amenable to detailed modeling studies. For Diesel fuels the use of even larger ketones was suggested which turned out to have a limited stability at high temperatures. The larger aliphatic chains enhance the reactivity of the carbonyl group.

The smallest aldehyde, formaldehyde (HCHO), tends to polymerize and is therefore difficult to handle as a dopant. Its next larger homologous molecule, acetaldehyde (CH_3CHO) has been used as a tracer in internal combustion engines [57]. Its low boiling point (21 °C) allows high seeding concentrations. Its spectral properties are comparable to those of acetone. Because acetone is considered less harmful, acetaldehyde is not frequently used as a tracer substance. Aldehydes with different molecular weights have been used to trace different boiling fractions in multi-component fuels [58].

The fluorescence quantum yields ($\phi = 0.0008$–0.0018 for acetaldehyde depending on the excitation wavelength and $\phi = 0.002$ for acetone [59,60]) are small compared to those of aromatic compounds in the absence of oxygen. In realistic situations where fuel is mixed with air, however, resulting signals are comparable. Hexafluoroacetone has been suggested as an alternative that has fluorescence quantum yields about an order of magnitude stronger than that of acetone [61,62]. Because of the toxicity, however, this substance has not been further considered as a tracer for practical applications.

Biacetyl (CH_3–CO–CO–CH_3) is frequently used as a fluorescent tracer. With a boiling point of 88 °C, the room temperature vapor pressure is too low for many applications. On the other hand, the boiling point is significantly below that of typical fuels. This intermediate position, the stability and the strong odor might be the reasons why biacetyl, despite its attractive spectroscopic properties and its extensively studied photophysics [63–65], is less popular than ketones. For seeding oxygen-free flows, biacetyl is especially attractive because of its high phosphorescence quantum yield (15%, but strongly quenched by O_2).

Amines do fluoresce upon UV excitation. Some studies include ethylamine [66], and *N*,*N*-dimethyl aniline [67]. Strong quenching by oxygen often hinders the practical

application, and an unpleasant (fish-like) smell and toxicity might deter people from using this class of tracers. Amines, such as TMPD [41,68] triethylamine (TEA) [69], and diethylmethylamine (DEmA) [70], have found some attention as part of exciplex systems. TEA and DEMA do not contribute significantly to the overall gas phase signal but play an important role in forming the excited complex that is responsible for a shift of the liquid phase fluorescence relative to that of the monomers.

2.1.3.3. Organic dyes. Organic dyes with larger chromophores can be tailored for absorption and emission properties, minimized intersystem crossing, maximum fluorescence quantum yield, and fluorescence lifetime [71]. This class of molecules is well known as laser dyes [72] or as fluorescence tracers that are used in the liquid phase down to single-molecule detection level [73,74]. A wide variety of molecules is available that allow choosing tracers with spectral properties that have minimal interference with the properties of the base fuel [75,76]. While these substances are attractive for measuring fluorescence from the liquid phase, e.g. in sprays [75,77] or wall films [33], they are not applicable for vapor phase diagnostics since they have either negligible vapor pressures or they disintegrate before vaporization. Because this paper focuses on vapor phase diagnostics, this class of tracers is not further considered.

2.1.3.4. Purity of fuels and tracers. Laser-induced fluorescence is a very sensitive diagnostic technique, and even trace amounts of substances other than the ones under study can compromise the integrity of the signals and introduce systematic errors into the measurement. The ideal case is that non-fluorescing base fuels are used and the fluorescing tracer is responsible for all measured signals. Thus, care has to be taken to choose adequately pure chemicals. Fuels like methane, propane, *n*-heptane, and *iso*-octane are available with high purity levels that guarantee negligible levels of LIF signal in wavelength ranges coinciding with tracer LIF signals. Reports on fluorescence in these fuels (like *iso*-octane [78]) must be attributed to impurities or to partially oxidized by-products that form in the hot but not yet burning fuel/air mixture (cf. Section 2.2.3). Therefore, spectroscopic grade or HPLC-grade fuels should be used to ensure high quality measurements; unfortunately this comes at a higher price compared to regular high-purity grades. Since the base hydrocarbon fuels include larger carbon chains the purification process becomes increasingly more difficult and expensive. Fuels like decane or higher hydrocarbons are hard to produce in spectroscopic purities. It should be mentioned that the purity specification itself is a poor indicator for its suitability as 'non-fluorescing' fuel. Chemically very similar isomers of the desired hydrocarbon are counted as impurities as well as aromatic compounds, whose fluorescence yields could be higher by several orders of magnitude. Therefore, it is almost mandatory to run a 'blind test' and to perform LIF measurements with just the parent fuel, and it is highly advised to check the quality of the fuel at least when purchasing from a new vendor or changing to another quality.

As for tracers, toluene and acetone are available in spectroscopic grade. Biacetyl and 3-pentanone are typically sold in purities of 98% and are usually adequate for quantitative measurements.

2.2. Natural tracers

There are several practical situations where fluorescing substances are naturally present in the system of interest and do not have to be added for LIF measurements.

2.2.1. Aromatics in commercial fuels

Gasoline and Diesel fuels as well as typical aviation fuels contain a variety of fluorescing aromatic compounds. A full quantification of fluorescence intensities is difficult because several compounds with different evaporation and transport properties as well as different photophysical behavior fluoresce at the same time. The broad-band absorption allows simple, qualitative visualization of fuel (liquid [36] and vapor [4]) distributions in practical situations. Based on several assumptions, semi-quantitative interpretation of the data was possible [34]. However, it was shown that for gasoline the fluorescence is dominated by naphthalene [33], a strongly fluorescing compound with significantly higher boiling point (217 °C) than the rest of the fuel (50% evaporated point at 109 °C). In systems where the evaporation kinetics determines the distribution of the fuel compounds, the 'natural' LIF signal might therefore be misleading. To alleviate this, 3-pentanone was added to regular gasoline for a stronger representation of mid-boiling point fractions [79]. For imaging diagnostics in gas turbines the use of naphthalene or even higher boiling point substances like fluoranthene, on the other hand, can be beneficial for a better representation of the kerosene fuel [80].

2.2.2. Odor markers in natural gas

For safety reasons the suppliers of natural gas usually add so-called odor markers to natural gas at small quantities. Substances typically used for this purpose are mercaptanes (sulfur analogs to alcohols) and tetrahydrothiophen (THT, thiophane, C_4H_8S). The latter strongly fluoresces upon UV excitation, which allows for easy tracing of natural gas concentrations in mixing systems. THT is strongly quenched by oxygen. The resulting fluorescence intensity can therefore, similar to the case of aromatic compounds, be used as a measure for local fuel/air equivalence ratios [81].

2.2.3. Naturally generated tracers

Fluorescing species might also form through chemical reactions within the system under study. In some combustion situations close to auto-ignition partially oxidized species are generated in a process called 'cool flame' [28].

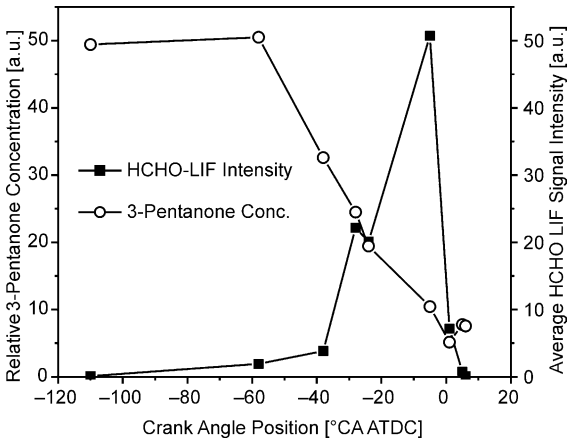

Fig. 1. Temporal variation of 3-pentanone concentration and formaldehyde LIF intensity in an HCCI engine [82]. While the fuel and the added tracer disintegrate, formaldehyde is formed in the 'cool flame' at high concentrations and suddenly disappears at the onset of the hot combustion phase. Reprinted with permission from SAE Paper 2001-01-1924 © 2001 SAE International.

At high temperatures and high pressures the fuel disintegrates and is partially oxidized before the onset of the 'hot' combustion phase. This gives rise to ignition in Diesel engines, is involved in the process that causes engine knock, and is of major importance in so-called *homogeneous-charge compression-ignition* (HCCI) engines that rely on auto-ignition of (more or less) homogeneous gasoline/air mixtures. During the cool flame phase, formaldehyde (HCHO) is formed at high concentrations (up to the percent level), while—depending on the fuel—added tracers disintegrate (Fig. 1) [82]. The slow disappearance of the tracer can be correlated to the slow breakdown of the parent fuel [83]. These first reaction steps, however, are not connected with strong heat release. The regions where the tracer signal disappears should, therefore, not be confused with the zones where the 'hot' combustion is active.

The HCHO-LIF intensity for a selected excitation wavelength shows local variations which can be interpreted as local temperature variations [84]. The regions where the HCHO-LIF signal disappears, finally, indicate the locations of hot combustion.

Furthermore, fluorescing species forming as a consequence of partial combustion in fuel-rich flames are polycyclic aromatic hydrocarbons (PAH). Their fluorescence signal appears in many diagnostics situations as a nuisance [49]. Because it is emitted from a large number of different molecules that all have broad-band absorption and fluorescence spectra, the signal yields limited information only [85].

2.3. Tracers for measuring temperature

Atoms and small (mostly diatomic) molecules have well defined line spectra that allow the direct assessment of the population of different quantum states by tuning the excitation wavelength to appropriate transitions. This technique has been applied with atomic tracers [5,6,86] (cf. Section 2.1.1) and diatomic molecules, mainly OH and NO, yielding either vibrational or rotational temperatures [9,87–92] (cf. Section 2.1.2). Atomic tracers and OH, however, give no information about areas of unburned fuel/air mixtures. NO gives temperature information about non-reactive low temperature regions as well, but is not well suited to trace the fuel concentration distribution at the same time.

For a few larger organic molecules the temperature behavior of absorption cross-sections and fluorescence quantum yields is understood well enough to use them for gas phase temperature measurements. Acetone has been most thoroughly studied and used for temperature measurements in flows [43,93,94]. The understanding of 3-pentanone fluorescence has also evolved to a state [43,46] that makes this tracer useful for not only temperature measurements [95] but also simultaneous temperature and fuel concentration measurements in internal combustion engines [93]. The temperature effects in toluene LIF have been recently investigated [38,39,96]. It appears that toluene is also suited as a tracer for measuring temperature at least in oxygen-free environments [97]. The combination of simultaneous temperature and fuel concentration measurements is particularly interesting because it provides fuel number densities, fuel mole fractions, and equivalence ratios (based on the assumption that oxygen is evenly distributed within the air) [93]. The temperature-dependence of acetone, 3-pentanone, biacetyl, and toluene LIF will be presented in Sections 4.1.1, 4.2.1 and 4.3.1, respectively. The applications of ketones for temperature measurements will be discussed in further detail in Section 5.2.

The temperature-dependence of exciplex fluorescence was exploited with the use of 1,3-bis-(1′-pyrenyl)-propane and 3-(4′-dimethylaminophenyl)-1-(1′-pyrenyl)-propane as tracers in hydrocarbon liquids to measure temperatures up to 673 K [98].

After excitation in the UV, pyrene emits fluorescence in two transitions: $S_2 \rightarrow S_0$ and $S_1 \rightarrow S_0$. The ratio of these signals is temperature-dependent and was used to measure temperatures in low-pressure flames [99].

2.4. Inverse tracing

In some cases it is possible to deduce the concentration of a species via a tracer-based approach by visualizing another component in a mixture and determining the actual species of interest through a number balance. Deschamps and Baritaud [100] describe measurements of exhaust gas concentrations in an engine. Their approach uses biacetyl as a fluorescence tracer that indirectly indicates the presence of recirculated exhaust gas when images are compared to images from operating conditions without exhaust gas recirculation. In a similar manner, Frieden et al. [101] have used a combination of 3-pentanone and toluene to obtain

information on oxygen contents in an engine for different operating conditions that then also provides insight into the amount of residual gas. Reuss and Sick [11] have seeded the intake air of an HCCI engine with a mixture of acetone and toluene to observe ignition sites and combustion progress. The engine was fueled with a direct-injection strategy with *n*-heptane that was *not* doped with fluorescence tracers. In principle, this approach is suited to extract the fuel concentration from the difference of the measured signal and the total gas content. Modulations of the LIF signals were only measured early after the injection where local air (seeded) concentration decreased substantially. At later times during the engine stroke, the fuel was mixed well enough with the air to not produce significant modulation of the LIF signal that could have been analyzed as fuel concentration. (Note: for the fuel/air equivalence ratio of 0.5 that was chosen, the ratio of fuel to air volume is 1:30, which illustrates why the sensitivity of such an indirect method to measure fuel concentration is low).

3. Photophysics of organic molecules

3.1. Laser-induced fluorescence

The tracer techniques discussed here are based on laser-induced fluorescence detection. Molecules are electronically excited by absorbing a photon typically in the ultraviolet or visible spectral range. Spontaneous emission (fluorescence) from the excited molecule that occurs within 1–100 ns is then detected and is representative of the local tracer concentration. There is, however, a strong influence of the bath gas on absorption, energy transfer in the excited state, and non-radiative relaxation from the excited state on signal intensities and spectral distribution. An interpretation of measured signal intensities therefore requires a detailed knowledge of the underlying photophysical processes, as long as significant changes of these processes are expected relative to the calibration system. The following sections describe the fundamentals of photophysics of small organic molecules. In Section 4 the relevance of these processes to frequently used tracers (ketones and aromatics) is discussed. The reader not interested in the fundamental approach might therefore directly continue to Section 4.

3.2. Absorption

3.2.1. Classification of electronic transitions

Absorption of photons in the UV (and with larger molecules also in the visible) populates excited electronic levels in the respective absorbing molecules. The absorption strength is described by the wavelength-dependent absorption cross-section $\sigma_{abs}(\lambda)$. In organic molecules it is useful to describe the chemical bonds by linear combinations of the so-called s- and p-states (atomic orbitals) giving molecular orbitals with different symmetry: binding σ and π orbitals, anti-binding σ^* and π^*, and neutral (non-binding) n orbitals. Organic molecules typically have closed shells where the highest occupied molecular orbitals (HOMO) are bonding σ, π or neutral non-bonding n orbitals (localized at the O-atom in ketones, aldehydes and alcohols). The lowest unoccupied molecular orbitals (LUMO) usually are anti-bonding π^* or σ^* orbitals. The following typical optically active transitions occur:

- $\pi \rightarrow \pi^*$, i.e. in alkenes and aromatics
- $n \rightarrow \pi^*$, in molecules with carbonyl groups (ketones, aldehydes), azo- or thiocarbonylgroups (which are the analogous molecules with O replaced by N or S, respectively)
- $n \rightarrow \sigma^*$, i.e. in amines and alcohols
- $\sigma \rightarrow \sigma^*$, i.e. in alkanes (at vacuum UV-wavelengths).

Table 2
Wavelength of maximum absorptivity and absorption cross-sections for relevant chromophores [206]

Chromophore	Transition	λ_{max} (nm)	σ_{abs} (10^{-20} cm^2)
C=O	$n \rightarrow \pi^*$	280	8
Benzenes	$\pi \rightarrow \pi^*$	260	80
C=N	$n \rightarrow \pi^*$	240	50
C=C–C=C	$\pi \rightarrow \pi^*$	220	8×10^4
C=C	$\pi \rightarrow \pi^*$	180	4×10^4
C–C	$\sigma \rightarrow \sigma^*$	<180	400
C–H	$\sigma \rightarrow \sigma^*$	<180	400

This indicates that according to the photo-active groups or electronic systems (so-called chromophores) the molecules can be sorted into different classes with typical properties shown in Table 2. This is analogous to the classification for functional groups determining the reactivity and classes of chemical reactions of organic molecules.

3.2.2. Classification of electronic states

The electronic state of a molecule is characterized by its total spin and degree of excitation. In the ground state for most molecules, the total spin is $S=0$. Here, all electrons (each of them with $S=½$) are paired with anti-parallel spin. When exciting a single electron, the two resulting unpaired electrons can either be parallel ($S=1$) or anti-parallel ($S=0$). According to the resulting multiplicity of the states (number of potential realizations with the same total energy) the $S=0$ and 1 states are called singlet (S) and triplet (T), respectively. The level of excitation is indicated by subscript numbers. The ground state is 0, and 1 and 2 are excited states with increasing energy. Fig. 2 shows the population and the energy of the ground state and the first excited states of a carbonyl group.

3.2.3. Transition probabilities

The transition probabilities determining the absorption cross-section can be determined by perturbation calculations

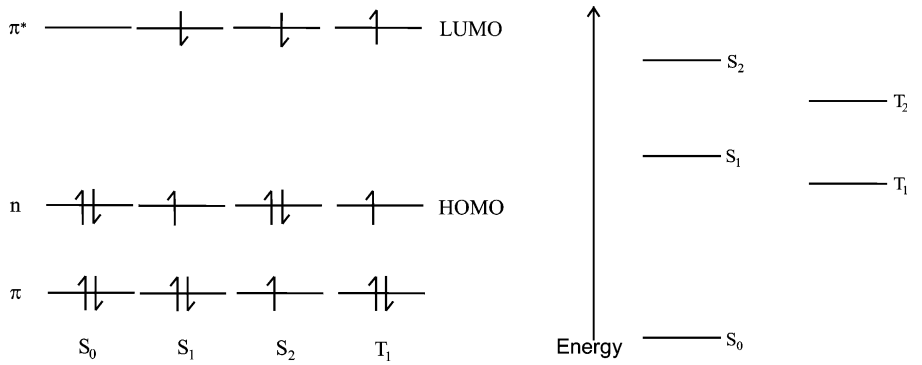

Fig. 2. Population of the molecular orbitals in the ground state and the first excited state of a ketone group. Right: Comparison of the relative energy of the various states.

using the wave functions of the ground and excited states of the molecule under study. Three factors determine their magnitude:

- The electronic contribution depends on the spatial overlap of the electronic wave functions. It is obvious that this might differ significantly depending on the symmetry of the contributing orbitals.
- The Franck–Condon contribution describes the spatial overlap of the wave function of the nuclei between ground and excited states.
- The spin wave function is zero for singlet–triplet transitions and unity for singlet–singlet and triplet–triplet transitions.

The combination of these contributions yields the selection rules. n and π^* orbitals in ketones ($S_0 \rightarrow S_1$ transition), for example have poor spatial overlap. The resulting transition is weak and sometimes called 'orbital-forbidden'. If the wave functions of ground and excited states have different symmetry, the integral determining the transition moment is zero; the respective transition is called 'symmetry forbidden'. This selection rule applies to $S_0 \rightarrow S_1$ transitions in ketones and aromatics. The reason that these molecules absorb light in contrast to the selection rules is that the Born–Oppenheimer approximation (which assumes the independence of the movement of electrons and nuclei: the typical timescale of the absorption is on the order of 10^{-15} s, that of vibrations 10^{-12} s) is partially violated. The intramolecular vibrations couple with the electronic system and therefore distort the electronic wave functions, breaking the perfect symmetry, which then introduces non-zero contributions to the integral. The resulting transitions are called 'vibrationally allowed'. With increasing vibrational excitation (i.e. temperature) the transition moments increase. This effect explains the relatively small transition moments compared to fully allowed transitions like $\pi \rightarrow \pi^*$ in alkenes (cf. Table 2). In small and highly symmetric molecules vibrations are responsible for a clear band structure of the absorption spectrum, whose relative intensities depend on the Franck–Condon overlap argument. In organic molecules at room temperature, the large number of degrees of freedom causes broad, only weakly structured absorption bands. The shape of this spectrum, however, is still determined by Franck–Condon's principle.

These arguments focus on the interaction of the electronic dipole moment with the electric field of a light wave. The respective magnetic interaction is usually negligible. In some cases, however (i.e. $n \rightarrow \pi^*$ transition in formaldehyde HCHO), symmetry-forbidden and vibrationally forbidden transitions are observed anyway, because they coincide with allowed magnetic dipole transitions.

Finally, spin-forbidden transitions should completely prevent singlet–triplet transitions because of their orthogonal wave functions. The validity of this rule, however, is limited due to coupling of the spin with the orbital's angular momentum. In this case the selection rules are determined by the resulting total angular momentum. In organic molecules the coupling between the orbital and the electronic angular momentum is weak, and the selection rule is strongly obeyed. Coupling, however, increases in the presence of heavy atoms (with the fourth power of the atomic mass). Organic molecules with heavy atoms (i.e. Br, I) show an increased coupling and a limited validity of the spin selection rule.

3.2.4. Deactivation of excited molecules

So far we discussed the excitation of molecules leading to the population of highly excited states well above their thermal equilibrium population. From these states the excess energy can be lost on different paths via chemical (dissociation, photo-induced reaction) and physical processes. The latter fall into three categories:

- *Radiative processes*: The excess energy (or a part of it) is emitted by spontaneous emission, i.e. fluorescence
- *Non-radiative processes*: The excess energy is thermalized by vibrational and rotational energy transfer
- *Collisional quenching*: Electronic excitation of colliding molecules, i.e. electronic energy transfer

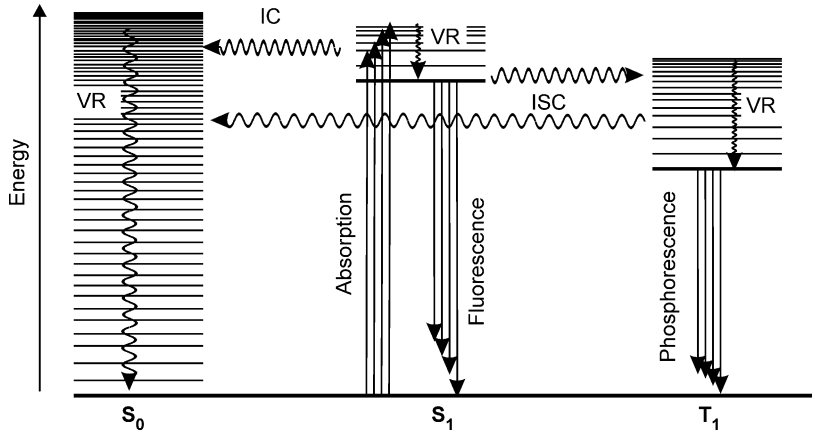

Fig. 3. Jablonski diagram showing the photophysical processes during deactivation of excited organic molecules.

The processes of the first two categories are shown in the Jablonski diagram in Fig. 3. Radiative and non-radiative processes are indicated by straight and curved lines, respectively. The excited molecule can loose energy by emitting light (fluorescence and phosphorescence) or by exciting vibrations and rotations in colliding molecules (external *vibrational relaxation*, VR). Radiationless, intramolecular electronic transitions occur 'horizontally' without changing the total energy. When the spin multiplicity changes, the process is called *intersystem crossing* (ISC), when the multiplicity is maintained: *internal conversion* (IC).

3.2.5. Radiative processes

Spontaneous emission has the same dependence on transition moments like the absorption cross-sections and must satisfy the same selection rules. The probability of spontaneous emission, however, increases with the energy difference between the coupled states.

3.2.5.1. Fluorescence. The $S_1 \rightarrow S_0$ transition due to spontaneous emission of light is fast; it is typically observed during an interval of 1–100 ns. In ketones the $S_1 \rightarrow S_0$ transition is symmetry and orbital forbidden. The radiative lifetime is therefore on the order of microseconds. The fast depopulation of the excited state due to intersystem crossing, however, limits the effective fluorescence lifetime to the values given above.

3.2.5.2. Phosphorescence. Triplet states are significantly longer lived due to spin-forbidden radiative relaxation to the singlet ground state. Intersystem crossing populating the S_0 state is inefficient due to the large energy difference. The spontaneous transition $T_1 \rightarrow S_0$ is called phosphorescence and has a typical lifetime of milliseconds to seconds.

3.2.6. Non-radiative processes

3.2.6.1. Dependence of the transition probability on the energy difference (energy gap law). The transition probabilities of non-radiative relaxation processes (*intersystem crossing* and *internal conversion*) decrease with increasing energy difference between the involved quantum states. The overlap of the vibrational wave functions decreases with increasing energy difference. This explains why ISC in simple ketones ($\Delta E \sim 20$ kJ/mol (0.22 eV)) is much faster than in benzene and toluene ($\Delta E \sim 120$ kJ/mol (1.3 eV)). This difference in triplet–singlet energy difference is also important for the understanding of quenching processes (Section 3.4). Due to this importance, we further discuss the background of the energy gap between the triplet and singlet states.

3.2.6.2. Singlet–triplet energy difference. When comparing singlet and triplet systems with otherwise identical quantum numbers, the triplet is systematically lower in energy. This reflects Hund's first rule, stating that in open shell systems the configuration with maximum spin multiplicity is preferred.

A simple interpretation of this effect is based on Coulomb repulsive forces between the electrons. With maximum spin, the spin wave function is fully symmetric, and hence, according to Pauli's law, the spatial wave function must be anti-symmetric. This means, however, that the average distance between the electrons increases (relative to the symmetric case), and the Coulomb forces decrease. The result is an overall lowered energy of the triplet compared to the singlet.

The resulting energy difference depends on the electronic structure of the respective molecule. In single ring aromatic molecules the π and π^* molecular orbitals (that contain the two unpaired electrons) have a larger spatial overlap than the n and π^* orbitals in ketones.

Table 3
ISC-rates for molecules with similar singlet–triplet energy gaps but different symmetries (8–21 kJ/mol, 0.08–0.2 eV) [207,208]

Molecule	Transition	Selection rule	Rate for ISC (s^{-1})
Anthracene	$S_1(\pi, \pi^*) \rightarrow T(n, \pi^*)$	'Forbidden'	1.4×10^8
Acetone	$S_1(n, \pi^*) \rightarrow T(n, \pi^*)$	'Forbidden'	5×10^8
Benzophenone	$S_1(n, \pi^*) \rightarrow T(\pi, \pi^*)$	'Allowed'	10^{11}

Therefore, the aforementioned effect of Coulomb repulsion is more pronounced in benzene and toluene compared to acetone and 3-pentanone, for example. This effect ultimately contributes to different susceptibility towards oxygen fluorescence quenching that is observed in these two classes of molecules (cf. Section 3.4.3).

3.2.6.3. Intersystem crossing, ISC. The non-radiative transition between states of different spin multiplicity is called intersystem crossing. The total energy is typically preserved, which means that after a $S_1 \rightarrow T_1$ transition the molecule gains vibrational excitation. The dependence on the energy gap between the two states was discussed above (energy gap law). Additional geometry-dependent selection rules ('El-Sayed's rules') must be satisfied. ISC is allowed for $S(n, \pi^*) \rightarrow T(\pi, \pi^*)$ and $S(\pi, \pi^*) \rightarrow T(n, \pi^*)$ and forbidden for $S(n, \pi^*) \rightarrow T(n, \pi^*)$ and $S(\pi, \pi^*) \rightarrow T(\pi, \pi^*)$ transitions. The transition probabilities of forbidden transitions are not exactly zero due to interaction of the electronic wave function with vibrations. They are, however, significantly reduced compared to allowed transitions (cf. Table 3).

For ketones and benzene derivatives (toluene) ISC is symmetry-forbidden. Nevertheless, it is 3 and 1 orders of magnitude faster than the respective rates of spontaneous $S_1 \rightarrow S_0$ emission. ISC can be significantly increased in the presence of oxygen. This is discussed in the collisional quenching Section (3.4).

3.2.6.4. Internal conversion. Internal conversion (IC) is the non-radiative transition between states of the same spin multiplicity. This process is symmetry-allowed. Because of the large energy difference between S_0 and S_1, according to the energy gap law, IC is of minor relevance for the species typically used as fluorescence tracers. This argument can be applied to motivate Vavilov's law that states that fluorescence is emitted from the S_1 state only. The energy difference between excited singlet states is small enough to enable fast IC (i.e. $S_2 \rightarrow S_1$) transitions.

3.2.6.5. Vibrational relaxation. Vibrational relaxation (VR) occurs through collisions with bath molecules with almost unity probability. Therefore, in the liquid phase, VR is very fast. In the gas phase, however, VR does not fully relax the molecules to the vibrational ground state during the fluorescence lifetime, which makes signals pressure-dependent. While VR takes place, competing processes (ISC and spontaneous emission) are active on the same timescale. The entire process, therefore, often requires dynamic modeling for a full explanation of the observed behavior [102].

3.3. Kinetics of photo-physical processes

3.3.1. Radiative and effective lifetimes

If fluorescence emission of photons $h\nu$ is the only pathway of relaxation of the excited molecules M^* according to $M^* \rightarrow M + h\nu$, the temporal variation of the concentration $[M^*]$ of excited molecules is described by a first order differential equation

$$-\frac{d}{dt}[M^*] = k_{fl}[M^*] \tag{3.1}$$

leading to an exponential decay with the rate k_{fl} of the fluorescence process and the initial concentration $[M^*]_0$

$$[M^*] = [M^*]_0 \exp^{-k_{fl}t}. \tag{3.2}$$

Within the radiative life time, τ_{rad}, the number of the excited molecules decays to $1/e$ of the initial value

$$\tau_{rad} = \frac{1}{k_{fl}} \tag{3.3}$$

Typical values are shown in Table 4.

In practical systems the decrease of $[M^*]$ is increased because non-radiative processes ISC and IC (with rates k_{isc} and k_{ic}) occur simultaneously:

$$-\frac{d}{dt}[M^*] = (k_{fl} + k_{isc} + k_{ic})[M^*] \tag{3.4}$$

k_{tot} is then the total rate of depopulation of the excited state including all individual depopulating processes i

$$k_{tot} = \sum k_i, \tag{3.5}$$

yielding the experimentally accessible effective fluorescence lifetime:

$$\tau_{eff} = \frac{1}{k_{tot}}. \tag{3.6}$$

In 3-pentanone, for example, the radiative lifetime of approx. 1 μs [60] is reduced to approximately 2 ns mainly due to fast ISC [45].

Table 4
Radiative lifetimes for systems obeying different selection rules

	Dipole allowed	Dipole allowed, vibrationally forbidden	Spin forbidden
σ_{Abs} (10^{-20} cm^2)	2×10^3	5	5×10^{-3}
τ_{rad} (μs)	1×10^{-3}	5	5×10^3

3.3.2. Fluorescence quantum yield

Non-radiative processes reduce the fraction of excited molecules that actually emit fluorescence. This fraction is called fluorescence quantum yield ϕ_{fl} which is unity in the absence of non-radiative relaxation and decreases otherwise. It is the ratio of fluorescence rate $\tilde{k}_{fl}[M^*]$ over the absorption rate $\tilde{k}_{abs}[M][h\nu]$ with $[h\nu]$ being the photon density:

$$\phi_{fl} = \frac{\tilde{k}_{fl} h [M^*]}{\tilde{k}_{abs}[M][h\nu]}. \tag{3.7}$$

Within a typical ns laser pulse duration a steady-state population of M^*, $d[M^*]/dt[M^*]=0$, is quickly established. Then with the rate coefficient of non-radiative excited state depopulation $\tilde{k}_{nr} = \tilde{k}_{tot} - \tilde{k}_{fl}$, the temporal variation of excited state population

$$\frac{d}{dt}[M^*] = \tilde{k}_{abs}[M][h\nu] - (\tilde{k}_{fl}[M^*] + \tilde{k}_{nr}[M^*]) \tag{3.8}$$

can be used to express $[M^*]$, which is experimentally not easily accessible, as

$$[M^*] = \frac{\tilde{k}_{abs}[M][h\nu]}{\tilde{k}_{fl} + \tilde{k}_{nr}}. \tag{3.9}$$

This leads to the interpretation of the fluorescence quantum yield as the ratio of the rate coefficients of fluorescence and total depopulation or the inverse ratio of the respective lifetimes:

$$\phi_{fl} = \frac{\tilde{k}_{fl}}{\tilde{k}_{tot}} = \frac{\tau_{eff}}{\tau_{rad}}. \tag{3.10}$$

Measurements of the fluorescence quantum yield and the effective fluorescence lifetime then yield the radiative lifetime. Rate coefficients are denoted with $\tilde{k}$. For spontaneous processes these are converted to rates by multiplying with a concentration. For most relevant processes in the following sections the excited molecule concentration $[M^*]$ cancels in many equations. We therefore adopt the somewhat sloppy convention that is frequently found in literature. We drop $[M^*]$ and call the remaining k-values rates and omit the tilde notation. We only use it again when collisional processes are considered for which the rate depends not only on the concentration of the excited molecule but also of the number density of a collider (cf. Section 3.4.1).

The detected fluorescence signal intensity S_{fl} is proportional to the number of fluorescence photons, which is the product of absorbed photons and the fluorescence quantum yield (times the efficiency of the detection system η and the observed solid angle $\Omega/4\pi$)

$$S_{fl} = (E/h\nu) V n_{fl} \sigma_{abs} \phi_{fl} \eta \Omega/4\pi \tag{3.11}$$

$E/h\nu$ is the photon flux (in cm^{-2}), n_{fl} the number density of the fluorescence tracer in the observed volume V that have the absorption cross-section σ_{abs} (in cm^2).

3.4. Collisional quenching

The non-radiative processes leading to depopulation of the excited state discussed so far were intra-molecular processes. Depending on the properties of colliding molecules, strong inter-molecular deactivating processes can occur. First, we will focus on the kinetics of these processes, and then we will discuss possible mechanisms.

3.4.1. Stern–Volmer coefficient

If quenching collisions occur, an additional term must be added to the denominator of the formulation of the fluorescence quantum yield, ϕ_{fl} (Eq. (3.10)), given in Section 3.3.2. The probability of fluorescence quenching is proportional to the collision rate with the respective species times a species-specific quenching cross-section. This is usually expressed by the number density of the colliding (quenching) species, n_q, times a rate coefficient, $\tilde{k}_q$, changing the equation for ϕ_{fl} to

$$\phi_{fl} = \frac{k_{fl}}{k_{tot} + \tilde{k}_q n_q}. \tag{3.12}$$

Note, we distinguish between rates of energy transfer processes (like k_{tot}, k_{fl}) and the rate coefficient $\tilde{k}_q$ by adding a tilde on top of the k. It becomes a rate by multiplying with the respective number density of quenching molecules, n_q.

In some practical applications it can be argued that the denominator is dominated by the quenching term and that ϕ_{fl} is inversely proportional to the quencher concentration. This assumption, however, is limited and must be carefully checked for particular situations, e.g. the direct measurement of air/fuel ratios in Section 4.3.3. The variation of signal intensity with increasing concentration of quenching molecules is given by:

$$\frac{S_{fl}^0}{S_{fl}} = \frac{k_{fl}}{k_{tot}} \frac{k_{tot} + \tilde{k}_q n_q}{k_{fl}} = 1 + \frac{\tilde{k}_q}{k_{fl}} n_q. \tag{3.13}$$

S_{fl}^0 is the fluorescence intensity in the absence of quenching. If measurements with varying quencher concentrations under otherwise identical conditions are carried out, this equation can be used to evaluate the ratio of $\tilde{k}_q/k_{tot}$, the so-called Stern–Volmer coefficient k_{SV}:

$$k_{SV} = \tilde{k}_q/k_{tot} = \tilde{k}_q \tau_{eff}. \tag{3.14}$$

k_{SV} indicates the relevance of fluorescence quenching and is therefore experimentally important. The plot for graphical analysis of this relation is called the Stern–Volmer plot (cf. Fig. 4). The Stern–Volmer coefficient can be temperature-dependent, as will be shown for toluene in Section 4.3.

With the assumption that quenching occurs as a consequence of short-range interactions (collisions), the quenching constant can be understood as a product of the collisional frequency, Z_{coll}, as obtained from kinetic gas

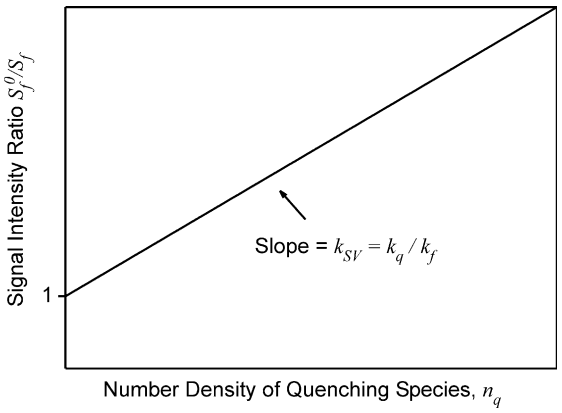

Fig. 4. Stern–Volmer plot.

theory, and a probability, $\langle p \rangle$, of an effective collision

$$\tilde{k}_q n_q = Z_{coll} \langle p \rangle. \tag{3.15}$$

3.4.2. Electronic energy transfer

One important process leading to collisional quenching is electronic energy transfer. The ground-state collider Q is electronically excited during the collision according to

$$M^* + Q \rightarrow M + Q^*. \tag{3.16}$$

This process can in principal involve the emission of a photon by M with subsequent absorption by Q (radiative energy transfer). The non-radiative process can, however, be much more efficient. In this case M is called donor and Q acceptor. Two fundamentally different processes must be considered.

3.4.2.1. Fluorescence resonance energy transfer. Fluorescence resonance energy transfer (FRET) was first described by Förster [103]. Dipole–dipole interaction distorts the electronic structure of the donor and acceptor molecules. The dipole oscillation of M^* then induces an oscillation in Q without direct physical contact between the two. This interaction depends strongly on the distance between the molecules but allows energy transfer over the distance of several molecule diameters (up to 10 nm). The probability, dP_n, of the energy transfer within the time interval, dt, is

$$dP_n = \tau_{eff}^{-1} \left(\frac{r_0}{r}\right)^6 dt, \tag{3.17}$$

with the fluorescence lifetime, τ_{eff}. The 'critical radius', r_0, determines the strength of the interaction and depends on the spectral overlap between the emission spectrum of the donor and the absorption spectrum of the acceptor.

Electrons are not exchanged between the molecules. Therefore, the spin selection rules must be satisfied. Possible processes are

$$^1M^* + {}^1Q \rightarrow {}^1M + {}^1Q^* \quad \text{or} \tag{3.18}$$

$$^1M^* + {}^3Q \rightarrow {}^1M + {}^3Q^*. \tag{3.19}$$

3.4.2.2. Short-range energy transfer. The mechanism first described by Dexter [104] involves the exchange of electrons between the two molecules. Direct contact leading to spatial overlap of the different molecular orbitals is therefore a requirement. The maximum distance is on the order of 0.5–1 nm. The probability of this process depends on the spectral overlap of the two molecules as well. Selection rules, however, do not apply. For this process the following reactions are spin-allowed:

$$^1M^* + {}^1Q \rightarrow {}^1M + {}^1Q^* \quad \text{and} \tag{3.20a}$$

$$^1M^* + {}^1Q \rightarrow {}^1M + {}^3Q^*. \tag{3.20b}$$

3.4.3. Fluorescence quenching by molecular oxygen

The ground state of molecular oxygen is a triplet state. It is therefore very efficient in quenching fluorescence of organic molecules by facilitating the transition into triplet states. The energy transfer reactions can be written as [105]:

$$^1M^* + {}^3O_2 \leftrightarrow {}^3(M, O_2)^* \rightarrow {}^3M + {}^1O_2^* \tag{3.21a}$$

$$^1M^* + {}^3O_2 \leftrightarrow {}^3(M, O_2)^* \rightarrow {}^3M + {}^3O_2 \tag{3.21b}$$

The colliding molecules form a short lived exciplex (transition state). Different states with localized excitation (e.g. $^3(^1M^*, ^3O_2)$, $^3(^3M^*, ^3O_2)$,…) and charge transfer ($^3M^{\cdot+}, {}^2O_2^{\cdot-}$) are possible. This coupling between states with different spin multiplicity enables the otherwise spin-forbidden intersystem crossing. Decreasing quenching rate coefficients $\tilde{k}_q$ with increasing ionization potentials indicate that at least partial charge transfer occurs in the transition state [106]. However, this process can only happen if the energy difference between M's singlet and triplet state is larger than the energy required for excitation of O_2 into its singlet state (91 kJ/mol, 0.98 eV). This is the case for aromatic molecules, but not for ketones (cf. Section 4.1.2). Therefore, aromatic molecules are efficiently quenched by molecular oxygen, while small aliphatic ketones are only mildly influenced. The effects of collisional quenching in aromatics is, therefore, well described by the mechanism shown above [107].

In ketones, however, it was not clear for a long time whether oxygen has any influence at all. Nau and Scaiano [108] finally found a weak influence and use the aforementioned mechanism also for this class of molecules to describe an 'oxygen-enhanced intersystem crossing'. The reduced $\tilde{k}_q$ compared to aromatic systems is then explained with the observation that as in aromatics, $\tilde{k}_q$ decreases with a decreasing singlet–triplet energy difference and when the formation of the exciplex $(M, O_2)^*$ is endothermic [107]. Both arguments apply to aliphatic ketones. Furthermore, the fluorescence lifetime of ketones is much shorter than that of

aromatics because of faster ISC. Therefore, the Stern–Volmer coefficient that describes the quenching effect relative to the sum of all depopulation effects is much reduced, making the oxygen quenching influence on ketones almost negligible.

3.5. Sensitized fluorescence

Energy transfer during collisions between organic molecules can happen with almost unity probability, as long as the emission spectra of the excited molecule and the absorption spectra of the collider molecules overlap (cf. Section 3.4.2). This has been used for mixing studies where two flows were seeded with two different tracers (called donor and acceptor). The donor is selectively excited by laser radiation and then transfers its excitation to the acceptor in areas where the two gas flows are mixing. The fluorescence emitted by the acceptor can then be used as an indicator for the mixing process. Yip et al. [109] demonstrated this process with acetone as the donor and biacetyl as the acceptor.

It should be mentioned that the same process also occurs as a nuisance in practical diagnostics situations. Tracer combinations of aliphatic ketones and small aromatics have been applied because their emission signals can be spectrally separated. They were used for the simultaneous observation of the distribution of different volatility classes of multi-component fuels [29] and to measure oxygen concentrations [101,110]. It was found that 3-pentanone quenches toluene fluorescence with almost the same efficiency as oxygen (collision limited). At the same time the fluorescence of 3-pentanone strongly increases due to additional electronic energy transfer from collisions with toluene (see Sections 4.3.5 and 5.3). While corrections are possible in special situations where the signals of both tracers are detected individually, erroneous signal intensity might occur in simpler diagnostics arrangements. This energy transfer can also happen if tracers are added to fuels that contain absorbing molecules (e.g. aromatic compounds) and in the gas phase of vaporized exciplex–tracer mixtures, where energy transfer occurs between the two components of an exciplex system (cf. Section 6).

4. Photophysics of typical fuel tracers

For quantitative measurements of fuel concentrations, acetone, 3-pentanone, biacetyl and toluene are the most frequently used tracers (cf. Section 2). Ketones (acetone and 3-pentanone) have been studied quite extensively in order to describe the dependence of their LIF intensities on temperature, pressure, and excitation wavelength. They are therefore an excellent example to demonstrate the capabilities of tracers when their photophysical behavior is well understood. Many of these dependencies appear negative at first glance but can be used to measure additional quantities, like temperature and fuel/air ratio. In turn, this additional information has the potential for the quantitative determination of fuel concentrations in systems with strong temporal and spatial fluctuations in temperature and gas phase composition, like modern IC engines.

As a typical and most frequently used class of tracers, we will discuss aliphatic ketones, like acetone and 3-pentanone (diethylketone), in Section 4.1 and compare their properties to those of toluene, a representative for small aromatic compounds (cf. Section 4.3).

4.1. Aliphatic ketones: influence of pressure, temperature and excitation wavelength

Under ambient conditions, due to the high density of states, aliphatic ketones like acetone and 3-pentanone show broadband absorption spectra from 220 to 330 nm. They can be conveniently excited in the UV with various laser systems in practical situations where wavelengths at and above 248 nm are of interest. This leads to the population of the S_1 state through a $n\rightarrow\pi^*$ transition that is symmetry-forbidden and therefore has relatively small absorption cross-sections (8×10^{-20} cm^2 at 280 nm, cf. Table 2). Additional transition probability is 'borrowed' from higher lying symmetry-allowed transitions through vibronic coupling [111]. Fast vibrational relaxation towards lower vibrationally excited S_1 states is responsible for the red-shift of the emission spectrum to approx. 300–550 nm (Fig. 5). The radiative lifetime of this symmetry-forbidden transition is on the order of microseconds. The effective lifetime under ambient conditions, however, is reduced to the nanosecond scale [60] due to intersystem crossing (ISC) with rates approximately three orders of magnitude faster than those of spontaneous emission. This results in a small fluorescence quantum yield (acetone: $\phi_{fl}=0.002$ [112]).

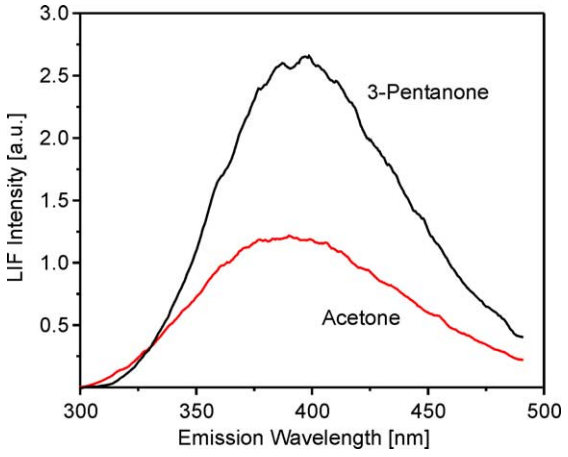

Fig. 5. Emission spectra of acetone and 3-pentanone upon excitation at 266 nm at 295 K with 13 mbar tracer in 1 bar N_2. 3-Pentanone has comparable absorption cross-sections at 266 nm but approximately twice the fluorescence quantum yield compared to acetone.

The triplet state that is populated via ISC is long-lived because of the spin-forbidden transition to the ground state. It emits phosphorescence on the time scale of milliseconds to seconds. Experiments with short-pulse excitation report on photodissociation out of the S_1 state on a timescale of femtoseconds [113].

The temperature- and pressure-dependence of acetone and 3-pentanone LIF was investigated in numerous experiments [43–46,48,50,114,115]. These effects will be discussed in the following sections. Thurber et al. [115] succeeded in setting up a conceptual model combining the various observations. This model for acetone fluorescence was recently extended to include 3-pentanone [46] and will be described in Section 4.1.3. Acetone and 3-pentanone show a similar behavior. We therefore restrict the detailed discussion to acetone and report the parameters of the resulting photophysical models for both compounds (Section 4.1.3).

4.1.1. Temperature-dependence of ketone fluorescence

In early applications, acetone was chosen as a fuel tracer because of its reduced temperature-sensitivity. Under certain experimental conditions negligible temperature-dependence was found [50]. More recent studies, however, showed that the acetone and 3-pentanone fluorescence intensity indeed depends on temperature. Different researchers reported results that seemed inconsistent in the beginning. Tait and Greenhalgh [49] observed an increase in signal intensity per molecule with increasing temperature upon excitation at 308 nm. While Großmann et al. [43] verified this behavior for 312-nm excitation, they found the inverse characteristics with 248- and 276-nm excitation, which they attributed to a red-shift in absorption cross-sections with increasing temperatures.

The fluorescence signal $S_{fl}(\lambda, T)$ is governed by both the temperature-dependent absorption cross-section $\sigma_{abs}(\lambda, T)$ and the fluorescence quantum yield $\phi_{fl}(\lambda, T)$ (cf. Eq. (3.10)). Some confusion arises from the fact that the LIF signals can be either measured on a per-molecule (i.e. per unit number density) or on a per volume basis (i.e. per unit mole fraction). In the first case the relation

$$S_{fl} \propto n_{fl}\sigma_{abs}(\lambda, T)\phi_{fl}(\lambda, T) \tag{4.1}$$

is used when determining number densities (i.e. $S_{fl} \propto n_{fl}$ for fixed λ and T). In turn, the fluorescence intensity, S_{fl}^{+}, has an additional $1/T$ dependence when relating the measured signal intensity to unit mole fractions $S_{fl}^{+} \propto x_{fl}$:

$$S_{fl}^{+} \propto x_{fl}p/T\sigma_{abs}(\lambda, T)\phi_{fl}(\lambda, T). \tag{4.2}$$

In an experimental situation both quantities can be relevant and must be clearly distinguished. The excitation strategy that gives minimal temperature sensitivity depends on the desired quantity.

Temperature-dependent absorption cross-sections of acetone are presented in Fig. 6 for 290–870 K. The absorption cross-section increases with temperature at all wavelengths because the coupling with higher vibrational states relaxes the selection rules. An additional red-shift of the band center of approximately 10 nm per 100 K [43] is responsible for the fact that the temperature sensitivity of the absorption cross-section strongly increases with excitation wavelength up to ~290 nm. The red-shift of absorption features of organic molecules is also well known for many other molecules and can be explained by the Sulzer–Wieland mechanism [116,117].

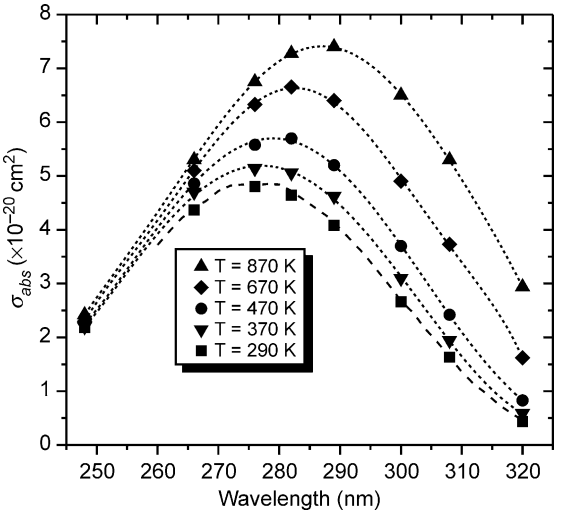

Fig. 6. Absorption spectra of acetone at different temperatures (300–870 K) [115]. Reprinted from [115] with permission from Optical Society of America.

At the same time, the fluorescence quantum yield (Fig. 7) decreases with increasing temperature with a smaller dependence on excitation wavelength. An interpretation of this behavior is presented in Section 4.1.3. The resulting

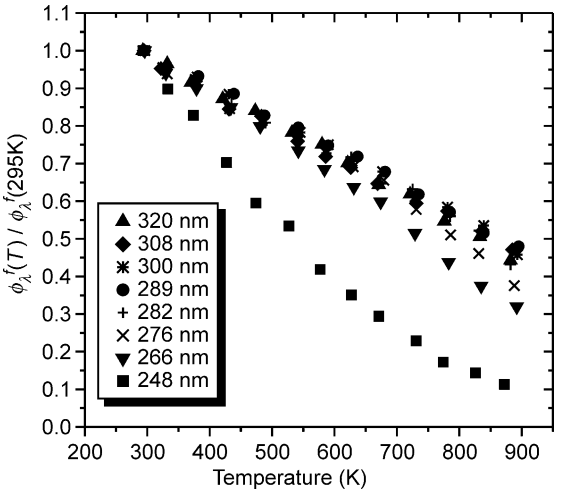

Fig. 7. Acetone fluorescence quantum yield at 300–870 K for different excitation wavelengths [115]. Reprinted from [115] with permission from Optical Society of America.

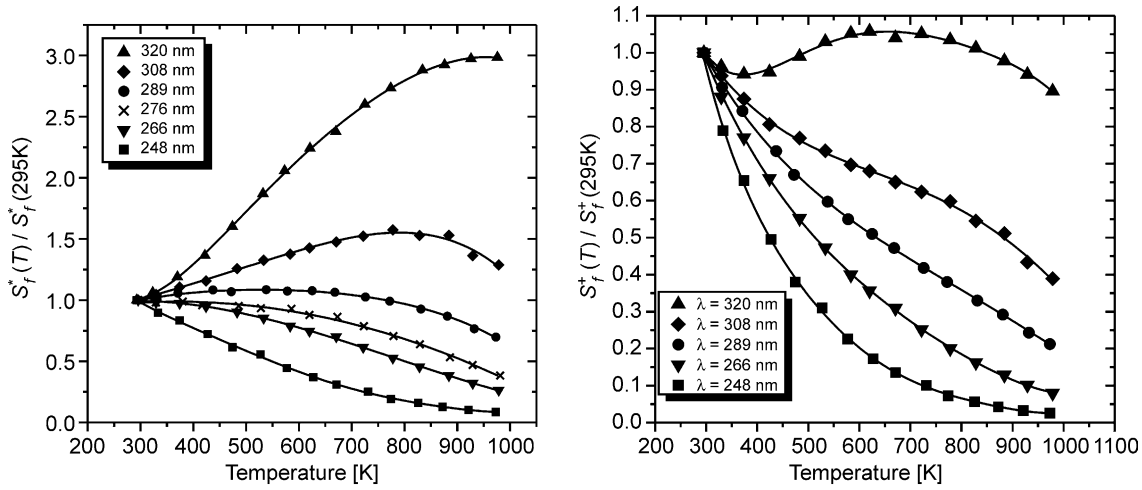

Fig. 8. Temperature dependence of the acetone fluorescence signal relative to room temperature at 1 bar for 248–320 nm excitation. Left: per unit number density, right: per unit mole fraction [115]. Reprinted from [115] with permission from Optical Society of America.

overall temperature dependence that is relevant for experimental applications is shown in Fig. 8. For experiments that aim at temperature insensitive measurements of tracer number densities, excitation at 276–300 nm reduces the signal uncertainty to $\pm 20\%$ for temperatures from room temperature up to 800 K. When measuring tracer mole fractions, however, 320-nm excitation is advisable to reduce the signal uncertainty to $\pm 10\%$ in the same temperature range.

The strongly temperature-dependent acetone LIF signal, in turn, can be used for measuring temperatures. In systems where the acetone concentration is constant (both spatially and temporally) the LIF signal can be directly used to quantify local temperatures. Depending on the respective temperature range, it is advisable to measure the signal ratio upon excitation with two different wavelengths. This is also the only possibility in systems with temporal and spatial variation in tracer concentration. Two-line temperature measurements have been demonstrated by Großmann et al. [43] and Thurber et al. [94], who presented a thorough analysis for homogeneous systems, discussing the advantages and disadvantages of single- and dual-wavelength temperature imaging techniques. An application of a dual wavelength technique for measuring quantitative temperatures and fuel concentrations inside the cylinder of an internal combustion engine [93] is presented in Section 5.2.

4.1.2. Pressure-dependence of ketone fluorescence

The fluorescence quantum yield of acetone was shown to depend on pressure. While Heicklen et al. [112] report on minor pressure dependence at 280–313 nm excitation, experiments with shorter excitation wavelengths showed more significant effects. Yuen et al. [44] report increasing acetone fluorescence quantum yields upon 266 nm excitation from ambient pressure up to 8 bar, with a total variation of approx. 30–60%. At the same excitation wavelength Ossler et al. [45] made the equivalent observation that fluorescence lifetimes rise with increasing pressure. Großmann et al. [43] and Thurber and Hanson [118] investigated the dependence of effects of pressure on excitation wavelength in more detail. They showed that the initial signal rise is more pronounced with short excitation wavelengths. At pressures relevant for the compression stroke in IC engines, however, the acetone fluorescence quantum yield becomes relatively pressure-independent, which makes the signal a good measure for fuel number density.

The pressure effect depends on the bath gas composition. However, as is expected for molecules where the lifetime of the excited state is limited by fast collision-independent processes, the sensitivity to the bath gas composition is much lower than in aromatic compounds that are strongly quenched by molecular oxygen (cf. Section 4.3.2). For acetone and 3-pentanone it was observed that, while the fluorescence quantum yield continuously increases beyond 8 bar in nitrogen, it becomes pressure-independent in air and slightly decreases with pressure in pure oxygen [43]. The resulting pressure-independence in tracer/air mixtures makes this class of tracers very attractive for the direct measurement of tracer (i.e. fuel) concentrations in practical diagnostics situations.

As pointed out in Section 3.4 it was not clear for a long time if acetone fluorescence is at all quenched by oxygen. Both the short excited state lifetime and the small energy difference between the singlet and triplet states are not in favor for collisional quenching by O_2. However, the small effect that is experimentally observed is attributed to a so-called oxygen-assisted intersystem crossing [108]. This opens an additional loss-channel out of the excited state that depends on the local oxygen concentration.

4.1.3. Photophysical model for aliphatic ketones

The observed temperature-, pressure- and wavelength-dependence of acetone-LIF can be explained by a conceptual model. The lifetime of the excited state is limited by fast intersystem crossing. The intersystem-crossing rate increases with the level of excitation in the excited state. This decreases the lifetime (and hence the fluorescence quantum yield) with increasing vibrational excitation in the S_1 state. These levels, however, get preferentially populated with short excitation wavelengths and with high temperatures. This explains the observation of decreasing fluorescence quantum yield with increasing temperature and decreasing excitation wavelength. At the same time, collisionally induced vibrational relaxation within the S_1 state leads to the population of lower, longer-lived states. Therefore, increasing pressure increases the fluorescence quantum yield. The observation of increased pressure-sensitivity with short excitation wavelengths is a result of this behavior. In the case of short-wavelength excitation the initial S_1 population distribution is above thermal. Collisions, therefore, effectively dump the highly excited states to lower ones, which leads to an overall increase of the fluorescence quantum yield. With long-wavelength excitation in turn, the initial excited-state population is close to thermal, and the influence of collisions is reduced.

Thurber et al. [115,118] developed a multi-step model that is based on these ideas. Schematically, this model is described in Fig. 9. It treats an 'average molecule' rather than a statistical ensemble. The molecule in the S_0 state has a thermal (average) ground state energy $\Delta E_{\text{thermal}}(T)$. It is excited with photons of energy $h\nu$ to the S_1 state. The laser-coupled upper state relaxes towards thermal equilibrium by collisional processes. This relaxation is treated as a multi-step process. From each level, the excited molecule can either cross to the triplet state with a rate $k_{\text{nr}}(E)$ (and additionally k_{O_2} in the presence of oxygen-enhanced ISC, here also considered as collisional quenching), fluoresce with a rate k_{fl}, or relax to a lower vibrational level with a rate $k_{\text{coll}}(T, p)$ until thermal equilibrium in the S_1 state is reached (from where finally further loss occurs through fluorescence and ISC only). The average energy transferred per collision

$$\Delta E_{\text{coll}}(E) = \alpha(E - \Delta E_{\text{thermal}}) \tag{4.3}$$

is a linear function of excess energy above thermal equilibrium [119]. $\Delta E_{\text{thermal}}$ is calculated as a function of

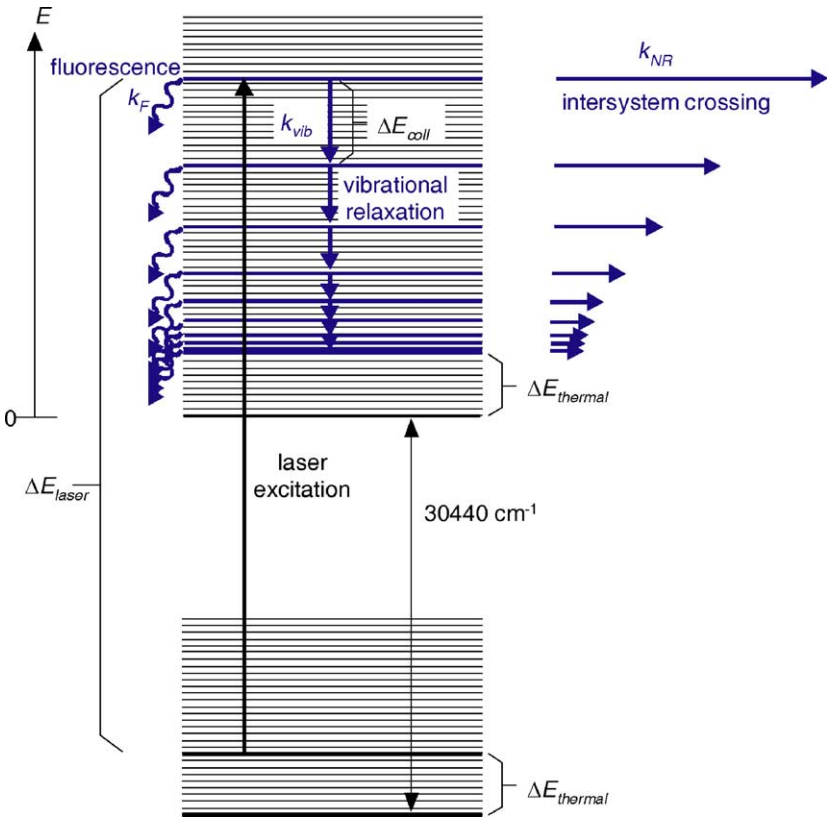

Fig. 9. Schematic of ketone photophysics: simplified model based on a multi-step vibrational decay in the S_1 state and an energy-dependent intersystem crossing rate (see text) [115,118]. Reprinted from [115] with permission from Optical Society of America.

Table 5
Model parameters for the multi-level model for acetone and 3-pentanone fluorescence [46,118]

Parameter	Value for acetone	Value for 3-pentanone
k_{fl}^{a} (s^{-1})	8×10^{5}	1.1×10^{5}
k_{coll} (300 K, 1 bar) (s^{-1})	1.1×10^{10}	1.1×10^{10}
k_{nr} (s^{-1})	$-3.82\times10^{9}+8.82\times10^{5}\exp((E/cm^{-1})/1650)$ $+4.08\times10^{9}\exp((E/cm^{-1})/77{,}300)$	$-3.52\times10^{8}+8.75\times10^{6}$ $\exp((E/cm^{-1})/2567)$
α	0.021	0.032
k_{O_2} (s^{-1})	1.65×10^{-12} $1.65\times10^{-12}n_{O_2}$ (cm^3)	–

T assuming harmonic oscillators for all 24 normal modes with energies according to [120].

The overall fluorescence quantum yield ϕ_{fl} is then the sum over the individual fluorescence yields of all different levels between level '1' (the laser-coupled level) and a level 'N' close to thermal equilibrium in the $\Delta E_{thermal}(T)$ S_1 state (cf. Eq. (4.4)):

$$\phi_{fl} = \frac{k_{fl}}{k_{fl}+k_{coll}+k_{nr,1}+\tilde{k}_q n_q} + \sum_{i=2}^{N-1}\left(\frac{k_{fl}}{k_{fl}+k_{coll}+k_{nr,i}+\tilde{k}_q n_q} \times \prod_{j=1}^{i-1}\left[\frac{k_{coll}}{k_{fl}+k_{coll}+k_{nr,j}+\tilde{k}_q n_q}\right]\right) + \frac{k_f}{k_{fl}+k_{nr,N}+\tilde{k}_q n_q}\prod_{j=1}^{N-1}\left[\frac{k_{coll}}{k_{fl}+k_{coll}+k_{nr,j}+\tilde{k}_q n_q}\right] \quad (4.4)$$

k_{fl} is assumed constant with vibrational energy [121]. The model parameters are α (from Eq. (4.3)) to scale the efficiency of collisional energy transfer and a bi-exponential expression for k_{nr}. The best fit to experimental data for acetone and 3-pentanone is shown in Table 5. Model results for the 3-pentanone-LIF temperature-dependence at atmospheric pressure (Fig. 10) and pressure-dependence at 296–473 K (Fig. 11) are in very good agreement with the measurements.

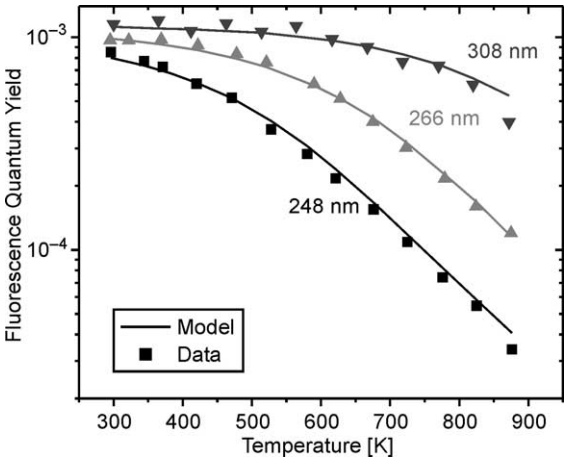

Fig. 10. Benchmark fluorescence quantum yield data for 3-pentanone as a function of temperature in 1 bar nitrogen (data are relative from [46] but calibrated to absolute measurements [209]). The model adequately combines the effects of temperature and wavelength by considering the non-radiative decay rate as a function of the vibrational energy of the excited molecule [39].

4.1.4. 3-Pentanone-LIF under engine conditions

3-Pentanone-LIF (as well as acetone-LIF) has not yet been systematically studied under conditions with simultaneously elevated temperature *and* pressure. This case, however, is of high interest if tracers are used to quantify fuel concentrations in the compression stroke in internal combustion engines, for example. While the pressure-dependence at room and slightly elevated temperature and the temperature-dependence at atmospheric pressure is well described by the model presented above, recent experiments in the compression stroke of an optically accessible IC engine showed that the model cannot yet predict the LIF intensities per molecule with sufficient accuracy. Open questions are, for example, if T and p are high: does sufficient collisional relaxation negate the decrease in signal

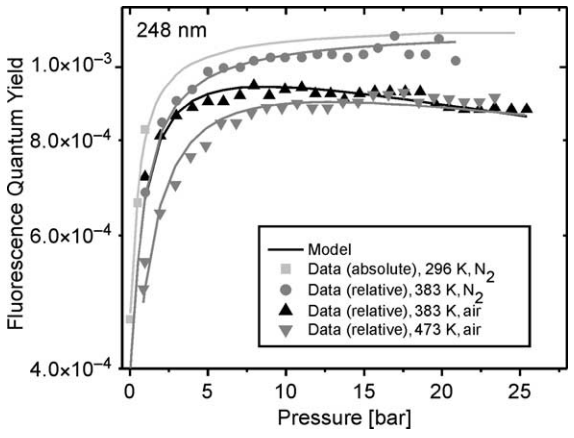

Fig. 11. Fluorescence quantum yield model results and data (from [43,209]) as a function of pressure for 3-pentanone. The model accounts for an increasing ϕ_{fl} (up to a high-pressure limit) via collisional transfer of excess vibrational energy [39]. A secondary quenching effect due to oxygen is also present, becoming significant at elevated pressures. Reprinted from [39] with permission from the Combustion Institute.

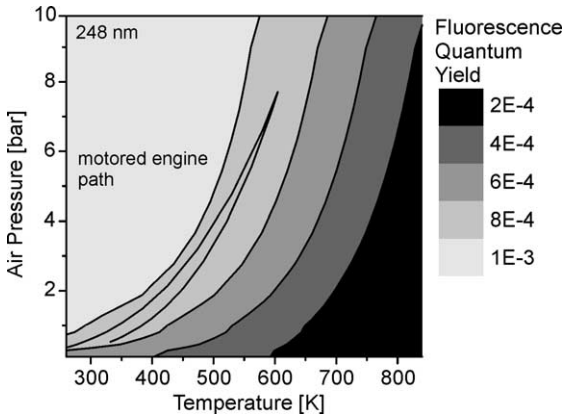

Fig. 12. Map of fluorescence quantum yield predictions for 3-pentanone through a range of temperatures and pressures. Since the absorption cross-section is constant for 248-nm excitation, the change in ϕ_{fl} is directly proportional to the relative fluorescence per molecule. The path of the motored engine shows that the pressure and temperature effects on the fluorescence signal may roughly cancel [39].

due to temperature? With the data obtained in a motored engine the model predictions can be evaluated. For 248-nm excitation, the absorption cross-section is constant with temperature to within 10% [46]. Hence, the relative fluorescence quantum yield reflects the change in fluorescence signal per molecule and can be compared directly with the fluorescence data (per molecule) from the motored engine. An extended T–p contour of the fluorescence quantum yield ϕ_{fl} predictions is shown in Fig. 12.

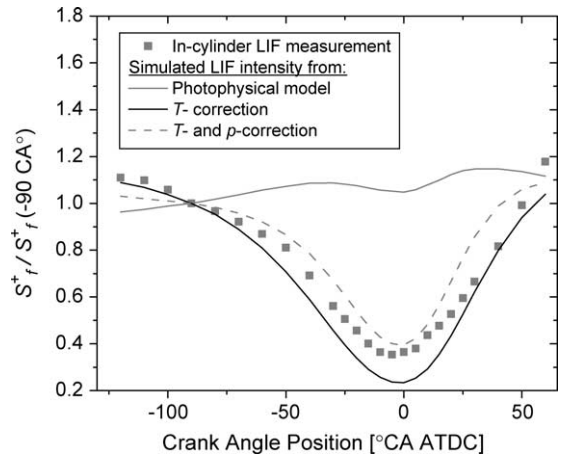

Fig. 13. Comparison of engine LIF data and fluorescence quantum-yield model for 3-pentanone. The engine data show that the fluorescence per molecule continues to decrease at high temperatures, despite the presence of high pressure, a trend not predicted by the model. In this case, multiplicative corrections for temperature and pressure from the fundamentally measured data results in the best agreement [39]. Reprinted from [39] with permission from the Combustion Institute.

The path that the motored engine takes through the T–p plane shows that little change in ϕ_{fl} is expected; the increase in p essentially balances the increase in T to keep the predicted ϕ_{fl} between 6×10^{-4} and 8×10^{-4}. This prediction is shown (as the flattest line) in Fig. 13 as a function of the crank angle (normalized to -90 crank angle degrees after top dead center, CA ATDC, at 0.82 bar and 360 K). The prediction shows a marked difference from the engine data. The measured fluorescence per molecule drops as p and T are increasing, but the model indicates that the p-dependent collisional relaxation dominates, even to the point of slightly increasing the fluorescence signal with crank angle. The modeled fluorescence per molecule is insensitive to the ±20 K uncertainties in temperature calculation from the pressure trace.

A second simulation can be obtained by extrapolating to simultaneously elevated pressures and temperatures from the benchmark data of Koch [46] and Großmann [43]. That is, the relative change in fluorescence is approximated as the product of the change due to temperature as measured at 1 bar and the change due to pressure as measured at 473 K. In this case, the agreement is improved as shown in Fig. 13. It too, however, seems to overemphasize the increase in signal due to pressure and thus predicts a slightly higher-than-measured value for much of the cycle. By looking at the change in signal due only to temperature, we see that neglecting the influence of pressure altogether gives results that are slightly too low. It thus seems that higher temperatures consistently lead to lower fluorescence signals for 3-pentanone, regardless of p (at least for 248-nm excitation). The best predictive method, in this case, is simply the multiplicative combination of the measured T- and p-dependencies. This may not be true in general. To understand its physical basis, work is underway to improve some of the model assumptions like introducing an energy distribution among the excited molecules rather than using an average vibrational energy. In addition, we might speculate that oxygen plays a more important role than first considered at high T and p, either due to increased chemical reactivity or a photochemical/quenching process that varies with excited state energy. Further fundamental experiments are necessary to investigate such a hypothesis.

4.2. Temperature- and pressure-dependence of biacetyl LIF

4.2.1. Temperature-dependence of biacetyl LIF

The use of biacetyl opens another wavelength range for tracer-LIF applications. With absorption from 350 to 460 nm and a peak near 417 nm excitation can be achieved with frequency-tripled Nd:YAG lasers. Strong absorption bands in the UV are not suitable since they lead to photodissociation and are thus not useful for fuel imaging. Fluorescence emissions are observed from 440 to 520 nm, while phosphorescence extends even further into the visible spectral range. Phosphorescence is strongly temperature-dependent and disappears at around 470 K. Although

biacetyl was used in several imaging studies, which demonstrated that it has the potential to be a good tracer, little detailed information is available on the temperature-dependence of biacetyl LIF signals. Heinze and Baritaud [122] determined a modest temperature sensitivity of less than 1.6% signal change per 10 K in the range of 550–700 K when exciting with a frequency-tripled Nd:YAG laser at 355 nm. The strong temperature sensitivity of the phosphorescence is better documented (e.g. Liu et al. [65]).

4.2.2. Pressure-dependence of biacetyl LIF

Little specific information is available on quenching properties for LIF of biacetyl. The phosphorescence is quenched very strongly by oxygen. However, differences in biacetyl LIF signals in nitrogen vs. oxygen are reported to be less than 10% [122]. Overall, the properties of biacetyl appear to be attractive enough for it to be reconsidered as a viable tracer for practical imaging diagnostics.

4.3. Temperature- and pressure-dependence of toluene LIF

4.3.1. Temperature-dependence of toluene LIF

Although toluene is frequently used for fuel mixing diagnostics in internal combustion engines, the temperature-dependence of toluene fluorescence is not yet fully characterized. Most authors implicitly assumed temperature-independent fluorescence yields and Stern–Volmer coefficients. However, recent experiments show a strong temperature effect on absorption cross-sections, fluorescence quantum yield, and Stern–Volmer coefficients [38,39,96], which is important when aiming at quantitative measurements.

Unlike absorption spectra of ketones the absorption spectrum of toluene is strongly structured at ambient conditions. Most investigations were carried out with spectrometers with somewhat limited resolution. Therefore, the variation of the absorption coefficient with temperature (and pressure) that affects narrowband laser excitation in LIF experiments cannot be extracted from most available measurements. 266 nm, i.e. the wavelength of the fourth harmonic of Nd:YAG lasers, is right in the wing of one of the peaks. Pressure- and temperature-induced variations of the lineshape can therefore influence the overall signal significantly. The temperature-dependence of the shape of toluene absorption spectra is shown in Fig. 14. The fine structure observed at ambient conditions disappears with increasing temperature. At the same time the line center of the $S_0 \rightarrow S_1$ transitions shifts to longer wavelengths with increasing temperature. The maximum fluorescence occurs at 280 nm with a tail extending towards the red (Fig. 19). Due to the larger absorption cross-section and a fluorescence quantum yield $\phi_{fl} \sim 0.3$, the toluene LIF signal per unit tracer density is approximately 300 times stronger than the signal of ketones in the absence of quenching colliders.

Fig. 15 shows recent measurements of toluene absorption cross-sections at 248 and 266 nm [96]. The room temperature measurement by Burton [123] (which is commonly regarded as a standard) agrees well with the new room temperature data; the new data, however, extend to higher temperatures from measurements in a static cell and in shock-heated gases. At 248 nm only minor variations in absorption cross-sections are observed below ~1000 K. At higher temperature the red tail of the S_2 absorption feature becomes significant. At 266 nm, however, the absorption cross-section changes by more than a factor of three within the 300–1000 K temperature interval. In the same interval the fluorescence quantum yield

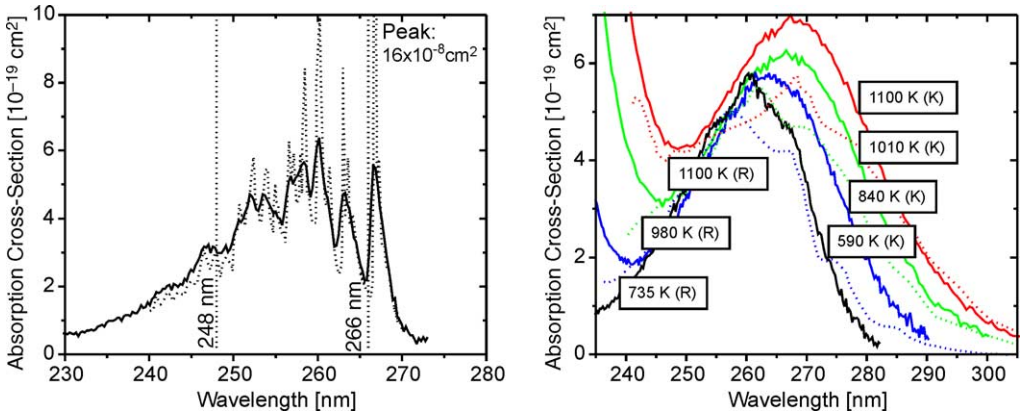

Fig. 14. Absorption spectra of toluene. Left: at 1 bar, 295 K with different spectral resolution: dashed: 0.003-nm resolution [123], solid: 0.25-nm resolution [96]. Right: absorption spectra in shock-tube experiments for different temperatures (0.25-nm resolution). Dashed lines labeled R [210], solid lines labeled K [96]. The solid lines were obtained from time-resolved measurements that exclude effects from thermal decomposition at the highest temperatures. Reproduced by permission of the PCCP Owner Societies.

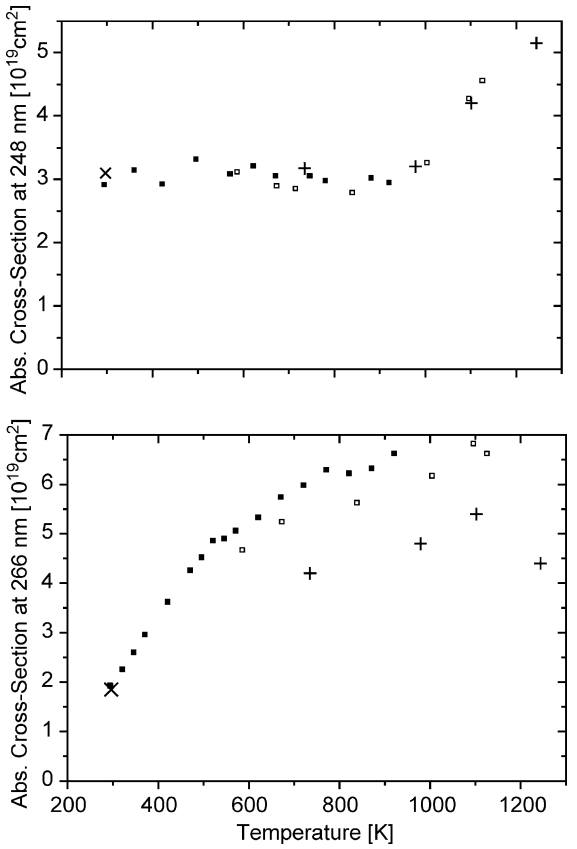

Fig. 15. Toluene absorption cross-sections at 248 nm (upper frame) and 266 nm (lower frame) as a function of temperature: ■ flow cell and □ shock tube from [96]; + from [210]; × from [123]. Reproduced by permission of the PCCP Owner Societies.

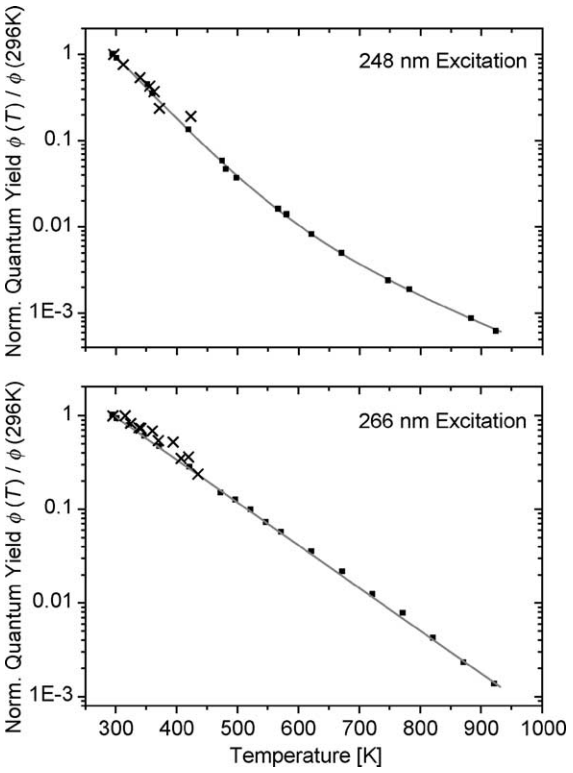

Fig. 16. Toluene fluorescence quantum yield as a function of temperature. Upper frame: 248-nm excitation, lower frame: 266-nm excitation, 20 mbar toluene in 1 bar N_2 [96]; × from [123]. Solid lines: exponential best-fit (lower diagram) and double-exponential best-fit (upper diagram). Reproduced by permission of the PCCP Owner Societies.

decreases by more than two orders of magnitude (Fig. 16). The overall toluene-LIF signal per molecule therefore depends strongly on temperature. On a per-volume basis the signal variation would be even stronger. These data indicate that in the absence of oxygen (which would disturb the simple correlation between temperature and LIF intensity) toluene can be used as a sensitive tracer for single line thermometry in homogeneously seeded gas systems.

The temperature-dependence of the fluorescence quantum yield decreases with increasing detection wavelength. Fig. 17 shows the temperature-dependent signal ratio of the toluene LIF signal detected around the peak (detected at $\lambda = 280 \pm 10$ nm) and the signal in the long-wavelength tail ($\lambda > 335$ nm) with excitation at 266 nm. The temperature sensitivity is similar to that used in 3-pentanone two-line thermometry (cf. Section 5.2.1). Furthermore, only one excitation wavelength is required for the two-line temperature measurement, which reduces experimental cost compared to the 3-pentanone two-excitation-color technique.

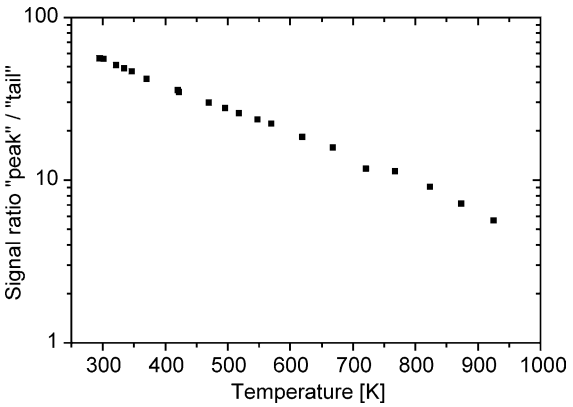

Fig. 17. Toluene-LIF signal ratio for detection at the 'peak' (detection at 280 ± 10 nm) and at the long wavelength 'tail' (detection at $\lambda > 335$ nm long pass) as a function of temperature. Excitation at 266 nm. The ratio is normalized to its value at room temperature [96]. Reproduced by permission of the PCCP Owner Societies.

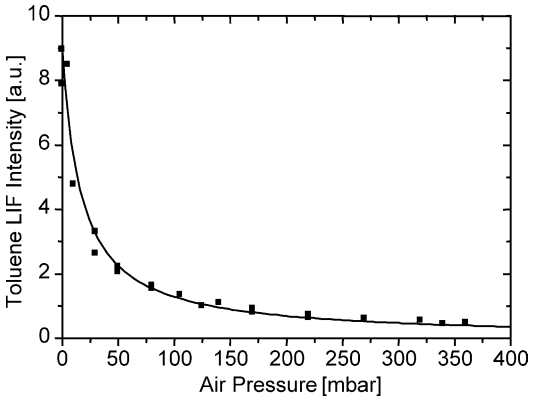

Fig. 18. Toluene-LIF signal intensity vs. air pressure.

Therefore, toluene is suited for temperature measurements in (again: oxygen-free) systems with inhomogeneous tracer concentration at reduced experimental cost [97].

4.3.2. Pressure-dependence of toluene LIF

The pressure-dependence of toluene LIF in practical applications is dominated by collisional quenching with molecular oxygen. Excited toluene is quenched by collisions with oxygen molecules with almost unity probability. The toluene-LIF signal-dependence on air pressure (Fig. 18) is therefore significantly different than that of aliphatic ketones (cf. Fig. 10). The difference is attributed to longer effective lifetimes in the S_1 state (i.e. a longer time where collisions can be active) and the larger singlet–triplet energy gap (i.e. a more effective energy transfer to the collider, cf. Section 3.4). The effect of quenching on fluorescence lifetime and quantum yield has been addressed in several studies. Vibrational relaxation by collisions with non-quenching colliders has been studied extensively for organic molecules in the S_0 state with high vibrational excess energy [119,124,125]. These data will become useful as a starting point to model the relaxation in the S_1 state that is relevant in our context. However, further experiments of pressure-dependence, i.e. in nitrogen, are desirable to validate such model calculations.

The strong dependence of toluene LIF on the oxygen concentration makes this tracer attractive for measuring local oxygen concentrations along with tracer concentrations. It should be noted that this is different from measuring equivalence ratios directly according to the method by Reboux that is further discussed in Section 4.3.3. The latter approach is valid only within a limited range of temperatures and oxygen partial pressures that do not fully cover the conditions that are expected in the compression stroke in IC engines. Even within the valid range this approach does not give information on the absolute *number densities*, i.e. the chemical energy stored in a combustible mixture, but on concentration *ratios*, i.e. mole fractions.

Oxygen concentrations have been determined from toluene fluorescence lifetimes [126]. Imaging measurements

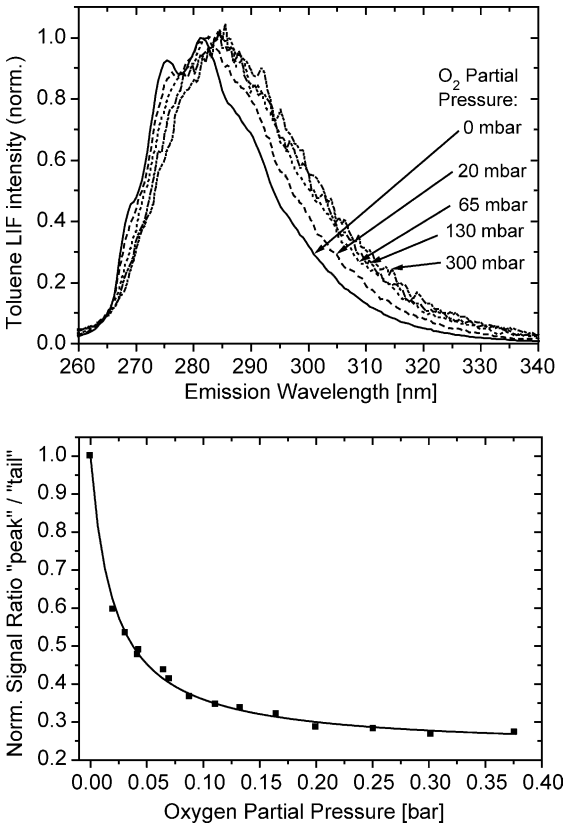

Fig. 19. Upper plot: toluene-LIF spectrum with excitation at 248 nm at room temperature with 0–300 mbar O_2. The intensity in the absence of oxygen is roughly 300 times higher than that of acetone with 248 nm excitation. The lower plot shows the ratio of the LIF signal obtained from the 'peak' ($\lambda = 280 \pm 10$ nm) and the 'tail' ($\lambda > 335$ nm) [38]. Reprinted from [38] with permission from Springer Verlag.

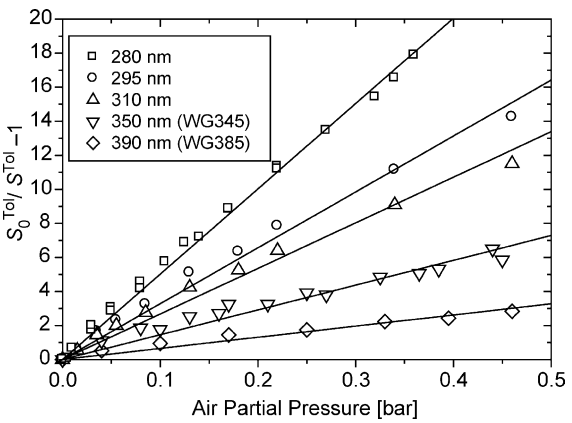

Fig. 20. Stern–Volmer Plots for toluene with 248-nm excitation for different detection wavelengths.

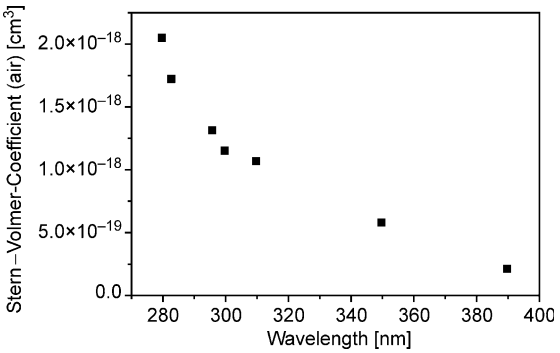

Fig. 21. Detection wavelength dependence of the Stern–Volmer coefficients for toluene after 266-nm excitation and quenching by air [127]. Reprinted from [127] with permission from Springer Verlag.

of oxygen concentrations (along with absolute fuel concentrations) have been performed by combining toluene and 3-pentanone tracers, taking advantage of their different response to oxygen, their spectrally separable emission signal, and their similar boiling and transport properties [101,110]. Recent experiments use the different Stern–Volmer coefficients in toluene at different detection wavelengths in order to obtain information about oxygen concentrations [127]. This technique is based on the observation that collisions with oxygen do not only change the total toluene LIF intensity but the spectral shape of the emission spectra as well (Fig. 19). The long-wavelength tail of the toluene signal is less influenced by oxygen quenching than the peak around 280 nm.

This behavior is more obvious in the Stern–Volmer plots for different toluene LIF emission wavelengths (Fig. 20). The Stern–Volmer coefficients decrease by more than a factor of five between 280 and 380 nm (Fig. 21). This variation in fluorescence quenching at different detection wavelengths can be used for measuring oxygen concentration in isothermal systems [127] similar to the thermometry technique mentioned above using a single excitation wavelength and simultaneous detection within two sections of the emission spectrum.

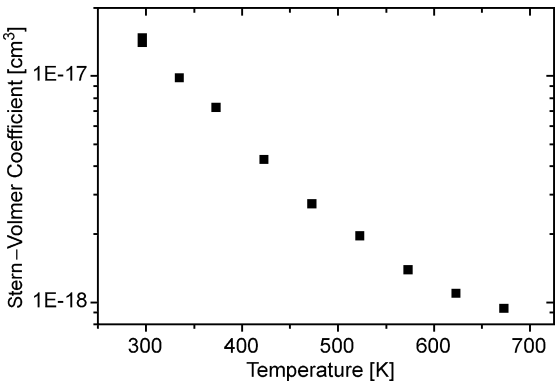

Fig. 22. Variation of the Stern–Volmer coefficient with temperature (266-nm excitation).

Temperature and oxygen-quenching effects on toluene LIF, however, are strongly coupled. Therefore, the evaluation of oxygen concentrations (or fuel/air ratios according to [37], cf. Section 4.3.3) in non-isothermal systems are critical. The same applies to temperature measurements in situations where oxygen is present. The reason for that is the strong temperature-dependence of the Stern–Volmer coefficient (Fig. 22). Within the temperature range found for the mixing and compression stroke in IC engines, the Stern–Volmer coefficient changes by more than an order of magnitude.

4.3.3. Direct measurement of equivalence ratio with toluene LIF?

Reboux et al. [37] suggested to take advantage of the strong quenching of toluene LIF by O_2 in order to use toluene as a fluorescent tracer to directly measure the fuel/air equivalence ratio ϕ. This technique is often referred to as FARLIF and it has also been applied to measurements with other tracers that are strongly quenched by oxygen [69]. Reboux et al. found that the toluene fluorescence in air at room temperature is proportional to ϕ for $p > 3$ bar with 248 nm excitation. Since then, toluene has become a popular tracer to study mixing behavior in the compression stroke of IC engines. Until recently, however, no data was available on absorption or fluorescence at elevated temperatures. In IC-engine applications the decrease of total fluorescence with increasing crank angle (i.e. increasing p, T) was observed for excitation at 248 nm [101,128]. Recent studies at elevated temperatures in a flow cell revealed a strong temperature-dependence of the fluorescence quantum yield ϕ_{fl} and the Stern–Volmer factor. ϕ_{fl} changes by more than two orders of magnitude within the temperature-range of the compression stroke in engines, and the relative strength of oxygen quenching was dependent on the oxygen number density itself [38,39,96]. With these new findings, the technique of measuring fuel-air equivalence ratios in IC engines using toluene fluorescence must be reconsidered [129]. The following discussion focuses on excitation with 248 nm; the concept, however, is valid for any other excitation wavelength.

The fluorescence signal S_{fl} of a molecular tracer state quenched by oxygen can be described by

$$S_{\mathrm{fl}} \sim \sigma_{\mathrm{abs}}(\lambda, T)\frac{k_{\mathrm{fl}} n_{\mathrm{fl}}}{k_{\mathrm{tot}} + \tilde{k}_{\mathrm{q}} n_{\mathrm{q}}}, \tag{4.5}$$

where k_{fl} denotes the rate of spontaneous emission, k_{tot} the sum of all intra-molecular de-excitation pathways, $\tilde{k}_{\mathrm{q}}$ the quenching rate coefficient, and n_{fl} and n_{q} the number densities of the tracer and quencher (O_2), respectively. In the case of toluene the absorption cross-section $\sigma_{\mathrm{abs}}(\lambda, T)$ at 248 nm has a negligible T-dependence (Fig. 15, [96]) and is therefore not further considered here. When quenching by

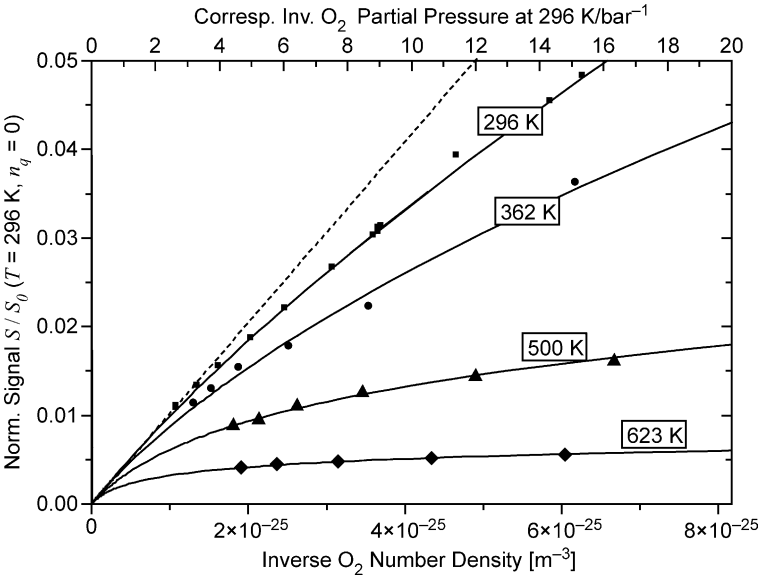

Fig. 23. Dependence of the toluene-LIF signal on the inverse oxygen concentration with a fixed tracer number density. Symbols: experimental data at 1 bar total pressure; Solid lines: fit based on Eq. (4.7); dashed line: expected signal dependence according to the 'common' assumption $S \sim \phi$ cf. Eq. (4.6). Excitation at 248 nm. Reprinted from [39] with permission from the Combustion Institute.

molecular oxygen is the dominant process, i.e. $\tilde{k}_q n_q \gg k_{tot}$, intra-molecular deactivation can be neglected, and the fluorescence signal is directly proportional to the ratio n_{fl}/n_{O_2} (with $n_{O_2} = n_q$), which scales with the fuel/air equivalence-ratio ϕ

$$S_{fl} \sim \frac{k_{fl}}{\tilde{k}_q}\phi_{fl}. \tag{4.6}$$

In the case of the toluene molecule, many different rovibrational states contribute to the emission. Thus, the fluorescence signal is the sum of n emitting states, populated with the fraction a_n following Eq. (4.5):

$$S_{fl}^{tol} \sim \sum_n a_n \left[\frac{k_{fl} n_{fl}^{tol}}{k_{tot} + \tilde{k}_q n_q}\right]_n. \tag{4.7}$$

The rates k_{tot}, k_{fl}, and the rate coefficient $\tilde{k}_q$ are now state-specific. At higher T, states with high k_{tot} contribute to the emission, and the assumption of O_2-quenching as the dominant deactivation process becomes questionable [38]. Additionally, the relative strength of O_2-quenching $\tilde{k}_q/k_{tot}$ becomes dependent on the oxygen number density n_q. This is due to the fact that the relative signal contribution of emission from states that are less affected by quenching (i.e. states with high k_{tot}) starts to dominate the total emission with increasing n_q. In other words, the signal from easily quenched states 'disappears' at high n_q.

4.3.4. Toluene-LIF under engine conditions

Based on the measured T- and n_{O_2}-dependence of toluene-LIF [38], Eq. (4.7) allows the prediction of toluene-LIF signal for the conditions of the compression stroke in an IC engine. In Fig. 23 we display the expected signal for a fixed amount of tracer molecules plotted over the inverse oxygen number density at different temperatures. The x-axis therefore scales with the fuel/air equivalence ratio ϕ. As a more intuitive scale, the corresponding inverse partial pressure at 296 K is displayed at the top of the figure. The signals are normalized to O_2-free conditions at 296 K. The straight dashed line in Fig. 23 illustrates the assumption from Reboux et al. according to Eq. (4.6) [37]. It can be

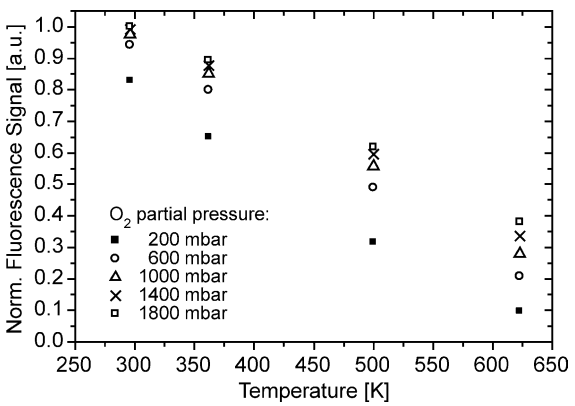

Fig. 24. Predicted dependence of toluene-LIF signal on oxygen partial pressure and temperature for a fixed value of ϕ. The opposing effects of p and T moderate the signal variations in the compression stroke of an engine (where p_{O_2} and T both increase). Quenching is dominant at each T when the signal becomes independent of p_{O_2}. The value of the high-pressure limit may depend on T (cf. Eq. (4.7)). Excitation at 248 nm. Reprinted from [39] with permission from the Combustion Institute.

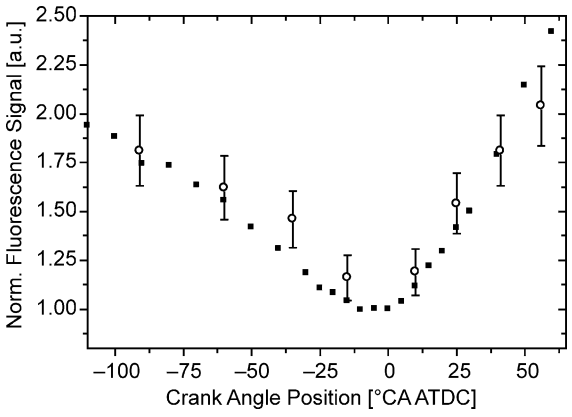

Fig. 25. Comparison of ○ predicted and ■ measured toluene signal intensities under engine conditions [39]. Reprinted from [39] with permission from the Combustion Institute.

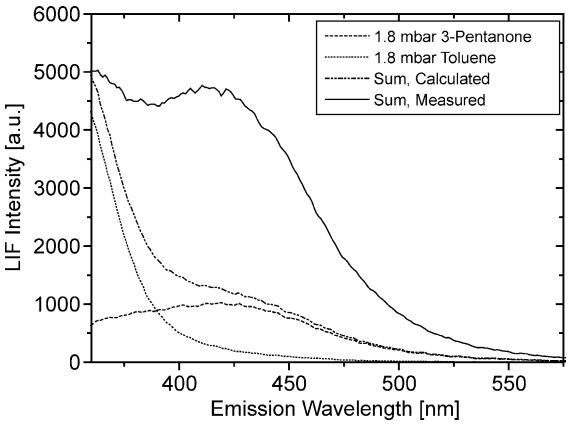

Fig. 26. Effect of energy transfer (sensitized fluorescence) in a toluene/3-pentanone mixture. Emission of pure toluene and 3-pentanone and of a mixture of both (identical individual number densities) in the 360–550-nm range.

clearly seen that this approximation is invalid over a wide range of engine-relevant conditions. In the experiments of Reboux et al., the signal is linear with ϕ for $p_{O_2} > 0.6$ bar ($1/p_{O_2} < 0.66$ bar^{-1}). At 362 K, deviation from linearity is less than 5% for $p_{O_2} > 0.7$ bar. At 500 K, however, the minimum oxygen partial pressure that justifies the use of Eq. (4.6) is already $p_{O_2} = 5$ bar (i.e. ~25 bar air pressure). Below this pressure the toluene LIF signal is *not* proportional to the equivalence ratio because a fraction of the excited molecules are in states with a competing, fast intra-molecular de-excitation (i.e. k_{tot} is not negligible). With increasing T, intra-molecular decay becomes faster [96]. Therefore, increasing n_q (i.e. n_{O_2}) is required for quenching to be the dominant process.

In Fig. 24 the predicted toluene-LIF intensity is displayed for a fixed equivalence ratio ϕ for different total pressures and temperatures that are typical for the compression stroke in an engine. According to the assumption of Eq. (4.6) *the same LIF intensity* should be measured for all variations shown. This again clearly shows that the common assumption of $S_{fl} \sim \phi$ does not hold. Temperature and gas density, however, have opposite effects and partially compensate each other. Therefore, the overall signal variation during the compression stroke in IC engines is small (which might give the illusion that the $S_{fl} \sim \phi$ hypothesis is correct). Increasing temperature lowers the signal of a mixture with fixed oxygen/toluene ratio whereas increasing pressure leads to stronger signals, especially at the higher temperatures. It is important to note that the common 'temperature correction,' (cf. [37]) as a calibration of signal intensities to crank angle, is in fact a correction for the combined effect of T and p_{O_2} and is only valid under the specific conditions of the experiment. In general, both effects cannot be treated independently. The same temperature correction curve applied at different pressures would give different results.

Predicted signal intensities for motored in-cylinder engine conditions are shown in Fig. 25 as a function of crank angle in the range of 1 bar, 350 K to 8 bar, 600 K [39]. The agreement is good and indicates that influence of total pressure is small compared to oxygen quenching and that the model (Eq. (4.7)) describes the signal behavior sufficiently well. Error bars of ±10% are displayed, estimated from extreme fits to the data measured under stationary conditions (Figs. 23 and 24). Predicted signal intensities are scaled to engine data at −90 CA ATDC at 0.82 bar and 360 K. This is close to conditions in the flow-cell experiment.

4.3.5. Toluene-LIF: a preliminary conclusion

Guidelines can now be given for the interpretation of signal intensities obtained from toluene. In general, the signal for a certain fuel/air equivalence ratio ϕ will change according to Fig. 24 for all deviations in T or n_q (i.e. n_{O_2}) relative to the calibration condition. Higher T will lower the signal, whereas increasing n_{O_2} will raise the signal of a constant fuel/air ratio. (For example when increasing the total pressure while maintaining the relative concentrations when increasing the load in an IC engine). In the latter case the relative influence of O_2-quenching decreases with increasing n_{O_2} leading to an increasing signal. The relative O_2-quenching effect significantly decreases with increasing p, and around TDC the uncertainty introduced by temperature will dominate. For example, changing temperature from 500 to 550 K at 5 bar air pressure for the same ϕ will cause a decrease in signal of ~15% whereas increasing p_{O_2} by 0.4 bar at 500 K, 5 bar air will increase the toluene LIF signal by ~6%. Thus, if local inhomogeneities or cycle-to-cycle variations in T can be neglected, the signal of a stratified charge will be perfectly proportional to ϕ over a wide range, since a varying fuel concentration affects ϕ but does not significantly change n_{O_2}. If T or n_{O_2} vary strongly

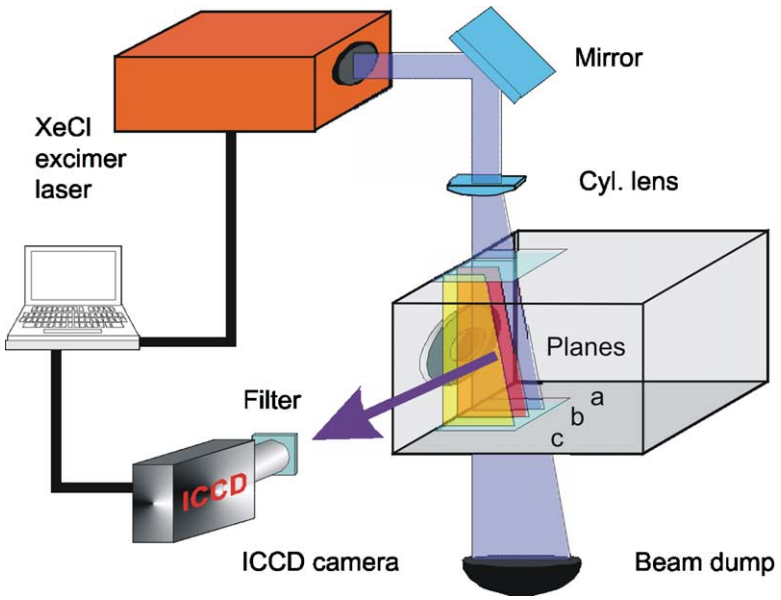

Fig. 27. Experimental setup for time-averaged measurements of fuel/air mixing in a swirl burner of a stationary gas turbine (in collaboration with R. Koch, ITS, Karlsruhe) [211].

during the investigation (e.g. strongly varying starting conditions or measurements over a wide range of crank angles), various calibration points or corrections according to Fig. 24 become necessary.

In the presence of varying amounts of residual gas, the oxygen number densities n_{O_2} changes spatially and temporally. If the fuel is homogeneously mixed and (when investigating cycle-to-cycle variations) a constant amount is injected, the relations shown Fig. 23 apply. While the overall behavior is non-linear, approximate linearity may be achieved over small ranges of n_{O_2} (or p_{O_2}), e.g. 2.5×10^{24} to 5×10^{24} m^{-3} (or 0.25–0.125 bar) at 362 K. For quantitative interpretation, however, two calibration points will be needed since the linear relation between ϕ and signal will have a non-zero value as $1/n_{O_2}\rightarrow 0$. A complete photophysical model that takes these effects into account will be very valuable but is not yet available (Fig. 25). When used in combination with other tracers, like ketones, additional energy trasfer processes can become important (see Fig. 26 and Section 5.3).

5. Applications: quantitative measurements of fuel concentrations in gas-phase systems

5.1. Isothermal systems

Although realistic combustion devices do not operate in isothermal mode, studies of mixing processes under isothermal conditions are valuable in assessing the validity of models in predicting mixing in specific geometries, thus adding credibility to predictions under non-isothermal conditions. Furthermore, in-cylinder conditions in internal combustion engines can often be approximated as spatially isothermal at fixed crank angles and therefore simplified concentration measurements will be possible. In fact, this is

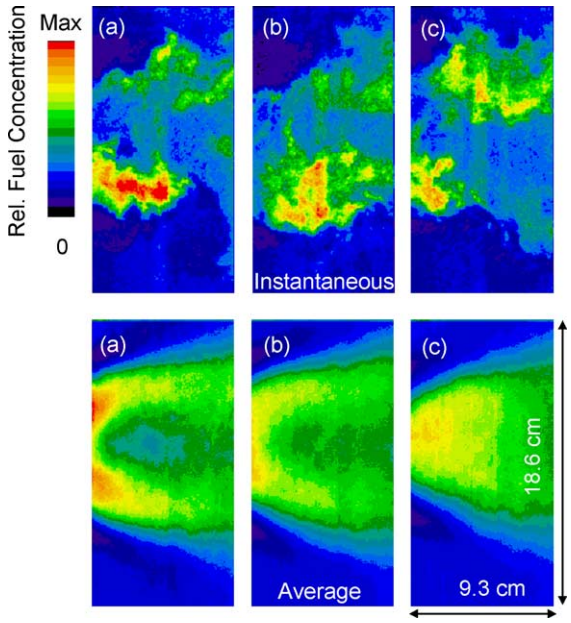

Fig. 28. Measurements of the fuel distribution (air doped with acetone) in three parallel planes in the mixing chamber. The fuel nozzle is 1 cm to the left end of the images. The planes a–c have a distance of 0, 15 and 30 mm to the burner axis, respectively. Upper row: randomly chosen single-shot images, lower row: averaged fuel distribution [211].

the most common application of LIF imaging in engines to investigate fuel/air mixing. Systems where spatial temperature inhomogeneities are measured and used to correct fuel concentration measurements are discussed in a subsequent section.

In isobaric, isothermal systems the use of tracer-LIF is straightforward. When seeding acetone to the desired gas flow, the local LIF intensity gives direct information about local concentrations. In later sections we will describe how temperature and pressure effects must be corrected in more general applications. Fig. 27 shows the setup for a measurement of fuel distributions in the combustion chamber of a stationary gas turbine (thermal power of the investigated segment ~1 MW). The gaseous fuel flow was simulated by air seeded with acetone, and the fluorescence was successively measured in three adjacent planes. Instantaneous and time-averaged images are shown in Fig. 28. The time-averaged concentration distributions from the adjacent planes were then used to reconstruct the average three-dimensional fuel distribution assuming cylindrical geometry [130]. The strong variation in local concentrations (upper row in Fig. 28) indicates, however, that an instantaneous view into the three-dimensional structure would deviate significantly from the average distribution.

For quasi-instantaneous 3D imaging measurements of fuel concentration distributions sweeping long-pulse or continuous (cw) laser beams (driven by scanning mirrors) have been suggested by Yip et al. [131]. Recent approaches using multi-laser excitation of three [132] and up to eight parallel planes [83] with subsequent imaging by multiple cameras or a high-speed camera yielded new results, however, at high experimental costs. Further measurements are based on simultaneous excitation with two crossed light-sheets [133–137]. One of the benefits of this method is the increasing resolution towards the crossing line and a small cylindrical volume up to approximately 1 mm around it. The resulting three-dimensional data matrix can be visualized by a 3D-visualization tool that assigns not only color but also transparency values to the given intensity values [130].

5.2. Non-isothermal systems

5.2.1. Measurement of temperature

The temperature-dependence of LIF signals from tracers is usually a detrimental effect for quantitative fuel concentration measurements. Without knowing the temperature the interpretation of LIF images is limited, since variation in signal intensities can originate from either concentration or temperature changes. However, the temperature-dependence can also be exploited beneficially to measure either temperature or to simultaneously measure temperature and fuel concentration.

Thurber et al. [94] determined temperature fields in a flow passing a heated cylinder using single line excitation of acetone at 248 nm. In this non-reacting flow the mole fraction of acetone in a nitrogen stream was constant. The quantitative evaluation of the LIF signals was based on previously measured absorption cross-sections and fluorescence yields per unit mole fraction and calibration at a single temperature. Temperature fields were determined with resolutions of a few Kelvin in a temperature range of ~350–500 K. Independence of the requirement of constant mole fraction is achieved when two-line excitation schemes are employed. Then, temperature can be determined from the ratio of two fluorescence signals, each of which is described by Eq. (3.11). The number density of the tracer molecules is thus eliminated from the data reduction process. This temperature measurement method was first demonstrated for 3-pentanone by Großmann et al. [43] and then expanded for applications with acetone by Thurber et al. [94,114]. Thurber investigated temperature and mole fraction fields in a turbulent jet of a heated acetone/air mixture introduced into ambient air. Excitation was achieved with two excimer lasers (248 and 308 nm) with a time delay between the two pulses sufficient to separate the LIF signals on subsequent frames of a non-intensified interline camera. The use of non-intensified cameras is restricted to non-reacting conditions since the effective exposure time of the CCD array is too long to suppress chemiluminescence signals that would spectrally overlap with the LIF signals of the fuel tracers. Thurber also compares single- and two-line acetone thermometry and assesses the conditions (for homogeneous distribution of tracers) where one of the two techniques has advantages in terms of temperature precision and signal-to-noise ratio [94].

The absorption spectrum of 3-pentanone exhibits a temperature-induced shift towards longer wavelengths of about 10 nm per increase of 100 K similar to acetone (depicted in Fig. 6). Upon excitation in this region, fluorescence is emitted between 330 and 550 nm, with a

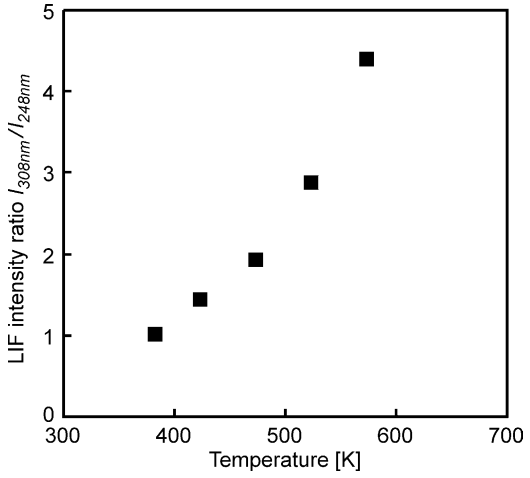

Fig. 29. Temperature-dependence of the ratio of LIF intensities in 3-pentanone with 308 and 248 nm excitation [93]. Reprinted from [93] with permission from Springer Verlag.

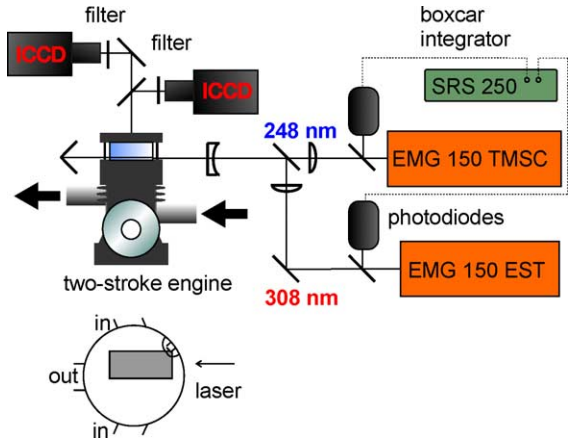

Fig. 30. Experimental setup for the simultaneous measurements of fuel concentration, temperature, and fuel/air equivalence ratio in a two-stroke engine. The lower figure shows the position of the measurements displayed in Fig. 31. Reprinted from [93] with permission from Springer Verlag.

spectral distribution almost independent of the absorbed wavelength. This spectral shift of the absorption, albeit undesired for concentration measurements with single wavelength excitation, can be used for measuring temperature, e.g. when 3-pentanone is seeded to non-fluorescing model fuels, as the fluorescence intensity is a function of the absorption coefficient for a given excitation wavelength, and thus, of temperature. After excitation at two different wavelengths the ratio of the fluorescence signal intensities reflects the local temperature. The temperature dependence

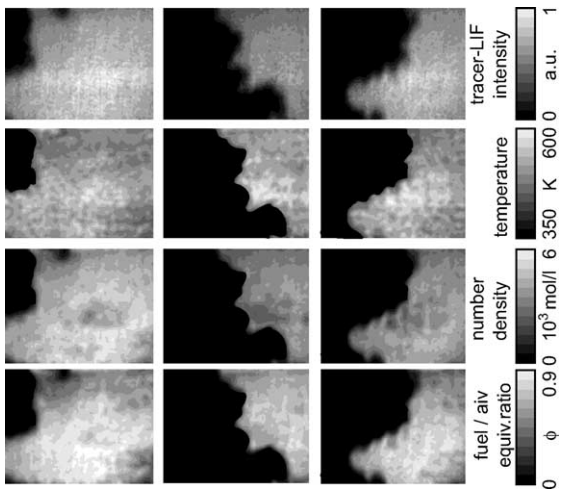

Fig. 31. Measurements of the tracer-LIF intensity (first row), temperature (second row), fuel number density (third row) and fuel/air equivalence ratio (fourth row) in a two stroke engine. The columns show three randomly chosen data sets for instantaneous measurements [93]. Imaged area: 68×52 mm^2. Reprinted from [93] with permission from Springer Verlag.

of the LIF signal ratio obtained with 248 and 308 nm excitation for these conditions is shown in Fig. 29 (using data for 308 nm from [138]).

In the imaging measurements the local temperature can be evaluated for each pixel from the relative signal intensities. Then, with the local temperatures now determined, signals from either of the two excitation wavelengths can be corrected for temperature effects to calculate the number density N of tracer molecules. A calibration with a known number density of tracer molecules at a known temperature scales N to absolute number densities. With the ideal gas law the local *mole fraction* can then be calculated. The fuel/air equivalence ratio ϕ can then be determined based on the assumption that the cylinder contains fuel and air only and that the oxygen concentration is homogeneous within the air. There are limitations for this assumption in systems with high levels of recirculated exhaust gases. Techniques to overcome this problem will be discussed in Section 5.3.

The engine measurements (Fig. 30) were conducted in a single-cylinder two-stroke engine (bore: 80 mm, stroke: 74 mm, compression ratio: 8.6) fueled with *iso*-octane (p.a.) doped with 10% (v/v) 3-pentanone at $\phi = 0.62$ [93]. Two excimer lasers, operated with KrF (248 nm) and XeCl (308 nm), respectively, were combined on a dichroic beam splitter. The dimensions of the two horizontal laser light sheets were 20 mm width and 0.5 mm thickness. The signals generated by the two laser pulses were split using a broadband beam splitter and each part was imaged onto a ICCD camera. Fig. 31 shows the LIF-intensities upon 308 nm excitation for three single-shot images (18 °CA). Temperature is obtained from the ratio of signal intensities with 248- and 308-nm excitation. The LIF signal with 308-nm excitation is then corrected for temperature effects and calibrated to absolute number densities (third row) using the measurements under perfectly mixed conditions. Finally, fuel/air equivalence ratios can be obtained based on the assumption that no exhaust gases are present that could cause inhomogeneous distribution of oxygen inside the cylinder.

5.2.2. Quantitative measurement of fuel concentration or equivalence ratio

The extraction of concentration information from LIF signals always requires certain corrections, like normalization to instantaneous laser pulse energy, light sheet inhomogeneity, and possibly others to account for the influence of pressure, temperature, and gas composition. Under favorable conditions and suitable selection of excitation and detection wavelength one or more of these factors can be assumed constant, and the interpretation of LIF signals is simplified. Furthermore, many studies that are presented in the literature discuss (relative) concentration distributions, where spatial homogeneity of pressure and temperature can be assumed. As such, statistical analysis of concentration variations, etc. is feasible and often done.

This even works when comparing different operating conditions as long as the changes in pressure and temperature are minor.

Wolff et al. [50] used acetone mixed with *iso*-octane to investigate fuel/air mixing in an SI engine. They characterized the LIF signals for their excitation wavelength (248 nm) and filter scheme (not specified) to be independent of temperature and pressure. Then, after calibration to a single, known value, the LIF signals can directly be interpreted as number density of fuel. Because in an engine the pressure varies with crank angle, normalization of the LIF signals to pressure yields fuel concentrations. Fujikawa et al. [139] investigated a range of tracers and then used acetone as the tracer for best performance under their conditions. They found a temperature and pressure dependence of LIF signals within their setup. More details and explanations on differences in reported temperature sensitivity for ketone LIF are discussed in Section 4.1. Additional applications and examples are summarized and listed in a review by Zhao and Ladommatos [140] from 1998. Since then, Richter et al. [141] developed a strategy to calibrate LIF images taken in mixtures of 3-pentanone and *iso*-octane with Raman scattering signals to obtain a quantitative measure of the equivalence ratio. Similarly, the use of an exciplex strategy in combination with Raman scattering is demonstrated by Ipp et al. [142] for quantitative fuel/air ratio measurements. Calibration of LIF signals against exhaust gas analysis when operating the engine with homogeneous fuel distribution was used by Neij et al. [55] for 3-pentanone/*iso*-octane mixtures. The only study where local variations in temperature were included for corrections of 3-pentanone LIF signals is reported by Einecke et al. [93]. These results have already been discussed in Section 5.2.1 on temperature measurements and were shown in Fig. 31.

Prevaporization of the fuel and mixing with the air in the intake system far upstream of the engine provided uniform fuel/air distributions for calibration purposes in a study of cold start strategies discussed by Weaver et al. [79]. LIF signals in that study originated from 3-pentanone and aromatic compounds that were contained in the base fuel. The signal intensity for known homogeneous equivalence ratio distributions was measured as a function of crank angle. Engine operation with port fuel injection was similar in performance and, thus, measured local variations could be interpreted as variations in fuel concentration after correction for crank angle- (i.e. pressure and temperature) dependent LIF signals. A few studies were performed with biacetyl as the tracer, which has been shown to exhibit a modest 20% signal change for fixed concentration over the temperature range from 550 to 700 K [122]. Only relative fuel distribution data are reported, however. The conversion of LIF signals to equivalence ratios is always based on the assumption that there is no spatial variation in the oxygen concentration and that the residual gas fraction is homogenously distributed and negligible within the uncertainty of the tracer-LIF measurement or not present at all. This is often a good assumption since many optical engine tests are run with skip-firing to keep the thermal load of the engine small but also to provide well-characterized composition conditions for validation purposes of CFD simulations.

In contrast to measurements with tracers like acetone, 3-pentanone, or biacetyl that determine the number density of the tracer, an approach later termed FARLIF (fuel/air-ratio laser-induced fluorescence) was proposed by Reboux et al. [37]. Details and potential restrictions of this technique, which relies on the strong quenching of electronically excited toluene by molecular oxygen, have been discussed in Section 4.3.2. Spatial inhomogeneity of the equivalence ratio was characterized in a four-stroke engine operated with different fuels and nominal equivalence ratios under port-fuel-injection conditions [143]. Although significant spatial variations of the equivalence ratio are observed under such conditions, studies of direct-injection engines reveal much more substantial differences in the fuel/air mixing. For late injection strategies, where the fuel is introduced only shortly before the spark ignites the fuel, highly stratified mixture conditions are found in comparison to homogeneous mixing conditions [128]. For full-load operating conditions, direct-injection gasoline engines are operated with an overall stoichiometric fuel/air mixture. The fuel is injected much earlier in these cases and should be completely mixed with the air by the time the spark is fired. A comprehensive study of the three-dimensional spray evolution in an optical direct-injection engine followed by mapping of the equivalence ratio and combustion progress with toluene-based LIF showed that changes the in-cylinder flow conditions substantially affected the fuel/air mixing and combustion [144]. Averaged three-dimensional maps of the equivalence ratio were obtained by sequentially scanning the laser sheet to a large number of planes across the cylinder. The spray atomization and hence the fuel distribution at later times was significantly affected by increases in swirl strength of the flow, as seen in Fig. 32. Note that these images show signals from liquid *and* vapor phase toluene. Also, the linear relationship between toluene LIF signal and equivalence ratio might no longer be valid for the very fuel-rich conditions shown for the sprays. Even though the fuel was injected very early in the engine cycle, differences in the fuel distribution that were observed during the injection event remained up to the time of ignition. The average equivalence ratio differed by approximately 0.2 for different swirl levels of the in-cylinder flows, as shown in Fig. 33.

Even though the use of toluene as a fluorescence marker can provide quantitative measures of the local equivalence ratio [39] under suitable conditions (cf. Section 4.3.3), it will not be possible to extract the absolute amount of fuel unless there is no residual gas present. The same restrictions apply to applications using triethylamine and benzene [145] or other exciplex systems (see Section 6 for more details)

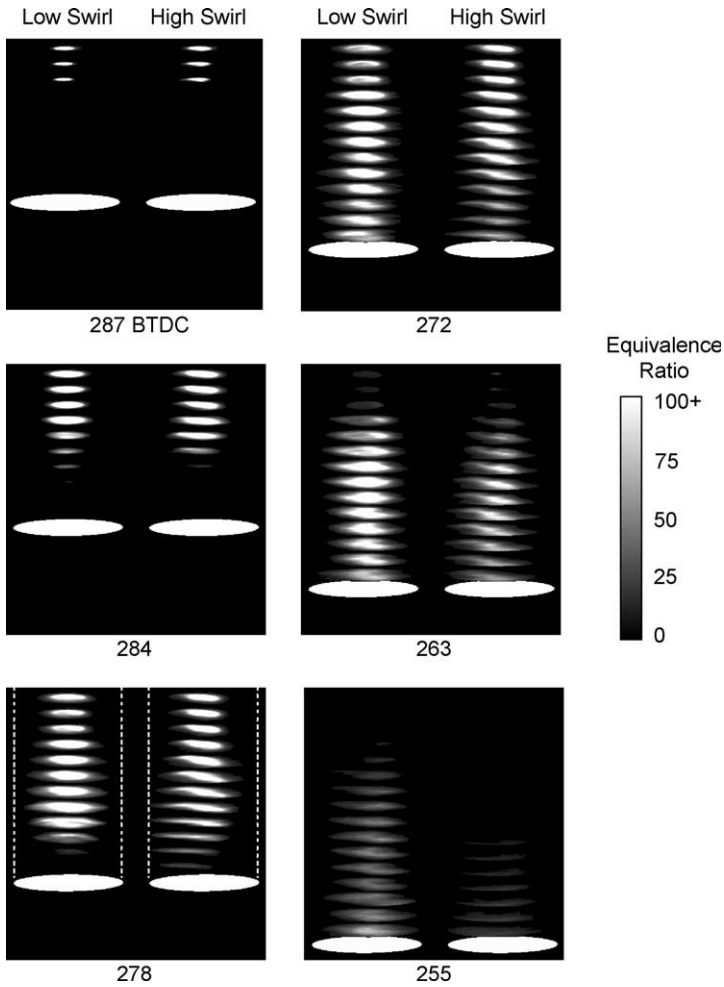

Fig. 32. In-cylinder swirl flows have a substantial impact on the spray structure and evaporation. Sprays in high-swirl conditions (shown in the right column of each sub-image) are more distorted at 2000 rpm as measured via toluene LIF in an optical direct-injection gasoline engine [144]. Crank position (°BTDC) varies as indicated above. The piston position is shown as a white disk. The individual elongated disk-like structures are LIF images taken at different height in the cylinder to obtain an overall quasi-3D view of the spray structure. Elevations shown are (from top) = 1, 4, 8, 12, 16 mm, etc. The view of the images is at a small angle with respect to the cylinder axis to illustrate the three-dimensional structure of the spray. Reprinted with permission from SAE Paper 2003-01-0068 © 2003 SAE International.

as the tracer. This is analogous to the determination of the equivalence ratio from measurements with ketones or biacetyl. Combinations of 3-pentanone and toluene provide both quantities and then also allow the determination of absolute residual gas amounts [101,144]. Details of this approach, when applied to systems with locally changing oxygen concentrations are presented in Section 5.3.

Measurements of fuel concentrations in Diesel engines are sparser and mostly address the atomization of sprays using exciplex techniques. The problem is twofold for measurements of fuel concentrations under Diesel engine conditions. First, suitable tracers for higher boiling point fuels have not yet been as well characterized as the tracers discussed here. Second, producing non-fluorescent fuels that mimic Diesel fuel is very difficult. The first investigations of Diesel sprays with 5-nonanone added as a fluorescent tracer to n-decane are reported in [146].

5.3. Systems with local variations in O_2 concentration

In modern highly energy-efficient combustion systems, like stratified-charge engines or homogeneous-charge compression-ignition (HCCI) engines, high concentrations of residual and recirculated exhaust gases strongly dilute the fuel/air mixture with inert gases. In these situations, ignitability, flame speed, and auto-ignition susceptibility are governed by fuel and oxygen concentrations (number densities) rather than equivalence ratios. Whereas several techniques for measuring fuel concentrations (see above) and equivalence ratios are available (measurements, for

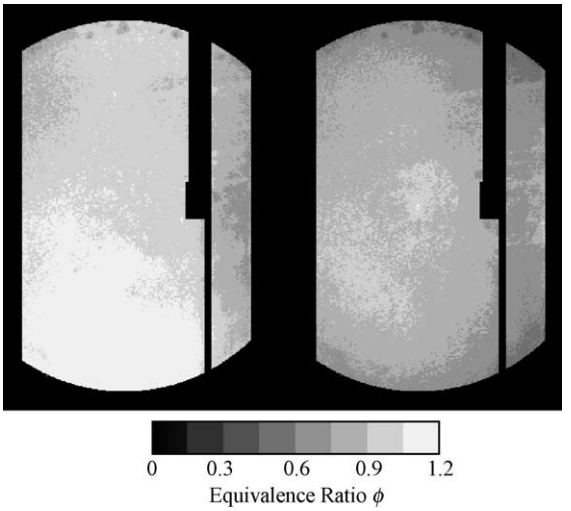

Fig. 33. Average equivalence ratio distributions at −20° ATDC, the time of ignition, at an engine speed of 2000 rpm for low- (left) and high- (right) swirl in-cylinder flow conditions. Reprinted with permission from SAE Paper 2003-01-0068 © 2003 SAE International.

example, based on the assumption that for tracers which are strongly quenched by oxygen—within a limited range [81]—the LIF signal is proportional to the equivalence ratio [37]), a technique to image oxygen distributions is desirable to characterize the local oxygen concentration. Mixing two jets at room temperature and atmospheric pressure, one of pure nitrogen, the other composed of mixtures of nitrogen with oxygen, is used to demonstrate an oxygen-imaging technique that is based on the use of 3-pentanone and toluene as tracers. A subsequent application to engine studies was referred to in the previous chapter [101]. The fluorescence properties of 3-pentanone and toluene (namely the effect of collisional

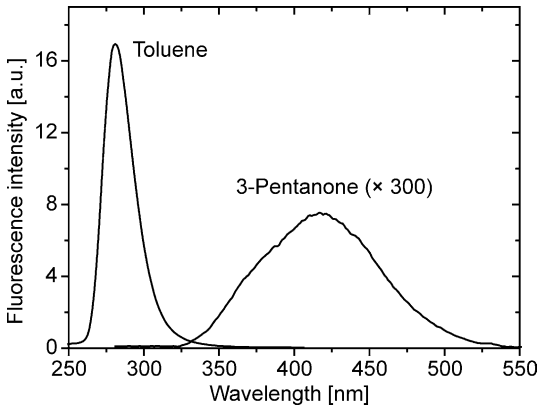

Fig. 34. Emission spectra of toluene and 3-pentanone with excitation at 248 nm. The signal of both species can be separated with appropriate filters. In pure nitrogen (shown here) the toluene signal is by far dominating (3-pentanone signal enhanced by a factor of 300) [110]. Reprinted from [110] with permission from Springer Verlag.

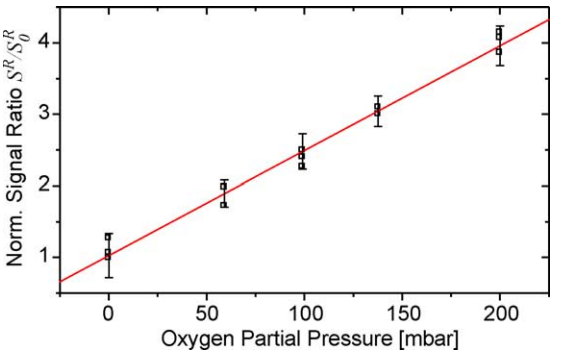

Fig. 35. Signal ratio of 3-pentanone- and toluene-LIF normalized to the ratio measured in pure nitrogen [110]. Reprinted from [110] with permission from Springer Verlag.

quenching by molecular oxygen) are markedly different, as discussed in detail in Section 4 of this paper. The spectral signature of their fluorescence spectra allows the separation of respective signals (Fig. 34).

For weak excitation the LIF signal intensity S_{fl} is given by Eq. (3.11). In zeroth order, molecular oxygen is regarded as the only relevant species quenching toluene fluorescence, while 3-pentanone fluorescence is considered independent of oxygen concentration. For a mixture of 3-pentanone (3P) and toluene (tol), the ratio of signal intensities $S_{\mathrm{fl}}^{\mathrm{R}}$ (Eq. (5.1)) is a function of the oxygen concentration only ($f(n_{\mathrm{O_2}})$) since all the other factors are either constant (like absorption cross-sections due to constant pressure and temperature) or cancel (like local laser intensity and detection volume)

$$S_{\mathrm{fl}}^{\mathrm{R}} = S_{\mathrm{fl}}^{\mathrm{3P}}/S_{\mathrm{fl}}^{\mathrm{tol}} = \mathrm{const}\ \phi_{\mathrm{fl}}^{\mathrm{3P}}/\phi_{\mathrm{fl}}^{\mathrm{tol}} = f(n_{\mathrm{O_2}}) \tag{5.1}$$

The fluorescence quantum yield ϕ_{fl}^{i} for species i is

$$\phi_{\mathrm{fl}}^{i} = \frac{k_{\mathrm{fl}}^{i}}{k_{\mathrm{tot}}^{i} + \tilde{k}_{\mathrm{q}}^{i} n_{\mathrm{q}}} \tag{5.2}$$

with the rate coefficient for spontaneous emission, k_{fl}^{i}, and the sum rate of all collision-independent de-excitation processes, k_{tot}^{i}. $\tilde{k}_{\mathrm{q}}^{i}$ is the rate coefficient for collisional quenching n_{q} the quencher (i.e. oxygen) number density.

For atmospheric pressure in 3-pentanone, as in all aliphatic ketones, quenching by oxygen can be neglected (because of $\tilde{k}_{\mathrm{q}}^{\mathrm{3P}} n_{\mathrm{q}} \ll k_{\mathrm{tot}}^{\mathrm{3P}}$). With the Stern–Volmer coefficient for toluene quenched by oxygen ($k_{\mathrm{SV}}^{\mathrm{tol,O_2}} = \tilde{k}_{\mathrm{q}}^{\mathrm{tol,O_2}}/k_{\mathrm{tot}}^{\mathrm{tol}}$) Eq. (4.6) can be rewritten [110]:

$$S_{\mathrm{fl}}^{\mathrm{R}} = \mathrm{const}\frac{k_{\mathrm{fl}}^{\mathrm{3P}}(k_{\mathrm{tot}}^{\mathrm{tol}} + \tilde{k}_{\mathrm{q}}^{\mathrm{tol}} n_{\mathrm{q}})}{k_{\mathrm{tot}}^{\mathrm{3P}} k_{\mathrm{fl}}^{\mathrm{tol}}} = c_1(1 + k_{\mathrm{SV}}^{\mathrm{tol,O_2}} n_{\mathrm{q}}). \tag{5.3}$$

The signal ratio of 3-pentanone versus toluene LIF therefore increases linearly with the oxygen number density. The offset, given by c_1, can be obtained from a single-point calibration. An experimental validation is shown in Fig. 35. This simple approach assumes that toluene and

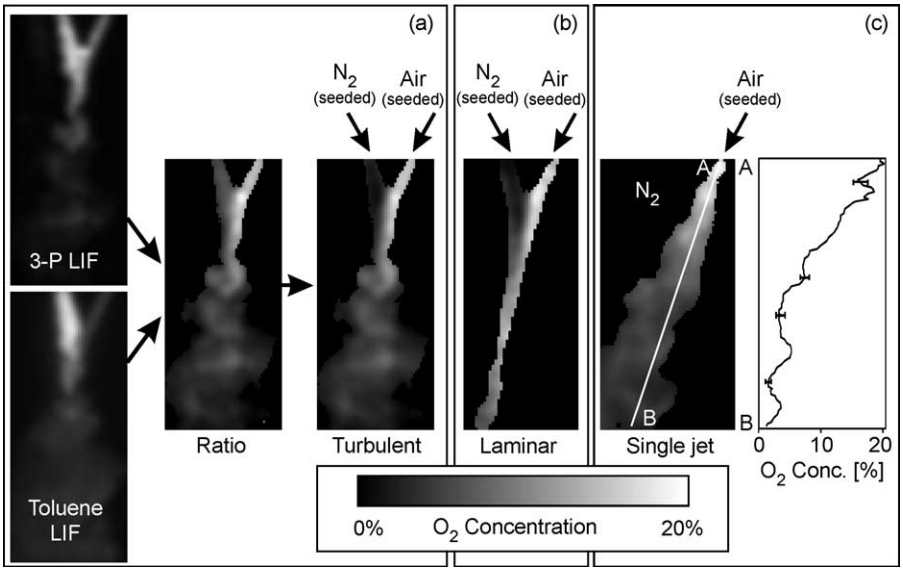

Fig. 36. Results of the O_2-imaging measurements in the mixing chamber [110]. For details see text. Reprinted from [110] with permission from Springer Verlag.

3-pentanone signals are detected independently without any spectral overlap and that oxygen is the only quenching species. Further corrections may be added in order to reduce the systematic errors caused by these assumptions [110].

The two gas jets emerged from metal tubes (exit diameter 1 mm) that were mounted 5 mm apart with the gas streams mixing at an angle of approximately 30°. The gas exit velocities were set to 5–15 m/s. The tubes were supplied with various mixtures of nitrogen and oxygen controlled by mass flow controllers. The gas mixtures were independently bubbled through a blend of the liquid tracers (3-pentanone and toluene, 50:50 per volume) which were kept at constant temperature of 293 K. The mixing cell was purged with an additional nitrogen flow that was quiescent compared to the velocities of the other two gas streams. For calibration of the LIF signal ratio, a single gas stream with identical tracer concentrations but at various well-known oxygen concentrations was used. A 248 nm laser sheet illuminated a plane up to 2 mm below the tube exits. The LIF signals were detected simultaneously with two image-intensified CCD cameras. For toluene detection a reflection bandpass filter centered at 295 ± 8 nm was used. 3-Pentanone LIF was detected with a 385 nm long-pass filter.

Results of the two-tracer imaging technique in an arrangement of interacting nitrogen (N_2) and air gas jets within a quiescent N_2-atmosphere are shown in Fig. 36. The first box 'a' shows separate LIF images from toluene and 3-pentanone. The '3P-LIF image' shows increased signal intensities in the nitrogen jet due to some spectral overlap from the strong toluene signal. This error is corrected by quantifying the relative contribution of toluene LIF to the 3-pentanone detection channel in additional experiments where the flow is seeded with toluene only. The second image shows that the ratio of signal intensities is not directly a function of oxygen number density (according to Eq. (5.3)) since the left jet (containing no oxygen) yields higher signal intensities compared to the mixing region. After correcting for energy transfer processes [110] (see also Fig. 26), this artifact disappears (right image in Fig. 36a), and the resulting signal is calibrated using a measurement in pure air. Fig. 36b shows the oxygen distribution in similar flows at slower exit velocities where the two laminar gas flows stay mostly separated. Fig. 36c shows the oxygen distribution in an air jet injected into a quiescent nitrogen atmosphere where the dilution of oxygen by entrainment of nitrogen is clearly visible. The line plot shows the oxygen concentration along the line in the 2D-image including error bars to demonstrate the sensitivity of the technique. Since only the incoming jets were seeded by tracers, the outer region does not yield any information in these measurements and is shown in black.

6. Applications: measurements in multiphase systems

In many practical combustion systems the atomization and evaporation of the fuel is the time-critical step, and combustion can occur when liquid fuel is still present. Measurement techniques that can work under such conditions and provide information about the phase and the amount of fuel that is already vaporized are important tools to study of such systems. The most promising diagnostic approach to date is based on the use of exciplex-based laser induced fluorescence [41]. This technique requires the use

of two tracers that act as an electronic donor and acceptor pair which form an excited complex or 'exciplex' after laser excitation. This complex is only stable in the liquid phase and the red-shifted fluorescence from the exciplex allows spectrally separated measurements of the liquid. The vapor phase is characterized through fluorescence from the separate monomer tracers. Particular issues with methods based on exciplex fluorescence are strong temperature-dependence of the signals of the monomers, a temperature-dependence of the formation of the excilex concentration in the liquid phase, and incomplete spectral separation of exciplex and monomer fluorescence. A clean detection of the vapor phase is especially difficult in the presence of droplets since there is also the possibility of remaining monomer molecules in the liquid phase. A more detailed discussion of this topic can be found in a review by Zhao and Ladommatos [140].

6.1. Measuring fuel concentrations

Quantitative applications to engine studies require that exciplex methods use tracer combinations that have similar evaporation characteristics as the fuel (component) that must be traced. As has been described in Section 4.3, the fluorescence signal strength for toluene (as well as for other aromatic compounds) depends strongly on the local oxygen concentration. Therefore, exciplex-based measurements that aim at the characterization of fuel concentrations usually have to be carried out in a nitrogen atmosphere. Ghandhi et al. [70] used fluorobenzene/diethylmethylamine tracer mixtures in hexane in a motored direct-injection two-stroke engine with nitrogen replacing the air. Fuel/air mixing is studied qualitatively with temperature effects on the LIF signal strength identified as a major obstacle towards quantification. Fröba et al. [69] describe the use of benzene/triethylamine mixtures to track *iso*-octane in oxygen-containing environments. They characterize the LIF signals for the tracer mixture to be inversely proportional to the local oxygen concentration. The measurements thus yield information on the local equivalence ratio, rather than the fuel concentration (cf. Section 4.3.3 for comments). This approach was applied to study the mixture formation process for different injectors in the intake runner of a port-fueled SI engine [147].

Diesel-type applications require the use of higher boiling point tracers, e.g. tetra-methyl-*p*-phenylene-diamine (TMPD)/naphthalene mixtures as they were first introduced by Melton [41]. An example of an application is the investigation of the evolution of a Diesel spray in nitrogen [148]. The same restrictions caused by the presence of oxygen as described above exist for such tracer combinations. More details on issues with quantification of this particular exciplex system are found in Felton et al. [68]. Kim et al. [149] used TMPD/naphthalene for quantitative investigations of the influence of ambient temperature and injection pressure on *n*-dodecane sprays in a high-temperature, high-pressure constant volume vessel.

6.2. Measuring phase-specific temperatures

Measurements of gas phase temperatures are reported by Beyrau et al. [150] for an evaporating *iso*-octane spray from an automotive fuel injector. Temperatures at a point in between fuel droplets could be measured with coherent anti-Stokes Raman scattering (CARS) and show the evaporative cooling in a spray. Temperature imaging via NO-LIF has been demonstrated in evaporating sprays and spray flames [151].

Mostly, temperature measurements in two-phase flows are reported for the liquid phase. The temperature-dependence of the fluorescence intensity in exciplex systems is different for the monomers and the exciplex. Murray and Melton [152] used measurements of the signal ratio of monomer and exciplex in two mixtures (0.04% DCNP/0.12% DEA/*m*-xylene and 1.0% naphthalene/2.5% TMPD/hexadecane) to determine temperatures. For non-evaporating conditions they achieved an accuracy of $\sim$1 K. Based on the same approach, Megahed [153] used a mixture of 99% hexadecane and 1% B-311(1,3-bis-(1′-pyrenyl)-propane) to measure temperature-images of sprays from a commercial Diesel fuel injector. The accuracy in this case is estimated to be 10 K. Picosecond laser excitation (35 ps) and precise timing of detection was implemented to improve the accuracy to $\sim$0.2 K for stationary conditions [154,155].

Other strategies for liquid-phase temperature measurements employ Raman scattering. Temperature-dependent linear Raman scattering in water allowed measurements of temperature profiles in stratified flows in gas and liquid phases [156]. The change of the Raman shift of methanol and ethanol with temperature was used to measure temperatures in droplets from a methanol/ethanol spray that was produced from an automotive injector [157].

Substantial effort also went into developing and using temperature measurement strategies for liquid phases that are based on fluorescence of non-evaporating laser dyes. Especially Rhodamin B has a high temperature-sensitivity to make it an attractive tracer molecule for this purpose [158–162].

7. Adverse effects of tracers

Mismatch in fuel and tracer properties with potential effects on a number of processes can lead to substantial systematic measurement errors that can prohibit quantitative interpretation of the measured LIF signals.

7.1. Droplet formation (Spray breakup)

Spray breakup depends sensitively on surface tension and viscosity of the liquid components. Different relations

are found in the literature to describe the influence of Weber *We* (momentum force/surface tension force) and Ohnesorge *Oh* (square root of Weber number/Reynolds number) numbers on droplet breakup. For a droplet of diameter d a critical relative velocity exists below which the droplet will not break up [163]. This critical velocity (represented by the critical Weber number) depends on the square root of the surface tension. Although the surface tension of a mixture does not exactly follow a simple linear relationship with mixture fraction [164], we will consider this to be the case for an estimate of the potential impact of a fluorescence tracer on the spray breakup. For *iso*-octane with a surface tension of approximately $\sigma = 18$ mN/m at 20 °C in a mixture with either 10% acetone ($\sigma = 23.7$ mN/m) or 5% toluene ($\sigma = 28.5$ mN/m) will experience a change in the critical breakup velocity of less than 2%. This effect can therefore be considered unimportant. This could change when surface-active tracers either accumulate or deplete near the surface. The effect of different viscosities via the Ohnesorge number is of similar magnitude and it is not expected to have a substantial impact on spray breakup.

7.2. Droplet vaporization

The separation of different components of a multi-component mixture via distillation is a technical process of enormous importance, e.g. to produce gasoline from crude oil or drinkable liquor from fermented fruit mixtures. In the case of a fuel/tracer mixture such a distillation effect is highly undesirable. If the fuel/tracer mixture can be evaporated and stirred before being introduced into the volume where measurements will be performed there is typically enough time and/or space to guarantee that the fuel and tracer are perfectly mixed. This method has been used to study mixing effects in engines where the fuel/tracer or air/tracer mixture was added upstream to the engine into preheated ducts (e.g. [11,165]). However, in recent years, more and more attention was put on systems where the liquid fuel and air are mixed shortly before combustion is initiated. Even in port-fuel injected systems spatial separation of different fuel components have been observed [29].

Especially for investigations of direct-injection gasoline engines, tracer LIF has found wide-spread application (see SAE technical paper series). As the fuel begins to evaporate inside the cylinder it is possible that sequential evaporation, or distillation occurs, and thus, the temporal and spatial distribution of the tracer might no longer accurately reflect the distribution of the fuel. Le Coz et al. [33] pointed out that mixtures of 3-pentanone and *iso*-octane will not evaporate like an ideal solution but that 3-pentanone concentrations in the gas phase were about twice that in the liquid phase for low 3-pentanone doping levels. More recently, Han and Steeper [30], Davy et al. [166], and Lin and Sick [32,167] have investigated this process more extensively. Han and Steeper [30] proposed the use of a ternary mixture of 3-pentanone/3-hexanone/*iso*-octane to replace 3-pentanone/*iso*-octane mixtures and their investigations indicate that measurements with a direct-injected fuel/tracer mixture that exhibits sequential evaporation indeed yields statistically different results compared to measurements performed for the ternary mixture [30].

Davy et al. [166] extended this work with numerical assessments of the 3-pentanone/*iso*-octane system. The pressure-, temperature-, and composition-dependence of phase compositions in binary tracer/fuel mixtures, like 3-pentanone/*iso*-octane and toluene/*iso*-octane was investigated numerically by Lin and Sick [32,167]. This work also addressed the influence of air on the vapor–liquid equilibrium to address the fact that the bulk of the in-cylinder mass in an engine is air and not just the tracer/fuel mixture. Neij et al. [55] found no conclusive difference in their combustion analysis for cases with added tracers. In a study of near-flame-front equivalence ratios, Rothamer and Ghandhi [168] concluded that, due to short time scales in the evaporation under engine conditions, the effect of sequential vaporization is not expected to be large. All studies essentially agree that 3-pentanone/*iso*-octane mixtures do have limitations for quantitative measurements when evaporation effects are important. This also applies to the study of evaporating fuel films [31]. However, with some evidence presented by Han and Steeper [30,169], there is no quantitative assessment of the potential implications for fuel distribution measurements available to date.

Computationally, Torres et al. [170] have developed a multi-component fuel model for KIVA 3V that describes sequential evaporation of individual fuel components when injected into an engine cylinder. Results of computations for binary mixtures of *iso*-octane/3-pentanone were performed as well but have not been published yet.

Separation of tracer and fuel in the gas phase (different transport properties) may not be important for practical fuels since the relevant mixing processes are not diffusion-controlled. For acetaldehyde/methane mixtures Tait and Greenhalgh [49] demonstrated that the differences in diffusion rates have no practical influence on imaging measurements, at least at mixture fractions higher than 0.6. Furthermore, the spatial resolution needed for measurements closer to flame fronts is not fully achieved in practical devices, and spatial averaging might alleviate the problem to some extent [168]. There could, however, be implications of differences in diffusion rates for measurements in hydrogen-fueled systems, if high-resolution measurements in the flame front are concerned and in slow flow systems where diffusion can compete with convective and turbulent mixing.

7.3. Ignition/combustion chemistry

Adding tracers of different chemical composition to a base fuel will change the overall mixture composition of

the fuel/air mixture if the amount of tracer/fuel mixture is not adjusted to reflect this change. In a spark-ignited direct-injection engine fueled with *iso*-octane Zhang et al. [171] observed an influence of the amount of added 3-pentanone on combustion performance; toluene had a much lesser effect. The amount of tracer/fuel mixture that is injected needs to be adjusted to bring the overall stoichiometry back to the undoped fueling case to avoid adverse effects on combustion.

7.4. Tracer stability

7.4.1. Breakdown in combustion environment

Typical tracers like ketones, aldehydes, aromatics, or amines have chemical structures that are quite different from model or surrogate fuels that are often used. Amongst them are *iso*-octane, *n*-heptane, and mixtures thereof. The breakdown of the molecular structure of those tracers during combustion can be substantially different from that of the parent fuel. Unimolecular reactions can lead to the decomposition of acetaldehyde and acetone [172], and if this reaction proceeds more rapidly than the decomposition of the parent fuel, the tracer will not track the fuel distribution faithfully. For acetaldehyde as a tracer in methane it was shown [49] that it is more reactive at all temperatures than the fuel. However, the difference in tracer and fuel mole fraction at mixture fractions between 1 and 0.6 is acceptably small to be ignored. Similar behavior is expected for 3-pentanone and *iso*-octane. Especially for conditions when combustion happens with regular flame propagation, any premature tracer consumption would happen close to the flame front and would not substantially affect measurements since usually the spatial resolution of imaging experiments on practical devices is not high enough to resolve the flame front anyway. This especially holds for application under elevated pressures, like in engines. However, if the fuel consumption proceeds on a more distributed scale, as is found in homogeneous-charge compression-ignition engines (HCCI), premature tracer consumption could pose a serious problem for quantitative measurements of fuel distributions. It was found that under HCCI combustion conditions 3-pentanone in *n*-heptane/*iso*-octane mixtures disappears before substantial heat release is measured [82] (cf. Section 2.2.3). Studies using *iso*-octane instead indicate no premature tracer destruction. The tracer seems to break down before the onset of the hot combustion at similar rates as the parent fuel [83]. The major difference is the presence of cool flames for low octane-number fuels. Radicals formed during the cool flame period remove the tracer. Reuss and Sick [11] have used toluene as a tracer in combination with *n*-heptane. The reactivity of aromatic compounds in flames is not that different from aliphatic compounds [173]; if anything they might be initially somewhat more stable.

7.4.2. Thermal stability in the gas phase

The thermal stability and breakdown of acetone was studied in a shocktube for temperatures of 1350–1650 K [172]. This temperature range is above temperatures that are usually of interest in fuel imaging studies. 3-Pentanone decomposition under conditions more typical for fuel imaging experiments (several hundred K) was studied by Großmann [174]. Gas chromatographic analysis showed a rapidly increasing decay of the 3-pentanone with increasing temperature. At a temperature of 573 K gas-phase 3-pentanone concentrations dropped by 50% within 1 h after injection into a heated stainless steel cell in the presence of 1 bar air. At 523 K no removal was noticed. It must be noted, however, that these experiments were conducted in a static cell where the 3-pentanone was in contact to heated stainless steel surfaces for several minutes and longer.

7.4.3. Stability in the liquid phase

Baritaud and Heinze [122] report that the decay rate for biacetyl LIF signal strength is 11% per hour. Neij et al. [55] report a decay of LIF signals in 3-pentanone/*iso*-octane mixtures over time. The origin of the observed decays is unclear at this time. Longterm studies of the chemical stability of 3-pentanone in *iso*-octane [175] indicate that 3-pentanone does not decompose. While biacetyl is chemically more reactive than 3-pentanone, it is unlikely that, in combination with *iso*-octane, the reactivity is enhanced compared to pure biacetyl. Not enough detail about the exact manner of how the tracer/fuel mixtures were stored is given in the literature, and as such it cannot be evaluated whether the higher vapor pressure of the tracers (as compared to the fuel) could be held responsible for the apparent decrease in LIF signal.

In the injection system fuel mixtures can be in contact with hot metal surfaces. Furthermore, conventional injection systems circulate fuel from the injection nozzle back to the fuel tank. The whole system is usually open to air; hence the fuel is saturated with oxygen. Under these conditions Schulz et al. [146] report the decomposition of 5-nonanone doped to n-decane fuel in experiments in a Diesel simulator. The fluorescence emission spectra change their shape after some hours of operation, and the fuel assumes a yellowish color. Changes in LIF emission spectra were observed at gas-phase temperature and detection delay after injection. However, for those conditions no tracer decomposition in the gas phase was expected according to previous measurements in shock-heated gases [146].

7.4.4. Photolytic destruction

The photolytic decomposition of fluorescence tracers is usually ignored in LIF imaging experiments. A simple experiment in open atmosphere above a small puddle of liquid where vaporized tracers like acetone, 3-pentanone or toluene are illuminated with a UV laser beam, e.g. 266 nm, reveals the presence of photolytic activity. Not only can a strong photo-acoustic signal be heard, but also the formation

of visible fumes and a change in the odor indicate that changes in the composition are happening. Diau et al. [113] report on details of the photolytic decomposition of ketones upon illumination with UV light, and Haas presents a review on photochemical a-cleavage of ketones, esp. acetone [176]. Biacetyl is especially prone to photodissociation when excited at short wavelengths, e.g. at 266 nm (frequency-quadrupled Nd:YAG laser) where the photodissociation quantum yield is 0.39; at longer wavelengths, photodissociation becomes less of a problem [177].

8. Alternative approaches to tracer techniques

8.1. Absorption

Hydrocarbon molecules (fuel) can be detected with absorption spectroscopy. A line-integrated signal is obtained in such a case. If multiple crossed absorption paths are used, tomographic reconstruction can be used to obtain multi-dimensional fuel distributions [178]. This has recently been applied to investigate a fuel spray [179]. More frequently fuel absorption measurements are used to determine the fuel concentration at the spark plug, e.g. Hall and Koenig [180]. Tomographic fuel imaging using infrared absorption was compared to LIF imaging of different fuel components by Krämer et al. [29]. Two different wavelengths in the absorption measurements were selected to be sensitive to aliphatic and aromatic hydrocarbons separately.

8.2. Raman scattering

The big advantage of Raman scattering compared to the tracer LIF techniques that were described in this paper is the potential to measure a more representative fuel concentration since all hydrocarbons will produce a Raman signal. However, no work has been done to analyze the sensitivity of the Raman signal intensity to the fuel composition. The book of Zhao and Ladommatos [181] serves as a good reference for Raman scattering studies in engines. As mentioned in Section 5.2.2, Raman scattering can be used to provide an absolute calibration signal for tracer-LIF measurements [141]. Measurements of fuel/air ratios before ignition with 1D spatial resolution have been achieved with KrF excimer lasers at 248 nm excitation [182–184]. Frequency-tripled Nd:YAG lasers (355 nm) were also used for engine research [145]. Miles discussed details of the application of frequency-doubled Nd:YAG lasers (532 nm) as a means to reduce interferences that often can plague measurements when UV lasers are used [185]. However, a range of factors is important to decide which strategy works best for a given situation. 2D-Raman in-cylinder measurement of methane [186] as well as a technique that uses a spectrometer [187] are reported but are certainly specialty applications. Slightly different Raman shifts for methanol in liquid and vaporized conditions allowed separate detection of the two phases in experiments with methanol [188].

It must be pointed out, however, that the intensity of the Raman signals is a complicated function of temperature. This is often neglected and can potentially lead to substantial errors, depending on the molecules probed and the temperature range. Full spectral simulations of the Raman spectra [189,190] or extensive calibration procedures [191] can be employed to account for this effect and are required for fully quantitative measurements.

8.3. Rayleigh scattering

The fuel distribution in a propane fueled engine was imaged with Rayleigh scattering by Zhao et al. [192]. Espey and Dec [193] have quantified the fuel concentration in the plume around a Diesel fuel jet with Rayleigh scattering. The large difference in scattering cross-sections for air compared to Diesel fuel makes this an attractive technique and allows a specific interpretation of the Rayleigh signals as representative of the fuel concentration. However, this only works in regions where no droplets are present, since otherwise Mie scattering would overwhelm the Rayleigh scattering signal. Andersson et al. [194] have studied mixing and combustion of dimethyl ether (DME) with Rayleigh imaging. Schulz et al. [146] and Vogel et al. [195] describe Rayleigh imaging experiments in a Diesel spray to assist numerical modeling of the spray and combustion process in such a spray. In comparison to LIF signals, Rayleigh signals can become comparably strong. This certainly depends on many experimental factors especially the wavelength of the exciting laser beam and the orientation of the polarization plane of the laser beam with respect to the direction of the detector [196]. Sick and Wermuth [197] reported simultaneous PLIF imaging of OH radicals and acetone for a range of mixing and combustion conditions. With an excitation wavelength of 266 nm the intensity of the Rayleigh scattering was within the same order of magnitude as the OH or acetone LIF signals.

A suitable fuel selection allowed analysis of the Rayleigh scattering cross-sections and thus permitted 2D temperature measurements in a research engine. In combination with simultaneous imaging of hydroxyl radicals, this is reported by Orth et al. [198]. Simultaneous measurements of temperature and nitric oxide distributions are presented by Schulz et al. [199].

9. Outlook

Much of the success that tracer-based imaging techniques have gained in recent years is based on improvements of the understanding of temperature-, pressure-, and composition-dependence of tracer LIF-signals. As such, it is expected that refinements of such studies will continue to

help in developing and applying quantitative imaging techniques for practical devices. The real challenges have to be faced when it comes to imaging diagnostics with regular fuels. As described in this paper, a quantification of the LIF signals from real fuels is usually not possible, at least not beyond a certain level of accuracy. This level of accuracy may be determined with a set of careful experiments to provide guidelines for measurements with real fuels. Adding tracers to real fuels, to at least enhance the quantitative measurement of some components, while overall maintaining the combustion properties of the real fuel, is a potential way towards more realistic fuel imaging. It has to be pointed out, however, that measurements with selected single- or (few) multiple-component fuels remain an interesting research field since the development of sophisticated CFD simulations with detailed chemistry will have to rely on validation experiments with well-defined boundary conditions and a limited set of chemical species. Improvements are most certainly needed in our capability of simultaneously measuring liquid and vapor phase concentration distributions as well as temperature fields.

10. Conclusions

In this paper an overview was presented on the photophysical background and strategies for applications of laser induced fluorescence imaging techniques based on fluorescence tracers to measure fuel, equivalence ratio and temperature distributions in the gas phase.

The motivation for using tracer LIF was introduced in Section 1 followed in Section 2 by an overview of tracers that had been introduced for use in gas phase systems. Section 2 covers tracers ranging from atoms to larger organic molecules. Subsequent sections of the paper focus on the characteristics and application of organic molecules. A section on the fundamental photophysics of organic molecules in general (Section 3) explained processes that form the background on which the understanding and description of laser-induced fluorescence signal generation is based.

Two types of molecules, ketones, and small aromatic compounds are most frequently used as tracer molecules. While literature is available on additional molecules, like amines and aldehydes, the use of ketones and small aromatics has found highest attention and widespread use in many applications. Section 4 describes specific details about the photophysics of acetone and 3-pentanone as representatives of ketones. Biacetyl, a representative for diketones, and toluene, an example of an aromatic, were addressed in this section as well.

Experimental investigations of the temperature-, pressure-, and composition-dependence of the fluorescence signal strength for ketones under well-defined conditions have led to the development of a phenomenological model for ketone photophysics. Along with descriptions of the experimental results, the successes and shortcomings of this model were explained. This illustrated how critical the fundamental understanding of the photophysics of a fuel tracer is when using the predictions of such a model for quantitative diagnostics. Despite the fact that ketones can be considered as the best-studied tracers for which elaborate models for signal predictions are available, recent experiments showed that there still is a significant lack of fundamental studies for the high-pressure, high-temperature regime that is highly relevant for applications in practical combustion environments. Current concepts that are based on the extrapolation of low-temperature or low-pressure data can lead to erroneous results. Further investigation of ketone photophysics will therefore continue to be an important and active field of research.

Only a brief excursion was given to address the use of biacetyl as a potential fluorescence tracer. Little has been published on the fluorescence behavior of biacetyl for application under high-pressure, high-temperature conditions but there is reason to believe that this should be done.

Toluene was chosen as a representative for aromatics because of its frequent use as a tracer. Because of the susceptibility of excited aromatic molecules to quenching by molecular oxygen, toluene LIF measurements have been suggested for direct assessment of fuel/air ratios. This technique quickly became popular for diagnostics in internal combustion engine experiments. Recent experiments, however, showed that the oxygen-susceptibility of toluene strongly decreases with increasing temperature. The applicable range of the fuel/air-LIF imaging technique is therefore limited. A simple model for toluene-LIF was presented that captured some of the observed signal behavior but the knowledge about aromatics fluorescence signal strength is far from satisfactory at this time.

In many tracer LIF applications signals have been calibrated at conditions close to that of the 'real' measurement. These approaches include calibration with motored engine operation to determine signal strength as a function of (combined) pressure and temperature. This approach has worked reasonably well since calibration conditions and unknown process conditions were very close to each other. Caution has to be applied when extrapolating far out beyond known signal conditions.

Section 5 described exemplary tracer-LIF applications. Without giving a complete overview, this section illustrates how tracer-LIF can be used to measure fuel concentrations, equivalence ratios, and temperature in different situations. Measurements of fuel/air mixing under isothermal conditions are amongst the simplest applications of tracer-LIF and provide substantial insight into technologically relevant processes. Two- and three-dimensional imaging measurements were discussed in this section. The temperature-dependence of ketone fluorescence was exploited as a means to measure temperature distributions in open atmosphere experiments as well as in engines. The issue with quantification of tracer-LIF measurements under variable pressure and temperature conditions was described for

a range of engine applications. Simultaneous variation of temperature and pressure can lead to ambiguous signal levels, in which case combinations of tracers can be used to gain additional information. For example, oxygen concentrations were measured using a combination of toluene and 3-pentanone as tracers, exploiting the difference in their susceptibility to quenching by molecular oxygen. Further concepts use detection or excitation at more than one wavelength in order to gain additional information.

The lack of discrimination between liquid and gas phase signals was introduced with these examples and remains one of the big problems of tracer-LIF for many applications. Since the scope of the present paper was to review the status and potential of tracer-LIF techniques for gas phase systems, Section 6 gave only a brief summary of approaches for multiphase systems.

Tracer addition can potentially affect many aspects of the investigated system. Section 7 addressed these issues ranging from physical processes, like droplet formation and evaporation, to effects on the chemistry in the case of combustion processes and tracer decomposition at high temperatures. Dynamic effects on the evaporation, i.e. preferential evaporation of either tracer or fuel, are not fully understood and are usually ignored. This will have to be quantified to allow high-fidelity measurements in systems where evaporation plays a dominant role in controlling the process under study, e.g. many direct-injection engine systems. Evidence was found that the addition of large amounts of tracers could alter the combustion process as well. If, for diagnostic reasons, e.g. signal strength, the amount of tracer cannot be reduced, the data analysis and especially comparison to models must include the presence of tracer in the fuel.

Section 8 addressed absorption and Raman and Rayleigh scattering as potentially alternative techniques to tracer-LIF along with a few examples. An outlook in Section 9 on some of the future issues with tracer-LIF techniques gives the authors' perspective on this subject.

This paper presented the state of the art of tracer-LIF application to a variety of combustion-related diagnostics situations. Tracer-LIF experiments falsely give the researcher the impression to be straight-forward. They often yield strong signals and do not require sophisticated, i.e. tunable, laser sources. Therefore, tracer-LIF applications quickly became popular in research and development. The photophysical background of the tracer-LIF signal, however, was often investigated a posteriori when applications indicated significant deviations from the expected results. Even recent measurements clearly indicated that there is still an important lack of fundamental understanding of the underlying photophysics. This still prevents the extrapolation of signal strengths from a calibration condition to high-pressure, high-temperature conditions in the compression stroke of internal combustion engines even for the best-studied tracers. What is characterized as 'quantitative measurement' in earlier papers must often be reconsidered as 'evaluated based on the best knowledge available at that time'. This especially applies if measurements are compared over a wide range of pressure, temperature, and gas composition conditions.

Tracer-LIF techniques will remain an important tool for a large variety of practical situations. They will become even more relevant in the future because many modern combustion systems require detailed knowledge of fuel distribution. This will raise the standards for quantitative data interpretation and multi-parameter measurements even more. The investigation of the photophysics of the underlying fluorescing tracer will therefore continue to be an important field of research.

Acknowledgements

The authors would like to thank Wieland Koban (PCI, University of Heidelberg) for critically reading the manuscript. Financial support from DFG within WO175/36, SCHU 1369/2 and SFB359, from the European Commission, and NSF under contract INT0089227 for Volker Sick is acknowledged.

References

[1] Neij H, Aldén M. Application of two-photon laser-induced fluorescence for visualization of water vapor on combustion environments. Appl Opt 1994;33:6514–23.
[2] Bessler WG, Schulz C, Lee T, Jeffries JB, Hanson RK. Carbon dioxide UV laser-induced fluorescence in high-pressure flames. Chem Phys Lett 2003;375:344–9.
[3] Roller A, Arnold A, Decker M, Sick V, Wolfrum J, Hentschel W. Non-intrusive temperature measurements during the compression phase of a DI Diesel engine. SAE technical paper series 952461; 1995.
[4] Drake MC, Fansler TD, French DT. Crevice flow and combustion visualization in a direct-injection spark-ignition engine using laser imaging techniques. SAE technical paper series 952454; 1995.
[5] Dec JE, Keller JO. High speed thermometry using two-line atomic fluorescence. Proc Combust Inst 1986;21: 1737–45.
[6] Kaminski CF, Engström J, Aldén M. Quasi-instantaneous two-dimensional temperature measurements in a spark ignition engine using 2-line atomic fluorescence. Proc Combust Inst 1998;27:85–93.
[7] Wolfrum J. Lasers in combustion: from basic theory to practical devices. Proc Combust Inst 1998;27:1–42.
[8] McMillin BK, Palmer JL, Hanson RK. Temporally resolved, two-line fluorescence imaging of NO temperature in a transverse jet in a supersonic cross flow. Appl Opt 1993; 32:7532–45.
[9] Bessler WG, Schulz C. Quantitative multi-line NO-LIF temperature imaging. Appl Phys B 2004;78:519–33.

[10] Bessler WG, Schulz C, Lee T, Jeffries JB, Hanson RK. Strategies for laser-induced fluorescence detection of nitric oxide in high-pressure flames: III. Comparison of A-X strategies. Appl Opt 2003;42:4922–36.
[11] Reuss DL, Sick V. Investigation of HCCI combustion with combined PLIF imaging and combustion analysis. In: Third joint meeting of the US sections of the Combustion Institute, Chicago, IL; 2003.
[12] Pitz RW, Wehrmeyer JA, Ribarov LA, Oguss DA, Batliwala F, DeBarber PA, et al. Unseeded molecular flow tagging in cold and hot flows using ozone and hydroxyl tagging velocimetry. Meas Sci Technol 2000;11:1259–71.
[13] Orlemann C, Schulz C, Wolfrum J. NO-flow tagging by photodissociation of NO_2. A new approach for measuring small-scale flow structures. Chem Phys Lett 1999;307:15–20.
[14] Dam N, Klein-Douwel RJH, Sijstema N, ter Meulen J. Nitric oxide flow tagging in unseeded air. Opt Lett 2001;26:36–8.
[15] Lee MP, Hanson RK. Calculations of O_2 absorption and fluorescence at elevated temperatures for a broadband argon-fluoride laser source at 193 nm. J Quant Spectrosc Radiat Transfer 1986;36:425–40.
[16] Miles RB, Lempert W, Zhang B. Turbulence structure measurement by RELIEF flow tagging. Fluid Dyn Res 1991; 8:9–17.
[17] Hiller B, Hanson R. Properties of the iodine molecule relevant to laser-induced fluorescence experiments in gaseous flows. Exp Fluids 1990;10:1–11.
[18] Greenough K, Duncan A. The fluorescence of sulfur dioxide. J Am Chem Soc 1961;83:555–60.
[19] Mettee H. Fluorescence and phosphorescence of SO_2 vapor. J Chem Phys 1968;49:1784–93.
[20] Strickler SJ, Howell D. Luminescence and radiation transitions in sulfur dioxide gas. J Chem Phys 1968;49: 1947–51.
[21] Sick V. Exhaust-gas imaging via planar laser-induced fluorescence of sulfur dioxide. Appl Phys B 2002;74:461–3.
[22] Rao T, Collier S, Calvert J. Primary photophysical processes in the photochemistry of sulfur dioxide at 2875 Å. J Am Chem Soc 1969;91:1609–15.
[23] Rao T, Collier S, Calvert JG. The quenching reactions of the first excited singlet and triplet states of sulfur dioxide with oxygen and carbon dioxide. J Am Chem Soc 1969;91: 1616–21.
[24] Caton R, Duncan A. Lifetime of the lowest triplet state of sulfur dioxide. J Am Chem Soc 1968;90:1945–9.
[25] Lozano A. Laser-excited luminescent tracers for planar concentration measurements in gaseous jets. PhD Thesis, Stanford University; 1992.
[26] Cattolica RJ. Combustion-torch ignition: fluorescence imaging of NO_2. Proc Combust Inst 1986;21:1551–9.
[27] Zhao F-Q, Taketomi M, Nishida K, Hiroyasu H. PLIF measurements of the cyclic variation of mixture concentration in a SI engine. SAE technical paper 940988; 1994.
[28] Warnatz J, Maas U, Dibble RW. Combustion. 3rd ed. Heidelberg: Springer; 2001.
[29] Krämer H, Einecke S, Schulz C, Sick V, Nattrass SR, Kitching JS. Simultaneous mapping of the distribution of different fuel volatility classes using tracer-LIF and NIR tomography in an IC engine. SAE Trans J Fuels Lubric 1998; 107:1048–59.
[30] Han D, Steeper RR. An LIF equivalence ratio imaging technique for multicomponent fuels in an IC engine. Proc Combust Inst 2002;29:727–34.
[31] Lin M-T, Sick V. Mixture evaporation characteristics prediction for LIF measurements using PSRK (predictive Soave–Redlich–Kwong) equation of state. SAE Trans J Fuels Lubric 2002;1490–9.
[32] Lin M-T, Sick V. Is toluene a suitable LIF tracer for fuel film measurements? SAE technical paper series 2004-01-1355; 2004.
[33] le Coz JF, Catalano C,Baritaud T. Application of laser-induced fluorescence for measuring the thickness of liquid films on transparent walls. In: Seventh international symposium on applications of laser techniques to fluid mechanics II; 1994. p. 29.3.1–8.
[34] Fansler TD, French DT, Drake MC. Fuel distributions in a firing direct-injection spark-ignition engine using laser-induced fluorescence imaging. SAE technical paper series 950110; 1995.
[35] Greenhalgh DA, Bryce DF, Lockett RD, Harding SC. Development of planar laser induced fluorescence for fuel: application to gas turbine combustion. In: AGARD PEP symposium on advanced non-intrusive instrumentation for propulsion engines, Brussels, Belgium; 1997.
[36] Hentschel W, Block B, Hovestadt T, Meyer H, Ohmstede G, Richter V, et al. Optical diagnostics and CFD-simulations to support the combustion process development of the Volkswagen FSI direct injection gasoline engine. SAE technical paper series 2001-01-3648; 2001.
[37] Reboux J, Puechberty D. A new approach of PLIF applied to fuel/air ratio measurement in the compression stroke of an optical SI engine. SAE technical paper series 941988; 1994.
[38] Koban W, Koch JD, Hanson RK, Schulz C. Toluene fluorescence quenched by molecular oxygen: non-constant Stern–Volmer coefficients. Appl Phys B 2004 (in review).
[39] Koban W, Koch JD, Sick V, Wermuth N, Hanson RK, Schulz C. Predicting LIF signal strength for toluene and 3-pentanone under engine-related temperature and pressure conditions. Proc Combust Inst 30 (in press).
[40] Kaiser, SA, Long MB. The effect of temperature and quenching on laser-induced fluorescence of naphtalenes as JP-8 tracers. In: Chemical and physical processes in combustion, 2003 Technical meeting of the eastern states section of the Combustion Institute, Pennsylvania State University, University Park, PA; 2003.
[41] Melton LA. Spectrally separated fluorescence emissions for Diesel fuel droplets and vapor. Appl Opt 1983;22: 2224–6.
[42] Lozano A, Yip B, Hanson K. Acetone: a tracer for concentration measurements in gaseous flows by planar laser-induced fluorescence. Exp Fluids 1992; 13:369–76.
[43] Großmann F, Monkhouse PB, Ridder M, Sick V, Wolfrum J. Temperature and pressure dependencies of the laser-induced fluorescence of gas-phase acetone and 3-pentanone. Appl Phys B 1996;62:249–53.
[44] Yuen L, Peters J, Lucht R. Pressure dependence of laser-induced fluorescence from acetone. Appl Opt 1997;36: 3271–7.

[45] Ossler F, Aldén M. Measurements of picosecond laser-induced fluorescence from gas-phase 3-pentanone and acetone: implications to combustion diagnostics. Appl Phys B 1997;64:493–502.
[46] Koch JD, Hanson RK. Temperature and excitation wavelength dependencies of 3-pentanone absorption and fluorescence for PLIF applications. Appl Phys B 2003;76:319–24.
[47] Koch J, Hanson RK. Ketone photophysics for quantitative PLIF imaging. AIAA paper 2001-0413; 2001.
[48] Ghandhi JB, Felton PG. On the fluorescence behavior of ketones at high temperatures. Exp Fluids 1996;21:143–4.
[49] Tait NP, Greenhalgh DA. 2D laser induced fluorescence imaging of parent fuel fraction in nonpremixed combustion. Proc Combust Inst 1992;24:1621–8.
[50] Wolff D, Schlüter H, Beushausen V, Andresen P. Quantitative determination of fuel air mixture distributions in an internal combustion engine using PLIF of acetone. Ber Bunsenges Phys Chem 1993;97:1738–41.
[51] Berckmuller M, Tait N, Lockett RD, Greenhalgh DA. In-cylinder crank-angle-resolved imaging of fuel concentration in a firing spark-ignition engine using planar laser-induced fluorescence. Proc Combust Inst 1994;25:151–6.
[52] Dawson M, Hochgreb S. Liquid fuel visualization using laser-induced fluorescence during cold start. SAE technical paper series 982466; 1998.
[53] Green RM, Cloutman LD. Planar LIF observations of unburned fuel escaping the upper ring-land crevice in an SI engine. SAE technical paper series 970823; 1997.
[54] Bryant R, Driscoll JF. Acetone laser induced fluorescence for low pressure, low temperature flow visualization. Exp Fluids 2000;28:417–76.
[55] Neij H, Johansson B, Aldén M. Development and demonstration of 2D-LIF for studies of mixture preparation in SI engines. Combust Flame 1994;99:449–57.
[56] Arnold A, Buschmann A, Cousyn B, Decker M, Vannobel F, Sick V, et al. Simultaneous imaging of fuel and hydroxyl radicals in an in-line four cylinder SI engine. SAE technical paper series 932696; 1993.
[57] Arnold A, Becker H, Suntz R, Monkhouse P, Wolfrum J, Maly R, et al. Flame front imaging in an internal-combustion engine simulator by laser-induced fluorescence of acetaldehyde. Opt Lett 1990;15:831–3.
[58] Swindal JC, Dragonetti DP, Hahn RT, Furman PA, Acker WP. In-cylinder charge homogeneity during cold-start studied with fluorescent tracers simulating different fuel distillation temperatures. SAE technical paper series 950106; 1995.
[59] Hansen DA, Lee EKC. Radiative and nonradiative transitions in the first excited singlet state of simple linear aldehydes. J Chem Phys 1975;62:3272–7.
[60] Hansen DA, Lee EK. Radiative and nonradiative transistions in the first excited singlet state of symmetrical methyl-substituted acetones. J Chem Phys 1975;62:183–9.
[61] Gandini A, Kutschke K. Primary processes in photolysis of hexafluoroacetone vapor. 2. Fluorescence and phosphorescence. Proc R Soc Lond Ser A 1968;306:511–28.
[62] Gandini A, Kutschke KO. The effect of mercury on the triplet state of hexafluoroacetone. Ber Bunsenges Phys Chem 1968; 72:296–301.
[63] Okabe H, Noyes WA. The relative intensities of fluorescence and phosphorescence in biacetyl vapor. J Am Chem Soc 1957;79:801–6.
[64] Sidebottom HW, Badcock CC, Calvert JG, Rabe BR, Damon EK. Lifetime studies of the biacetyl excited singlet and triplet states in the gas phase at 25 °C. J Am Chem Soc 1972;94:13–19.
[65] Liu JB, Pan Q, Liu CS, Shi JR. Principles of flow field diagnostics by laser induced biacetyl phosphorescence. Exp Fluids 1988;6:505–13.
[66] Pringsheim P. Fluorescence and phosphorescence. New York: Interscience Publishers; 1949.
[67] Itoh T, Kakuho A, Hishinuma H, Urushihara T, Takagi Y, Horie K, et al. Development of a new compound fuel and fluorescent tracer combination for use with laser-induced fluorescence. SAE technical paper series 952465; 1995.
[68] Felton PG, Bracco FV, Bardsley MEA. On the quantitative application of exciplex fluorescence to engine sprays. SAE technical paper series 930870; 1993.
[69] Fröba AP, Rabenstein F, Münch KU, Leipertz A. Mixture of triethylamine and benzene as a new seeding material for the quantitative two-dimensional laser-induced exciplex fluorescence imaging of vapor and liquid fuel inside SI engines. Combust Flame 1998;112:199–209.
[70] Ghandhi JB, Felton PG, Gajdezko DF, Bracco FV. Investigation of the fuel distribution in a two-stroke engine with an air-assisted injector. SAE technical paper series 940394; 1994.
[71] Arden-Jacob J, Frantzeskos J, Kemnitzer NU, Zilles A, Drexhage KH. New fluorescent markers for the red region. Spectrochim Acta 2001;57A:2271–83.
[72] Brackmann U. Lambdachrome laser dyes. Göttingen: Lambda Physik; 1997.
[73] Sauer M, Schulz C, Wolfrum J. Laser in combustion and biology: from diatomics to DNA. Heidelberg: Springer; 1999.
[74] Sauer M, Ankenbauer W, Angerer B, Földes-Papp Z, Göbel F, Han K-T, et al. Single molecule DNA sequencing in submicrometer channels: state of the art and future prospects. J Biotechnol 2001;86:181–201.
[75] Düwel I, Kunzelmann T, Schorr J, Schulz C, Wolfrum J. Application of fuel tracers with different volatilities for planar LIF/Mie drop sizing in evaporating systems. In: ICLASS-Europe, paper 9-3, Sorrento; 2003.
[76] Düwel I, Schorr J, Peuser P, Zeller P, Wolfrum J, Schulz C. Spray diagnostics using an all solid-state Nd:$YAlO_3$ laser and fluorescence tracers in commercial gasoline and Diesel fuels. Appl Phys B 2004;79:249–54.
[77] Jermy MC, Greenhalgh D. Planar dropsizing by elastic and fluorescence scattering in sprays too dense for phase Doppler measurement. Appl Phys B 2000;71:703–10.
[78] Andresen P, Meijer G, Schlüter H, Voges H, Koch A, Hentschel W, et al. Fluorescence imaging inside an internal combustion engine using tunable excimer lasers. Appl Opt 1990;29:2392–404.
[79] Weaver C, Wooldridge S, Johnson S, Sick V, Lavoie G. PLIF measurements of fuel distribution in a PFI engine under cold start conditions. SAE technical paper series 2003-01-3236; 2003.
[80] Greenhalgh DA. Laser imaging of fuel injection systems and combustors. Proc Inst Mech Eng 2000;214:367–76.
[81] Kazenwadel J, Koban W, Kunzelmann T, Schulz C. Fluorescence imaging of natural gas/air mixing without tracers added. Chem Phys Lett 2001;345:259–64.

[82] Graf N, Gronki J, Schulz C, Baritaud T, Cherel J, Duret P, et al. In-cylinder combustion visualization in an auto-igniting gasoline engine using fuel tracer- and formaldehyde-LIF imaging. SAE technical paper series 2001-01-1924; 2001.
[83] Nygren J, Hult J, Richter M, Aldén M, Christensen M, Hultqvist A, et al. Three-dimensional laser induced fluorescence of fuel distributions in an HCCI engine. Proc Combust Inst 2002;29:679–85.
[84] Schießl R, Maas U. Analysis of endgas temperature fluctuations in an SI engine by laser-induced fluorescence. Combust Flame 2003;133:19–27.
[85] Hildenbrand F, Schulz C, Sick V, Jander H, Wagner HG. Applicability of KrF excimer laser induced fluorescence in sooting high-pressure flames. In: VDI Flammentag Dresden, VDI Berichte 1492; 1999. p. 269–74 (ISBN 3-18-091492-0).
[86] Berten H-O, Kleinermanns K. Determination of spatial temperature distributions in a laminar premixed ethylene/air flame by laser-induced atomic fluorescence. Appl Phys B 1995;61:605–10.
[87] Cattolica R. OH rotational temperature from two-line laser-excited fluorescence. Appl Opt 1981;20:1156–66.
[88] Tamura M, Luque J, Harrington JE, Berg PA, Smith GP, Jeffries JB, et al. Laser-induced fluorescence of seeded nitric oxide as a flame thermometer. Appl Phys B 1998;66: 503–10.
[89] Tsujishita M, Hirano A, Yokoo M, Sakuraya T, Takeshita Y. Accurate thermometry using NO and OH laser-induced fluorescence in an atmospheric pressure flame. JSME Int J Ser B 1999;42:119.
[90] Meier UE, Wolff-Gaßmann D, Stricker W. LIF imaging 2D temperature mapping in a model combustor at elevated pressure. Aerosp Sci Technol 2000;4:403–14.
[91] Hartlieb AT, Atakan B, Kohse-Höinghaus K. Temperature measurement in fuel-rich non-sooting low-pressure hydrocarbon flames. Appl Phys B 2000;70:435–45.
[92] Bessler WG, Hildenbrand F, Schulz C. Two-line laser-induced fluorescence imaging of vibrational temperatures of seeded NO. Appl Opt 2001;40:748–56.
[93] Einecke S, Schulz C, Sick V. Measurement of temperature, fuel concentration and equivalence ratio fields using tracer LIF in IC engine combustion. Appl Phys B 2000; 71:717–23.
[94] Thurber MC, Grisch F, Hanson RK. Temperature imaging with single- and dual-wavelength acetone planar laser-induced fluorescence. Opt Lett 1997;22:251–3.
[95] Einecke S, Schulz C, Sick V, Dreizler A, Schießl R, Maas U. Two-dimensional temperature measurements in an SI engine using two-line tracer LIF. SAE technical paper series 982468; 1998.
[96] Koban W, Koch JD, Hanson RK, Schulz C. Absorption and fluorescence of toluene vapor at elevated temperatures. Phys Chem Chem Phys 2004;6:2940–5.
[97] Koban W, Lewerich B, Schulz C. Temperature imaging based on toluene laser-induced fluorescence. Appl Phys B (in preparation).
[98] Gossage HE, Melton LA. Fluorescence of pyrene. Appl Opt 1988;27:2256.
[99] Peterson DL, Lytle FE, Laurendeau NM. Flame temperature measurements using the anomalous fluorescence of pyrene. Appl Opt 1988;27:2768–75.
[100] Deschamps B, Baritaud T. Visualization of gasoline and exhaust gases distribution in a 4-valve SI engine; effects of stratification on combustion and pollutants. SAE technical paper series 961928; 1996.
[101] Frieden D, Sick V, Gronki J, Schulz C. Quantitative oxygen imaging in an engine. Appl Phys B 2002;75:137–41.
[102] Kienle R, Lee MP, Kohse-Höinghaus K. A scaling formalism for the representation of rotational energy transfer in OH A in combustion experiments. Appl Phys B 1996;63:403–18.
[103] Förster T. Zwischenmolekulare energieumwandlung und fluoreszenz. Annalen der Physik 1948;2:55–75.
[104] Dexter DL. A theory of sensitized luminescence in liquids. J Chem Phys 1953;21:836.
[105] Birks JB. Energy transfer in organic systems. J Phys B 1970; 3:417.
[106] Brown RG, Phillips D. Quenching of the first excited singlet state of substituted benzenes by molecular oxygen. Trans Faraday Soc II 1974;70:630.
[107] Kikuchi K, Sato C, Watabe M, Ikeda H, Takahashi Y, Miyashi T. New aspects on fluorescence quenching by molecular oxygen. J Am Chem Soc 1993;115:5180–4.
[108] Nau WM, Scaiano JC. Oxygen quenching of excited aliphatic ketones and diketones. J Phys Chem 1996;100:11360–7.
[109] Yip B, Lozano A, Hanson RK. Sensitized phophorescence: a gas phase molecular mixing diangostic. Exp Fluids 1994;17: 16–23.
[110] Koban W, Schorr J, Schulz C. Oxygen distribution imaging with a novel two-tracer laser-induced fluorescence technique. Appl Phys B 2002;74:111–4.
[111] Bunker PR, Jensen P. Molecular symmetry and spectroscopy, 2nd ed. Ottawa, Ont.: NRC Research Press; 1998.
[112] Heicklen J. The fluorescence and phosphorescence of biacetyl vapor and acetone vapor. J Am Chem Soc 1958; 81:3863–6.
[113] Diau EW-G, Kötting C, Zewail A. Femtochemistry of Norrish type-I reactions: 1. Experimental and theoretical studies of acetone and related ketones on the S1 surface. Chem Phys Chem 2001;2:273–93.
[114] Thurber MC, Kirby BJ, Hanson RK. Instantaneous imaging of temperature and mixture fraction with dual-wavelength acetone PLIF. In: 36th AIAA aerospace sciences meeting and exhibit, Reno, NV; 1998.
[115] Thurber MC, Grisch F, Kirby BJ, Votsmeier M, Hanson RK. Measurements and modeling of acetone laser-induced fluorescence with implications for temperature-imaging diagnostics. Appl Opt 1998;37:4963–78.
[116] Sulzer P, Wieland K. Intensitätsverteilung eines kontinuierlichen Absorptionsspektrums in Abhängigkeit von Temperatur und Wellenzahl. Helv Phys Acta 1952;25:653–76.
[117] Astholz DC, Brouwer L. High temperature ultraviolet absorption spectra of polyatomic molecules in shock waves. Ber Bunsenges Phys Chem 1981;85:559–64.
[118] Thurber MC, Hanson RK. Pressure and composition dependence of acetone laser-induced fluorescence with excitation at 248, 266 and 308 nm. Appl Phys B 1999;69: 229–40.
[119] Hippler H, Troe J, Wendelken H. Collisional deactivation of vibrationally highly excited polyamtomic molecules III. Direct observation for substituted cycloheptatrienes. J Chem Phys 1983;78:6718–24.

[120] Shimanouchi T. Tables of molecular vibrational frequencies, consolidated volume I. Natl Stand Data Ser Natl Bur Stand 1972;39.
[121] Lee EKC, Lewis RS. Photochemistry of simple aldehydes and ketones in the gas phase. Adv Photochem 1980;12: 1–95.
[122] Baritaud TA, Heinze TA. Gasoline distribution measurements with PLIF in an SI engine. SAE technical paper series 922355; 1992.
[123] Burton CS, Noyes WA. Electronic energy relaxation in toluene vapour. J Chem Phys 1968;49:1705.
[124] Lenzer T, Luther K, Reihs K, Symonds AC. Collisional energy transfer probabilities of highly excited molecules from kinetically controlled selective ionization (KCSI). II. The collisional relaxation of toluene: $P(E', E)$ and moments of energy transfer for energies up to 50 000 cm^{-1}. J Chem Phys 2000;112:4090–110.
[125] Toselli BM, Brenner JD, Yerram ML, Chin WE, King KD, Barker JR. Vibrational relaxation of highly excited toluene. J Chem Phys 1991;95:176–88.
[126] Ni T, Melton A. Fluorescence lifetime imaging: an approach for fuel equivalence ratio imaging. Appl Spectrosc 1991;45: 938–43.
[127] Koban W, Schulz C. Oxygen concentration imaging based on toluene laser-induced fluorescence. Appl Phys B (in preparation).
[128] Sacadura JC, Robin L, Dionnet F, Gervais D, Gastaldi P, Ahmed A. Experimental investigation of an optical direct injection SI engine using FARLIF. SAE technical paper series 2000-01-1794; 2000.
[129] Koban W, Koch J, Hanson RK, Schulz C. Toluene LIF at elevated temperatures: implications for fuel-air ratio measurements. Appl Phys B (in press).
[130] Hoffmann A, Zimmermann F, Scharr H, Krömker S, Schulz C. Instantaneous three-dimensional visualization of concentration distributions in turbulent flows with crossed-plane laser-induced fluorescence imaging. Appl Phys B (in press).
[131] Yip B, Fourguette DC, Long MB. Three-dimensional gas concentration and gradient measurements in a photoacoustically perturbed jet. Appl Opt 1986;25:3919–23.
[132] Landenfeld T, Kremer A, Hassel EP, Janicka J, Schäfer T, Kazenwadel J, et al. Laserdiagnostic and numerical studies of strongly swirling natural-gas flames. Proc Combust Inst 1998;27:1023–30.
[133] Knaus DA, Gouldin FC, Hinze PC, Miles PC. Measurement of instantaneous flamelet surface normals and the burning rate in a SI engine. SAE technical paper series no. 1999-01-3543; 1999.
[134] Knaus DA, Gouldin FC. Measurement of flamelet orientations in premixed flames with positive and negative Markstein numbers. Proc Combust Inst 2000;28:367–73.
[135] Sattler SS, Gouldin FC, Boertlein NT. Combined crossed-plane imaging and stereo-particle image velocimetry. In: Third joint meeting of the US sections of the Combustion Institute, Chicago, IL; 2003.
[136] Knaus DA, Gouldin FC, Bingham DC. Assessment of crossed-plane tomography for flamelet surface normal measurements. Combust Sci Technol 2002;174:101–34.
[137] Hoffmann A, Zimmermann F, Schulz C. Instantaneous three-dimensional visualization of concentration distributions in turbulent flows with a single laser. In: Arcoumanis C, editor. Optical and laser diagnostics. Bristol: Institute of Physics; 2002. p. 45–51.
[138] Tait NP, Greenhalgh DA. PLIF imaging of fuel fraction in practical devices and LII imaging of soot. Ber Bunsenges Phys Chem 1993;97:1619.
[139] Fujikawa T, Hattori Y, Aklhama K. Quantitative 2-D fuel distribution measurements in an SI engine using laser-induced fluorescence with suitable combination of fluorescence tracer and excitation wavelength. SAE technical paper series 972944; 1997.
[140] Zhao H, Ladommatos N. Optical diagnostics for in-cylinder mixture formation measurements in IC engines. Prog Energy Combust Sci 1998;24:297–336.
[141] Richter M, Axelsson B, Nyholm K, Aldén M. Real-time calibration of planar laser-induced fluorescence air–fuel ratio measurements in combustion environments using in situ Raman scattering. Proc Combust Inst 1998;27:51–7.
[142] Ipp W, Egermann J, Wagner V, Leipertz A. Visualization of the qualitative fuel distribution and mixture formation inside a transparent GDI engine with 2D MIE and LIEF techniques and comparison to quantitative measurements of the air/fuel ratio with 1D Raman spectroscopy. SAE technical paper series 2000-01-1793; 2000.
[143] Medaerts F, Puechberty D. In-cylinder fuel/air mixture and flame front visualization in a transparent engine using PLIF: a comparison between natural gas and gasoline used as a fuel. SAE technical paper series 982524; 1998.
[144] Frieden D, Sick V. Investigation of the fuel injection, mixing and combustion processes in an SIDI engine using quasi-3D LIF imaging. SAE technical paper series 2003-01-0068; 2003.
[145] Ipp W, Egermann J, Schmitz I, Wagner V, Leipertz A, Hartmann M, et al. 2D mapping and quantification of the in-cylinder air/fuel ratio in a GDI engine by means of LIF and comparison to simultaneous results from 1D Raman measurements. SAE technical paper series 2001-01-1977; 2001.
[146] Schulz C, Gronki J, Andersson S. Multi-species laser-based imaging measurements in a Diesel spray. SAE technical paper series 2004-01-1917; 2004.
[147] Münch K-U, Krämer H, Leipertz A. Investigation of fuel evaporation inside the intake of a SI engine using laser-induces exciplex-fluorescence with a new seed. SAE technical paper series 961930; 1996.
[148] Yeh C-N, Kamimoto T, Kobori S, Kosaka H. 2D imaging of fuel vapor concentration in a Diesel spray via exciplex-based fluorescence technique. SAE technical paper series 932652; 1993.
[149] Kim T, Beckman MS, Farrell PV, Ghandhi JB. Evaporating spray concentration measurements from small and medium bore Diesel injectors. SAE technical paper series 2002-01-0219; 2002.
[150] Beyrau F, Bruer A, Seeger T, Leipertz A. Gas-phase temperature measurement in the vaporizing spray of a gasoline direct-injection injector by use of pure rotational coherent anti-Stokes Raman scattering. Opt Lett 2004;29:247–9.
[151] Kronemayer H, Bessler W, Schulz C. Gas-phase temperature measurements in evaporating sprays and spray flames based on NO multiline LIF. Appl Phys B (in preparation).
[152] Murray AM, Melton LA. Fluorescence methods for determination of temperature in fuel sprays. Appl Opt 1985;24: 2783–7.

[153] Megahed M. First measurements of the liquid phase temperature in Diesel sprays. SAE technical paper series 930969; 1993.
[154] Parigger C, Plemmons DH, Litchford RJ, Jeng SM. Exciplex liquid-phase thermometer using time-resolved laser-induced fluorescence. Opt Lett 1998;23:76–8.
[155] Escobar S, González JE, Rivera LA. Laser-induced fluorescence temperature sensor for in-flight droplets. Exp Heat Transfer 2001;14:119–34.
[156] Karl J, Weiss T. Measurement of condensation heat transfer coefficients at stratified flow using linear Raman spectroscopy. In: The first Pacific symposium on flow visualisation and image processing, Honolulu; 1997. p. 479–84.
[157] Müller T, Grünefeld G, Beushausen V. High-precision measurement of the temperature of methanol and ethanol droplets using spontaneous Raman scattering. Appl Phys B 2000;70:155–8.
[158] Seuntiens HJ, Kieft RN, Rindt CCM, Van Steenhoven AA. 2D temperature measurements in the wake of a heated cylinder using LIF. Exp Fluids 2001;31:588–95.
[159] Sakakibara J, Adrian RJ. Whole field measurement of temperature in water using two-color laser induced fluorescence. Exp Fluids 1999;26:7–15.
[160] Lavieille P, Lemoine F, Lavergne G, Virepinte JF, Lebouché M. Temperature measurements on droplets in monodisperse stream using laser-induced fluorescence. Exp Fluids 2000;29:429–37.
[161] Lavieille P, Lemoine F, Lavergne G, Lebouché M. Evaporating and combusting droplet temperature measurements using two-color laser-induced fluorescence. Exp Fluids 2001; 31:45–55.
[162] Lavieille P, Lemoine F, Lebouché M. Investigation on temperature of evaporating droplets in linear stream using two-color laser-induced fluorescence. Combust Sci Technol 2002;174:117–42.
[163] Lefebvre AH. Atomization and sprays. 1st ed. New York: Taylor and Francis; 1989.
[164] Escobedo J, Mansoori GA. Surface tension prediction for liquid mixtures. AIChE J 1998;44:2324–32.
[165] Josefsson G, Magnusson I, Hildenbrand F, Schulz C, Sick V. Multidimensional laser diagnostic and numerical analysis of NO formation in a gasoline engine. Proc Combust Inst 1998; 27:2085–92.
[166] Davy M, Williams P, Han D, Steeper R. Evaporation characteristics of the 3-pentanone-isooctane binary system. Exp Fluids 2003;35:92–9.
[167] Lin SXQ, Chen XD. Improving the glass-filament method for accurate measurement of drying kinetics of liquid droplets. Chem Eng Res Des 2002;80:401–10.
[168] Rothamer DA, Ghandhi JB. Determination of flame-front equivalence ratio during stratified combustion. SAE technical paper series 2003-01-0069; 2003.
[169] Han D, Steeper R. Examination of iso-octane/ketone mixtures for quantitative LIF measurements in a DISI engine. SAE technical paper series 2002-01-0837; 2002.
[170] Torres DJ, O'Rourke PJ, Amsden AA. Efficient multicomponent fuel algorithm. Combust Theory Modell 2003;7: 67–86.
[171] Zhang R, Wermuth N, Sick V. Impact of fluorescence tracers on combustion performance in optical engine experiments. SAE technical paper series 2004-01-2975; 2004.
[172] Ernst J, Spindler K, Wagner HG. Untersuchungen zum thermischen Zerfall von Acetaldehyd und Aceton. Ber Bunsenges Phys Chem 1976;80:645–50.
[173] Fristrom RM. Flame structure and processes. In: Apel JR, editor. Applied physics laboratory series in science and engineering. New York: Oxford University Press; 1995. p. 510.
[174] Großmann F. Laserinduzierte Fluoreszenz von 3-Pentanon, Azeton und Azetaldehyd. Diploma Thesis, PCI, University of Heidelberg; 1994.
[175] Zhang R, Bohac S, Sick V. Chemical stability of LIF tracers. Exp Fluids (in preparation).
[176] Haas Y. Photochemical α-cleavage of ketones: revisiting acetone. Photochem Photobiol Sci 2004;3:6–16.
[177] Bell WE, Blacet FE. The photolysis of biacetyl. J Am Chem Soc 1954;76:5332–7.
[178] Sick V, McCann H. Imaging diagnostics for combustion control. In: Scott D, editor. Process imaging for automatic control. CRC Press (in press).
[179] Hindle FP, Carey SJ, Ozanyan KB, Winterbone DE, Clough E, McCann H. Near infra-red chemical species tomography of sprays of volatile hydrocarbons. Technisches Messen 2002;69:352–7.
[180] Hall MJ, Koenig M. A fiber-optic probe to measure precombustion in-cylinder fuel-air ration fluctuations in production engines. Proc Combust Inst 1996;26: 2613–8.
[181] Zhao H, Ladommatos N. Engine combustion instrumentation and diagnostics. Warrendale, PA: Society of Automotive Engineers; 2001.
[182] Grünefeld G, Beushausen V, Andresen P, Hentschel W. Spatially resolved Raman scattering for multi-species and temperature analysis in technically applied combustion systems: spray flame and four-cylinder in-line engine. Appl Phys B 1994;58:333–42.
[183] Schütte M, Finke H, Grünefeld G, Krüger S, Andresen P, Stiebels B. Spatially resolved air-fuel ratio and residual gas measurements by sponaneous Raman scattering in a firing direct injection fasoline engine. SAE technical paper series 2000-01-1795; 2000.
[184] Rothe EW, Andresen P. Application of tunable excimer lasers to combustion diagnostics: a review. Appl Opt 1997; 36:3971–4033.
[185] Miles PC. Raman line imaging for spatially and spectrally resolved mole fraction measurements in internal combustion engines. Appl Opt 1999;38:1714–32.
[186] Kyritsis DC, Felton PG, Bracco FV. On the feasibility of quantitative, single-shot, spontaneous Raman imaging in an optically accessible engine cylinder. SAE technical paper series 1999-01-3537; 1999.
[187] Tolboom RAL, Sijtsema NM, Dam NJ, ter Meulen JJ, Mooij JM, Maassen JDM. 2D stoichiometries from snapshot Raman measurements. 40th AIAA aerospace sciences meeting, 14–17 January, Reno, NV, 2002-0400; 2002.
[188] Mewes B, Bauer G, Brüggemann D. Fuel vapor measurements by linear Raman spectroscopy using spectral discrimination from droplet interferences. Appl Opt 1999; 38:1040–5.
[189] Geyer D, Dreizler A. Simulation of Raman spectra relevant for methane flames. Part I: diatomics (in preparation).

[190] Geyer D, Dreizler A. Evaluation of Raman scattering experiments in turbulent hydrocarbon–air flames. In: Laser applications to chemical and environmental analysis, Annapolis, MD; 2004.
[191] Barlow RS, Carter CD, Pitz RW. Multiscalar diagnostics in turbulent flames. In: Jeffries JB, editor. Applied combustion diagnostics. New York: Taylor and Francis; 2002. p. 384–407.
[192] Zhao F, Taketomi M, Nishida K, Hiroyasu H. Quantitative imaging of the fuel concentration in a SI engine with laser Rayleigh scattering. SAE technical paper series 932641; 1993.
[193] Espey C, Dec JE, Litzinger TA, Santavicca DA. Planar laser Rayleigh scattering for quantitative vapor-fuel imaging in a Diesel jet. Combust Flame 1997;109:65–86.
[194] Andersson Ö, Collin R, Aldén M, Egnell R. Quantitative imaging of equivalence ratios in DME sprays using a chemically preheated combustion vessel. SAE technical paper series 2000-01-2785; 2000.
[195] Vogel S, Hasse C, Gronki J, Andersson S, Peters N, Wolfrum J, et al. Numerical simulation and laser-based imaging of mixture formation, ignition and soot formation in a Diesel spray. Proc Combust Inst 30 (in press).
[196] Eckbreth AC. Laser diagnostics for combustion temperature and species, 2nd ed. Amsterdam: Gordon and Breach; 1996.
[197] Sick V, Wermuth N. Single-shot imaging of OH radicals and simultaneous OH radical/acetone imaging with a tunable Nd:YAG laser. Appl Phys B 2004;79:139–43.
[198] Orth A, Sick V, Wolfrum J, Maly RR, Zahn M. Simultaneous 2D-single shot imaging of OH concentrations and temperature fields in an SI engine simulator. Proc Combust Inst 1994;25:143–50.
[199] Schulz C, Sick V, Wolfrum J, Drewes V, Zahn M, Maly R. Quantitative 2D single-shot imaging of NO concentrations and temperatures in a transparent SI engine. Proc Combust Inst 1996;26:2597–604.
[200] Lide DR, editor. CRC handbook of chemistry and physics. 80th ed. CRC Press; 1999.
[201] Glassman I. Combustion, 3rd ed. San Diego: Academic Press; 1996.
[202] Bartok W, Sarofim AF. Fossil fuel combustion: a source book. New York: Wiley; 1991.
[203] Merck Product Catalogue. Merck, Darmstadt; 1999.
[204] Yaws CL. Handbook of transport property data—viscosity, thermal conductivity, and diffusion coefficients of liquids and gases. Houston: Gulf Publishing Company; 1995.
[205] Neij H. Development of laser-induced fluorescence for precombustion diagnostics in spark-ignition engines. PhD thesis, Lund Institute of Technology, Lund; 1998
[206] Gilbert A, Baggott J. Essentials of molecular photochemistry. Oxford: Blackwell; 1991.
[207] Turro NJ. Modern molecular photochemistry. Menlo Park: Benjamin/Cummings; 1978.
[208] Birks JB. Photophysics of aromatic molecules. London: Wiley-Interscience; 1970.
[209] Koch JD, Hanson RK, Koban W, Schulz C. Rayleigh-calibrated fluorescence quantum yield measurements of acetone and 3-pentanone. Appl Opt 2004;43:5901–10.
[210] Richardson WB, Lin SH, Evans DL. Analysis of the molecular electronic absorption-spectra of shock-heated aromatic-compounds. J Chem Soc Faraday Trans 1982;78:1–15.
[211] Schulz C. Advanced laser imaging diagnostics in combustion. In: Meeting of the European section of the Combustion Institute, Orléans, 2003.